The Solar Orbiter Solar Wind Analyser (SWA) suite

C. J Owen, R. Bruno, S. Livi, P. Louarn, K. Al Janabi, F. Allegrini, C. Amoros, R. Baruah, A. Barthe, M. Berthomier, et al.

A&A 642, A16 (2020)
https://doi.org/10.1051/0004-6361/201937259

Astronomy & Astrophysics
Special issue

The Solar Orbiter mission

The Solar Orbiter Solar Wind Analyser (SWA) suite

C. J. Owen[1], R. Bruno[2], S. Livi[3], P. Louarn[4], K. Al Janabi[1], F. Allegrini[3], C. Amoros[4], R. Baruah[4], A. Barthe[4], M. Berthomier[5], S. Bordon[4], C. Brockley-Blatt[1], C. Brysbaert[6], G. Capuano[7], M. Collier[8], R. DeMarco[2], A. Fedorov[4], J. Ford[3], V. Fortunato[9], I. Fratter[6], A. B. Galvin[10], B. Hancock[1], D. Heirtzler[10], D. Kataria[1], L. Kistler[10], S. T. Lepri[11], G. Lewis[1], C. Loeffler[3], W. Marty[4], R. Mathon[4], A. Mayall[1], G. Mele[12], K. Ogasawara[3], M. Orlandi[13], A. Pacros[14], E. Penou[4], S. Persyn[3], M. Petiot[4], M. Phillips[3], L. Přech[15], J. M. Raines[11], M. Reden[16], A. P. Rouillard[4], A. Rousseau[1], J. Rubiella[4], H. Seran[4], A. Spencer[1], J. W. Thomas[11], J. Trevino[3], D. Verscharen[1,10], P. Wurz[24], A. Alapide[12], L. Amoruso[9], N. André[4], C. Anekallu[1], V. Arciuli[13], K. L. Arnett[11], R. Ascolese[7], C. Bancroft[10], P. Bland[3], M. Brysch[3], R. Calvanese[7], M. Castronuovo[21], I. Čermák[17], D. Chornay[8], S. Clemens[11], J. Coker[1], G. Collinson[8], R. D'Amicis[2], I. Dandouras[4], R. Darnley[1], D. Davies[1,†], G. Davison[1], A. De Los Santos[3], P. Devoto[4], G. Dirks[3], E. Edlund[3], A. Fazakerley[1], M. Ferris[3], C. Frost[10], G. Fruit[4], C. Garat[4], V. Génot[4], W. Gibson[3,†], J. A. Gilbert[11], V. de Giosa[12], S. Gradone[1], M. Hailey[1], T. S. Horbury[18], T. Hunt[1], C. Jacquey[4], M. Johnson[3], B. Lavraud[4], A. Lawrenson[1], F. Leblanc[5], W. Lockhart[3], M. Maksimovic[19], A. Malpus[1], F. Marcucci[2], C. Mazelle[4], F. Monti[7], S. Myers[3], T. Nguyen[3], J. Rodriguez-Pacheco[20], I. Phillips[1], M. Popecki[10,25], K. Rees[1], S. A. Rogacki[11], K. Ruane[1], D. Rust[1], M. Salatti[21], J. A. Sauvaud[4], M. O. Stakhiv[11], J. Stange[3], T. Stubbs[8], T. Taylor[3], J.-D. Techer[5], G. Terrier[4], R. Thibodeaux[3], C. Urdiales[3], A. Varsani[1], A. P. Walsh[22], G. Watson[1], P. Wheeler[1], G. Willis[1], R. F. Wimmer-Schweingruber[23], B. Winter[1], J. Yardley[1], and I. Zouganelis[22]

(Affiliations can be found after the references)

Received 5 December 2019 / Accepted 8 July 2020

ABSTRACT

The Solar Orbiter mission seeks to make connections between the physical processes occurring at the Sun or in the solar corona and the nature of the solar wind created by those processes which is subsequently observed at the spacecraft. The mission also targets physical processes occurring in the solar wind itself during its journey from its source to the spacecraft. To meet the specific mission science goals, Solar Orbiter will be equipped with both remote-sensing and in-situ instruments which will make unprecedented measurements of the solar atmosphere and the inner heliosphere. A crucial set of measurements will be provided by the Solar Wind Analyser (SWA) suite of instruments. This suite consists of an Electron Analyser System (SWA-EAS), a Proton and Alpha particle Sensor (SWA-PAS), and a Heavy Ion Sensor (SWA-HIS) which are jointly served by a central control and data processing unit (SWA-DPU). Together these sensors will measure and categorise the vast majority of thermal and suprathermal ions and electrons in the solar wind and determine the abundances and charge states of the heavy ion populations. The three sensors in the SWA suite are each based on the top hat electrostatic analyser concept, which has been deployed on numerous space plasma missions. The SWA-EAS uses two such heads, each of which have 360° azimuth acceptance angles and ±45° aperture deflection plates. Together these two sensors, which are mounted on the end of the boom, will cover a full sky field-of-view (FoV) (except for blockages by the spacecraft and its appendages) and measure the full 3D velocity distribution function (VDF) of solar wind electrons in the energy range of a few eV to ~5 keV. The SWA-PAS instrument also uses an electrostatic analyser with a more confined FoV (−24° to +42° × ±22.5° around the expected solar wind arrival direction), which nevertheless is capable of measuring the full 3D VDF of the protons and alpha particles arriving at the instrument in the energy range from 200 eV/q to 20 keV/e. Finally, SWA-HIS measures the composition and 3D VDFs of heavy ions in the bulk solar wind as well as those of the major constituents in the suprathermal energy range and those of pick-up ions. The sensor resolves the full 3D VDFs of the prominent heavy ions at a resolution of 5 min in normal mode and 30 s in burst mode. Additionally, SWA-HIS measures 3D VDFs of alpha particles at a 4 s resolution in burst mode. Measurements are over a FoV of −33° to +66° × ±20° around the expected solar wind arrival direction and at energies up to 80 keV/e. The mass resolution ($m/\Delta m$) is >5. This paper describes how the three SWA scientific sensors, as delivered to the spacecraft, meet or exceed the performance requirements originally set out to achieve the mission's science goals. We describe the motivation and specific requirements for each of the three sensors within the SWA suite, their expected science results, their main characteristics, and their operation through the central SWA-DPU. We describe the combined data products that we expect to return from the suite and provide to the Solar Orbiter Archive for use in scientific analyses by members of the wider solar and heliospheric communities. These unique data products will help reveal the nature of the solar wind as a function of both heliocentric distance and solar latitude. Indeed, SWA-HIS measurements of solar wind composition will be the first such measurements made in the inner heliosphere. The SWA data are crucial to efforts to link the in situ measurements of the solar wind made at the spacecraft with remote observations of candidate source regions. This is a novel aspect of the mission which will lead to significant advances in our understanding of the mechanisms accelerating and heating the solar wind, driving eruptions and other transient phenomena on the Sun, and controlling the injection, acceleration, and transport of the energetic particles in the heliosphere.

Key words. instrumentation: detectors – plasmas – Sun: heliosphere – solar wind – Sun: particle emission

† Deceased.

1. Introduction

Solar Orbiter was formally selected by the European Space Agency (ESA) on October 4, 2011 to fill the first launch slot for "medium" class missions under the agency's "Cosmic Vision 2015−2025" programme. The mission, formally a collaboration between ESA and NASA, has top-level science goals which are centred on understanding how our Sun creates and controls the heliosphere, that is the volume of ionised material forming a "bubble" in interstellar space in which all of the planets of our Solar System reside.

As detailed elsewhere in this volume (e.g. Müller et al. 2020), and, for example, in Müller et al. (2013), the primary, overarching scientific objective above can be broken down into four inter-related scientific questions, all of which have strong, direct relevance to the Cosmic Vision theme "How does the Solar System work?". The four top-level scientific questions that will be addressed by Solar Orbiter, each together with three key targeted sub-questions, are as follows:

1. How and where do the solar wind plasma and magnetic field originate in the corona?
   - What are the source regions of the solar wind and heliospheric magnetic field?
   - What mechanisms heat and accelerate the solar wind?
   - What are the sources of solar wind turbulence and how does it evolve?
2. How do solar transients drive heliospheric variability?
   - How do coronal mass ejections (CMEs) evolve through the corona and inner heliosphere?
   - How do CMEs contribute to solar magnetic flux and helicity balance?
   - How and where do shocks form in the corona?
3. How do solar eruptions produce energetic particle radiation that fills the heliosphere?
   - How and where are energetic particles accelerated at the Sun?
   - How are energetic particles released from their sources and distributed in space and time?
   - What are the seed populations for energetic particles?
4. How does the solar dynamo work and drive connections between the Sun and the heliosphere?
   - How is magnetic flux transported to and re-processed at high solar latitudes?
   - What are the properties of the magnetic field at high solar latitudes?
   - Are there separate dynamo processes acting in the Sun?

These are currently fundamental open questions in solar and heliophysics. By addressing them with the observations made by the Solar Orbiter mission, major breakthroughs in our understanding of how the inner Solar System works, and how it is driven by solar activity, will be made.

To answer these questions, it is essential, in coordination with other observations, to make in-situ measurements of the solar wind plasma close enough to the Sun that it is still relatively pristine and has not had its properties modified by subsequent transport and propagation processes. This is one of the fundamental drivers for the Solar Orbiter mission, which will approach the Sun to distances as close as ∼0.28 AU. In addition, measurement of the solar wind plasma at high solar latitudes (several tens of degrees outside of the ecliptic) is also a primary driver for the mission. Making these critical measurement of the thermal and suprathermal components of the plasma population, including electrons, protons, alpha particles, and the minor heavy ion constituents, is the responsibility of the Solar Wind Analyser (SWA) suite of sensors, which is specifically detailed in this paper. The in-situ measurements of solar wind plasma made by SWA, together with those of the Magnetic fields and Radio and Plasma Wave instruments (MAG and RPW, Horbury et al. 2020; Maksimovic et al. 2020, both this issue, respectively), and the Energetic Particle Detector suite (EPD, Rodríguez-Pacheco et al. 2020) form a coherent description of the state of the solar wind local to the spacecraft. These measurements will be traced back to the source regions and structures on the Sun which can be observed using simultaneous, high-resolution imaging and spectroscopic measurements of the Sun, both in and out of the ecliptic plane, by the complement of remote sensing instruments (Auchère et al. 2020, and references therein) within the Solar Orbiter payload. The resulting combination of in-situ and remote sensing instruments on the same, purpose-built spacecraft (García-Marirrodriga et al. 2020), together with the new, inner-heliospheric perspective, distinguishes Solar Orbiter from all previous and current missions. This will enable breakthrough science which can be achieved in no other way.

We note also that the science goals of the Solar Orbiter mission are increasingly relevant to society, in that our own planet orbits within the heliospheric "bubble" and is subject to major disruptions to its near-space environment, which are of solar origin. Thus the mission not only promises to advance the fields of solar and heliospheric physics in their own right, but will make great progress on understanding the physics behind "space weather" and its impact on our technological society.

2. Requirements and expected results

2.1. Primary science motivations

The overarching objective of SWA is to provide the comprehensive in situ measurements of the solar wind which are critical if we are to establish the fundamental physical links between the Sun's highly dynamic and inhomogeneous magnetised atmosphere and the solar wind in all its quiet and disturbed states. This critical step requires comprehensive in-situ measurements of the various constituents of the solar wind plasma including high-time resolution velocity distributions of solar wind electrons and ions and composition up to suprathermal energies. These measurements are vital if we are to discover the fundamental links between, for example, solar eruptions, shocks and the suprathermal ions that are the seed populations of hazardous solar particle events.

The moments (i.e. density, bulk velocity, temperature, etc.) of the electron and proton VDFs provide the crucial information to link the global evolution of the solar wind to its local in-situ properties. These parameters characterise the solar-wind plasma that convects structures over the spacecraft. They also describe the medium through which CMEs and energetic particles propagate, making their measurement critical for the understanding of the evolution of these events. Therefore, the characterisation of the plasma environment around the spacecraft, in which it takes all in-situ measurements, heavily relies on knowledge of the plasma moments.

In addition to this general motivation for measuring the plasma environment, detailed knowledge of the particle properties will support Solar Orbiter's goal to link the coronal source regions with the in-situ solar wind. One such example is the electron strahl, a magnetic field-aligned beam of suprathermal electrons in the electron VDF, which usually propagates in the anti-Sunward direction (Feldman et al. 1975; Pilipp et al. 1987).

The orientation and density of the electron strahl are predictive tools to study the magnetic connectivity of the spacecraft with the solar corona (Steinberg et al. 2005; Owens et al. 2008, 2017). Furthermore, the ability to link solar wind to its solar sources is greatly enhanced by the inclusion of heavy ion measurements of both the ionic and elemental composition of solar wind plasma. Solar wind ion composition is determined by the electron density, temperature, and residence time in the ionising region during the solar wind's release from the low corona, usually freezing-in within 5 Solar radii (R_S) (Hundhausen et al. 1968; Gloeckler et al. 2003; Zurbuchen et al. 2002; Zurbuchen 2007; Ko et al. 1997; Landi et al. 2012). The fact that the ion composition is set within 5 R_S and remains unchanged during its transit through the heliosphere makes it a powerful tool for linking the solar wind to coronal source regions (Zurbuchen et al. 2002; Zhao et al. 2009; Landi et al. 2012). In addition, heavy ion elemental abundances are determined by processes in the chromosphere that can preferentially draw low first ionisation potential (FIP) ions up into closed fields in the corona for later release into the solar wind (e.g. see Laming 2015). Hence, different sources of solar wind (e.g. coronal holes vs. quiet Sun regions with initially closed fields) exhibit different enhancements in ions with low FIP, making elemental abundance measurements indicators of these sources (Feldman & Widing 2003; Zurbuchen et al. 1999, 2002; von Steiger et al. 2001). Combining measurements from SWA with SPICE (SPICE Consortium 2020), which remotely measures the ionisation of the corona will provide the most powerful set of measurements to date for linking the corona to the heliosphere.

By way of example of the contributions that SWA will make, we note that during intervals around perihelion, SWA will measure the solar wind plasma (electrons and ions) in magnetic flux tubes that can be readily traced back to their solar source regions, whose morphology, structure, and variability can be determined from Solar Orbiter's simultaneous remote-sensing observations. These sources can be observed over an extended period, compared to that available from Earth, and the observations will allow us to resolve outstanding questions about the origins of fast and slow wind, the distribution of open magnetic flux, the sources of solar wind turbulence and its dissipation to heat, and accelerate the wind (see Fig. 1). For example, the combined data set will allow us to determine how the nature of the fast solar wind relates to the 3D structure of coronal holes, whether the slow solar wind originates from the over-expanded edges of coronal holes or coronal loops outside of coronal holes. The measurements will help determine the distribution of open magnetic flux and the near-Sun drivers of solar wind turbulence.

Transient events such as CMEs and interplanetary shocks are characterised by rapid changes in the plasma parameters. Measurements by the SWA suite will facilitate studies of the evolution of plasma within these structures in unprecedented detail. For example, SWA measurements will advance our understanding of CME structure, the physical mechanisms of CME initiation, and the global influence of CMEs on the coronal and heliospheric magnetic fields. SWA measurements will provide tests of CME initiation, by utilising plasma signatures to differentiate between models (e.g. Lynch et al. 2011; Reinard et al. 2012), and will allow us to assess the impacts of CMEs on the magnetic configuration of the inner heliosphere. As Solar Orbiter traverses the inner heliosphere, approaching distances as close as 60 R_S from the Sun, SWA will measure the structure and evolution of shocks and other small-scale transients.

The particle VDFs in the solar wind often show deviations from the Maxwellian equilibrium state (Marsch 2006). These

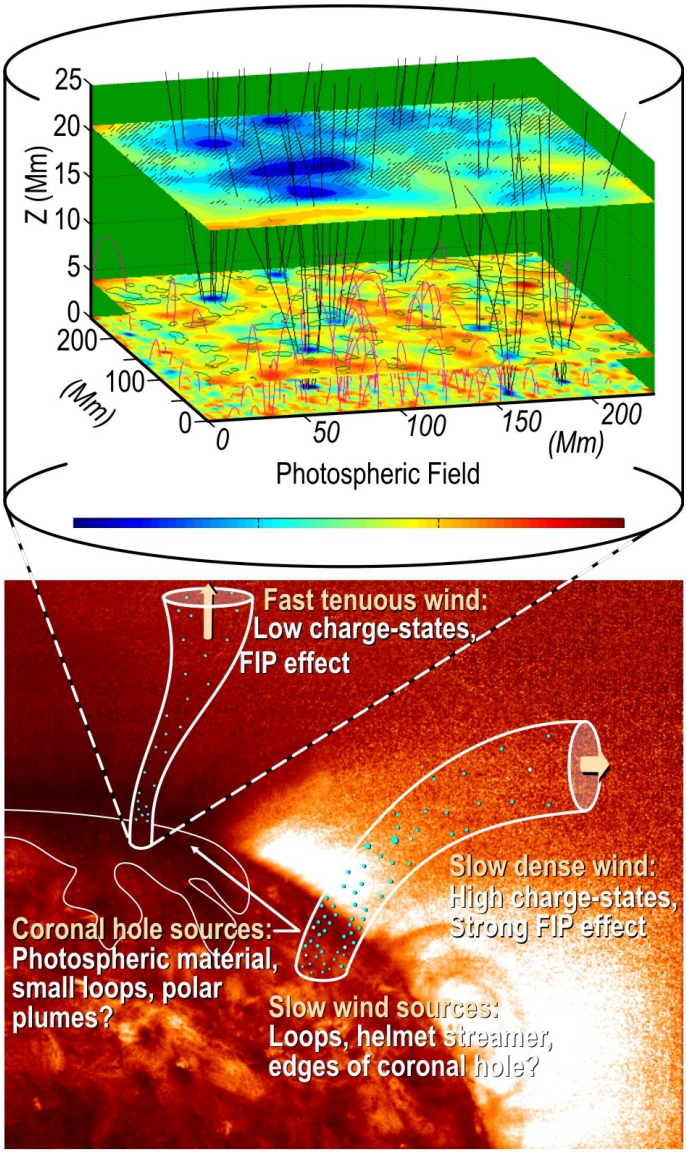

Fig. 1. Central goals of Solar Orbiter. These are to establish the physical links between the observed solar wind and its sources back on the Sun. The illustration shows some of the observed properties of fast wind from coronal holes and slow wind that may emanate from coronal hole edges, from loops beyond the coronal or the helmet streamer. The cut-out shows the complex magnetic structure modelled at the base of a fast wind flux tube that rapidly expands out of the chromosphere and into the corona. Understanding the dynamics of the solar magnetic atmosphere, and its signatures in the measured solar wind holds the key to understanding the sources of all solar wind (adapted from Tu et al. 2005; Schwadron & McComas 2003).

features are the result of a complex interplay between coronal heating, acceleration, global expansion, and local kinetic processes and thus give insight into the processes that determine the evolution of the solar wind plasma. Since the particle VDFs describe the local plasma thermodynamics at the spacecraft completely, the understanding of the solar wind thermodynamics and evolution requires that the particle VDFs, including their non-Maxwellian features, be measured and linked to the electromagnetic fields in the plasma in great detail and at high cadence and resolution. SWA will measure the kinetic microstate of the solar wind by measuring full 3D distributions and, at a higher cadence, 2D pitch-angle distributions of the plasma ions and electrons.

Non-equilibrium features in each particle species play a unique and prominent role. For example, the kinetic structure of the electron distribution is important for the global heat conduction in the plasma, while the kinetic structure of the ion distributions reflects momentum and energy transfer processes such as local heating and kinetic instabilities. These aspects of the solar wind particle distributions show a distinct evolution with heliocentric distance, latitude, and longitude (Verscharen et al. 2019). Solar wind internal energy is shared between all ions and electrons by wave-particle interactions, turbulence, and weak but unavoidable Coulomb collisions. Small-scale kinetic processes also act together with large-scale fluid processes in the acceleration of particles at reconnection sites and shocks. The comprehensive SWA sensor suite, with its novel observational strategy exploiting the Solar Orbiter orbital characteristics, will investigate the cross-scale couplings that constitute the Sun-heliosphere connections (Verscharen et al. 2019), from the global magnetohydrodynamic scales down to the local kinetic scales of wave-particle interactions in the solar wind.

If the non-equilibrium features in the VDF become large enough, the system will drive kinetic micro-instabilities that create small-scale electromagnetic fluctuations on which the particles scatter (Gary 1993). This scattering process reduces the deviation from equilibrium by bringing the shape of the VDF closer towards equilibrium. Known non-equilibrium features that drive instabilities include temperature anisotropies (Gary et al. 1976; Gary & Karimabadi 2006; Hellinger et al. 2006; Bale et al. 2009), ion beams (Gary et al. 1984; Gary 1991), differential streaming between protons and alpha particles (Gary et al. 2000; Verscharen et al. 2013), and electron heat flux (Gary et al. 1975; Verscharen et al. 2019), amongst others. Instabilities are important mechanisms for the overall thermodynamics of the plasma (Matteini et al. 2013; Verscharen et al. 2015; Yoon & Sarfraz 2017; Stansby et al. 2019). Therefore, the detailed study of non-equilibrium features that potentially drive instabilities and the search for the signatures that result from the action of instabilities are necessary to understand the impact of these micro-instabilities on the evolution of the solar wind. SWA will deliver on both of these requirements.

Measurements of the particle VDFs are also a critical component for the interpretation of the ubiquitous turbulent fluctuations in the solar-wind plasma. These fluctuations are characterised by self-consistent interactions between the fields and the particles. Therefore, the observation of the fluctuations in the particle VDF will give us insight into the nature of the turbulent fluctuations in general (Šafránková et al. 2019; Wu et al. 2019). Furthermore, the secular transfer of energy from the turbulent fluctuations into particle heating creates characteristic signatures in the velocity distribution such as the formation of quasi-linear plateaus through cyclotron-resonant and Landau-resonant dissipation (Dusenbery & Hollweg 1981; Marsch et al. 1982, 2003; Isenberg & Hollweg 1983) or flattening of the core of the distribution through stochastic heating (Klein & Chandran 2016). Finding these signatures in the velocity distributions will improve our understanding of the nature of the turbulent fluctuations and the relevant dissipation processes. These measurements of turbulent fluctuations in the VDFs and their moments require a high cadence in order to resolve small-scale fluctuations (Nicolaou et al. 2019) and a high resolution in order to resolve the characteristic signatures of heating. SWA will provide sufficient cadence and resolution to perform these studies.

Instabilities, turbulence, and other kinetic plasma processes result from, and participate in, a complex interplay between interactions in the solar-wind source regions, the large-scale expansion of the solar wind, and local plasma physics. These energy-transfer mechanisms have a strong impact on the thermodynamics and evolution of the solar wind and are thus important for our understanding (Verscharen et al. 2019). The radial evolution of turbulence and the continuous heating of the fast wind are clear examples of this kind of dynamical processes. SWA will measure the in-situ signatures of these processes mainly through provision of high-resolution solar wind VDFs. These distributions will show kinetic features like the electron strahl, ion temperature anisotropies, and differential streaming, which are most likely the results of a combination of local wave-particle interactions (near the Sun or in the solar wind) and global expansion effects.

The thermal and suprathermal particles in the solar wind also serve as part of the seed population for the acceleration of energetic particles through transient events such as interplanetary shock waves. Therefore, understanding the kinetic properties of these seed particles is important for the development of a better understanding of the production of energetic particle radiation in the inner heliosphere. SWA will characterise these particles completely down to kinetic scales, for example to determine the sources and acceleration mechanisms of the so-called large gradual solar energetic particle (SEP) events and determine the properties, composition, and evolution of suprathermal ions that seed these higher-energy particles.

During later phases of the mission, Solar Orbiter measurements will reveal the latitudinal dependence of these phenomena as the spacecraft climbs out of the ecliptic. Moreover, as the orbit repeatedly covers a range of heliocentric distances, the in situ instruments will also provide key information on the evolution of the solar wind with distance from the Sun, providing a separation of those processes which are inherent in the solar wind itself from those which play a role in the formation of the young, "pristine" wind near to the Sun. Solar Orbiter will thus extend our direct measurements of space plasmas into a new realm that will transform our view of the connections from the solar atmosphere into the solar wind, and help us project this understanding to other stellar environments.

2.2. General overview of SWA measurement requirements

The Solar Orbiter science goals, as expressed above, can only be achieved with the inclusion of a SWA-like package within the Solar Orbiter payload to provide moments and VDFs of electrons and ions. Indeed, measurements of the kind made by SWA are required for all of the mission science goals (Müller et al. 2013, 2020; Zouganelis et al. 2020). They are also fundamental to supporting modelling and analysis of the Sun-spacecraft connection (Rouillard et al. 2020), and multi-mission science opportunities requiring observations from more dispersed perspectives, such as those which will be achieved with Parker Solar Probe (Velli et al. 2020).

Electrons, protons, and alpha particles are the most abundant populations of the solar and heliospheric plasma. The electron strahl in the solar wind is generally the fastest of these plasma populations and thus provides the early information on any processes happening remotely from the spacecraft. The electron, proton, and heavy-ion VDFs with their moments and their typical non-Maxwellian features must be fully resolved by the SWA sensors, in order to provide critical information on the plasma globally and locally, its large-scale thermodynamics, its remote sources on the Sun, and furthermore about the transport processes (e.g. instabilities and turbulence) in operation between these sources and the spacecraft location. The compositional

signatures which must be measured by SWA are necessary to provide clearer constraints for theories on the origin of solar wind streams, and in particular of CMEs. For example, the kinetic properties of the heavy ions are required to provide information about the non-thermal processes heating the plasma and accelerating the solar wind. The ionic charge states of the local plasma must also be of sufficient quality to enable direct comparison with the remote observations of the coronal plasma., such that elemental and compositional signatures can be related to ultraviolet diagnostics of the solar source regions from remote-sensing observations.

SWA must consist of a suite of sensors that are able to measure the 3D VDFs of the major solar wind constituents: electrons, protons, and alpha particles. The basic moments of the distributions, such as density, velocity, pressure tensor, and heat flux vector must be obtained under all solar wind conditions and must be sampled with sufficient cadence to characterise fully the fluid and kinetic state of the wind. In addition, measurements supporting the derivation of relative elemental abundances, ionic charge state ratios and distributions, velocity space distributions and moments (population density, bulk flow speed and temperature) of representative high-FIP elements (the C, N, O group), and of low-FIP elements (such as Fe, Si or Mg) are required. These measurement challenges provide the motivation for our instrument suite comprising three distinct sensors:

– The Electron Analyser System (SWA-EAS) to measure the VDFs of electrons (including core, halo, and strahl electrons) and their moments at high time resolution;

– The Proton-Alpha Sensor (SWA-PAS) to measure the VDFs of major ion species and their moments at high time resolution and determine their moments;

– The Heavy Ion Sensor (SWA-HIS) to measure the VDFs of prominent minor ion species and determine their abundances and charge states.

To fully address the Solar Orbiter science goals, the SWA-EAS must resolve the full 3D velocity space distributions of solar wind electrons with high cadence (<10 s time resolution). Since the electron thermal velocity is much greater than their bulk velocity, the electrons arrive at the spacecraft from all directions. Therefore, even in the solar wind, such a measurement of the 3D electron VDF can only be achieved by a sensor (or a set of sensors) that has a combined FoV covering a large fraction of the full sky. In addition, the sensor is required to provide 2D pitch angle distributions (PADs) with high time resolution (ideally at a cadence of 0.125 s). Data from MAG (Horbury et al. 2020) are used onboard to determine the orientation of the magnetic field, which is necessary to produce the PADs and is thus required at this high cadence. The specific design goals for SWA-EAS, based on these general requirements, are presented in Sect. 3.1.6.

Fully addressing the Solar Orbiter science questions also requires the SWA-PAS sensor to be capable of resolving the full 3D VDFs of solar wind protons and alpha particles with high cadence (<10 s time resolution), as well as measuring the bulk plasma parameters (i.e. the moments) at ultra-high time resolution (as fast as ~0.1 s) to characterise the global structure and dynamics of the 3D inner heliosphere and improve our basic understanding of the kinetic processes, microstate, instabilities, and turbulence in the evolving solar wind from ~0.28–1.0 AU. The SWA-PAS energy coverage and resolution, FoV, angular coverage and resolution, geometric factor, and time resolution must be such that it can measure solar wind protons and alpha particles for more than 99% of the time during the Solar Orbiter mission profile. The specific design goals for SWA-PAS, based on these general requirements, are presented in Sect. 3.3.6.

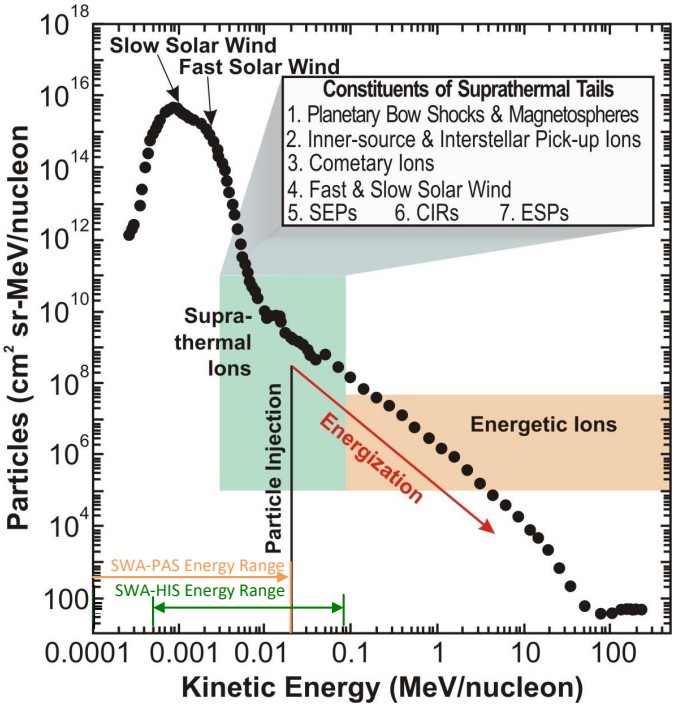

Fig. 2. SWA measurement range for the ion composition and energy distribution extending from the solar wind into the suprathermal domain and covering the energy range of SEP seed particles injected to shock acceleration (adapted from Mewaldt et al. 2003; shown here are oxygen fluences from ACE measured over a 3-year period). SWA-PAS and SWA-HIS energy ranges are shown at the bottom of the figure for comparison.

Finally, the SWA-HIS must address two fundamentally different sets of measurement objectives. First, SWA-HIS must measure the composition and 3D VDFs of heavy ions in the bulk solar wind as well as that of pick-up ions. Second, SWA-HIS must measure the composition and 3D VDFs of the major constituents in the suprathermal energy range (see Fig. 2). The sensor must be able to resolve the full 3D VDFs of the prominent heavy ions at a resolution of 5 min in normal mode and 30 s in burst mode. Additionally, SWA-HIS must measure 3D VDFs of alpha particles at 4 s resolution in burst mode. Measurements must be made up to 60 keV/e, with mass resolution ($m/\Delta m$) of ~5. These will be the first such measurements in the inner heliosphere. The specific design goals for SWA-HIS, based on these general requirements, are presented in Sect. 3.2.6.

In summary, the measurements by the SWA suite are central to addressing critical parts of the Solar Orbiter top-level science questions related to the in situ solar wind, the connectivity between the spacecraft, the wind's coronal source regions, and suprathermal ion populations throughout the heliosphere. Through its capability of measuring the 3D VDFs of electrons and ions, SWA is a pivotal and indispensable instrument suite for establishing the links between processes remotely observed in the corona and the resulting heliospheric plasma properties measured in situ, and for revealing their complex multiple connections.

3. SWA sensor descriptions

In this section we provide a summary of the technical details of each of the four hardware elements that comprise the SWA suite. For each of the three scientific sensors, we provide an

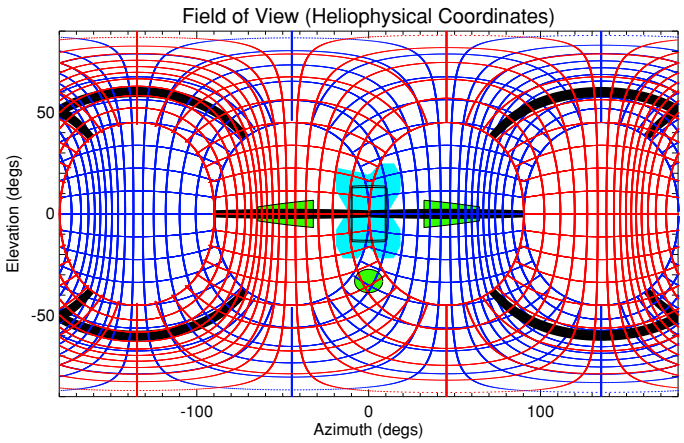

Fig. 3. Expected combined FoV for the 2-head SWA-EAS unit. The figure covers the full sky (±90° in elevation and ±180° in azimuth), with the blue grid indicating the regions of sky sampled by SWA-EAS1 and the red grid that sampled by SWA-EAS2. The black bars indicate regions of the sky occluded by sensor structure, in this case the three support pillars on each sensor which are clearly visible in Fig. 4. The green shaded regions indicate the approximate projection of spacecraft appendages in the FoV, namely the solar arrays and the high gain antenna. The blue shaded region indicates the blockage to the FoV due to a boom-mounted baffle designed to shield the instrument from direct impingement of thruster exhausts. (The relative projection of the spacecraft itself is indicated by the rectangle within this latter region).

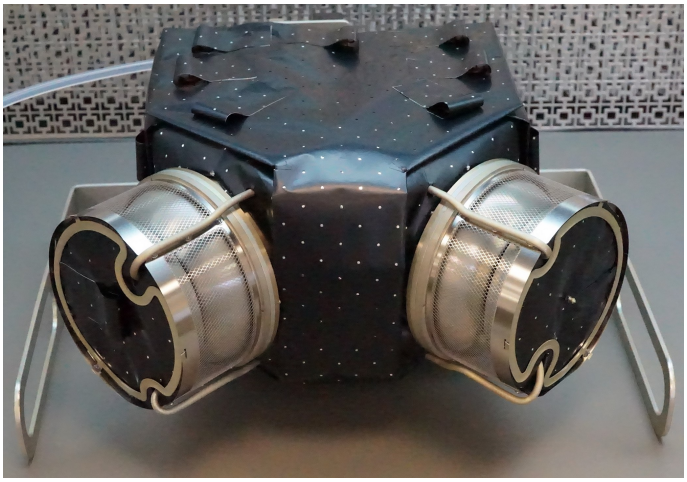

Fig. 4. Flight model of the SWA-EAS unit, showing the two orthogonally-mounted cylindrical electron optics subsystems attached to the control electronics box (which is housed beneath the black multi-layer insulation (MLI) blankets). The curved aperture deflector plates, lying either side of the apertures themselves, can be seen through the entrance grid on both heads.

overview of the design, discuss the principles behind the making of the measurements before describing the details of some of the key and novel features of the design at subsystem level. We summarise the testing and calibration procedures that each of the hardware elements has undergone before summarising the design specification of each sensor as delivered to the spacecraft. In the case of the SWA-DPU, we also provide an overview of the software design and the on board scientific data processing algorithms.

3.1. The SWA Electrostatic Analyser System (SWA-EAS)

3.1.1. SWA-EAS introduction

To address the Solar Orbiter mission science goals, the SWA-EAS unit must be able to resolve the full 3D velocity space distributions of solar wind electrons with high cadence (<10 s time resolution). This basic measurement requirement can only be achieved by a sensor, or sensors, that have a combined FoV covering a large fraction of the 4π steradians of the full sky.

To achieve the requirement, the SWA-EAS consists of two identical top-hat electrostatic analysers, each with an aperture deflection plate system. Both are mounted on a common electronic box, which in turn is mounted at the end of a boom extending into the shadow of the spacecraft. Orthogonal mounting of the two sensor heads and an aperture deflection capability of ±45° on each head provides a full 4π FoV, with some degree of overlap and subject only to blockage by the spacecraft and its appendages.

With this deployment configuration, the expected FoV of the combined sensor system is as shown in Fig. 3. This shows the full sky FoV (±90° in elevation and ±180° in azimuth) with the Sun (and spacecraft) direction centred at (0,0). The blue grid represents the pixelated FoV of SWA-EAS head 1 (SWA-EAS1), while the red grid represents that of head 2 (SWA-EAS2). Some regions of sky are covered only by SWA-EAS1 or SWA-EAS2, while others are sampled by both heads. Sensor and spacecraft related blockages to the FoV are marked by the coloured regions, as described in the caption.

The sensor will measure electron fluxes and the SWA-DPU will calculate onboard and return moments of the electron distribution with a cadence of 4 s. In normal mode SWA-EAS will also return full 3D distributions at 100 s cadence. However, the sensor is capable of returning these at 1 s cadence where resources allow. The sensors will also provide 2D electron PADs at ~0.125 s cadence during short periods of burst mode. To achieve this at high cadence, the sensor will use information provided on board by the MAG sensor (Horbury et al. 2020) to steer the sensor look-direction using the aperture deflection system such that the unit samples only the plasma at elevations which contain the parallel and anti-parallel magnetic field directions. Since data is taken at all azimuth angles simultaneously, rebinning this data with respect to the magnetic field direction allows the assembly of a PAD in the time needed to perform two energy sweeps. This cadence has been selected to allow synchronisation with magnetometer data rates.

3.1.2. SWA-EAS design overview

The flight model (FM) configuration of the two SWA-EAS analyser heads and common electronics box is as shown in Fig. 4. Each head consists of three key modular sub-systems:

i. Electron optics (EO) system: consisting of the top-hat electrostatic analyser system (EA), aperture deflection system (ADS) and "top-cap" variable geometric factor system (VGFS);

ii. Detector and readout element: consisting of a microchannel plate (MCP) mounted onto an anode and readout board, including high-voltage (HV) coupling capacitors and readout electronics;

iii. EAS low voltage (LV) and HV distribution and control circuitry.

Sub-systems (i) and (ii) consist of a number of functional elements. Figure 5 shows a cross-section through a single analyser head and the location of the key functional elements, which are listed in the figure caption.

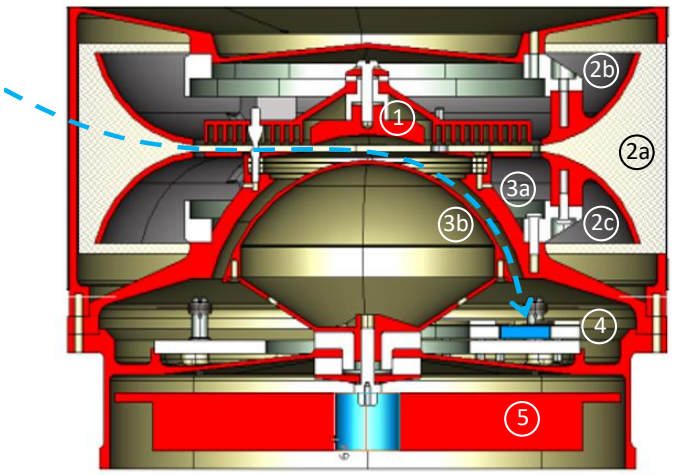

Fig. 5. Cross-section through a single SWA-EAS sensor head. Key subsystems are: (1) the VGF system "top-cap" anode; (2) (a) the entrance aperture shielding grid and (b,c) upper and lower plates of the deflection system; (3) (a,b) the upper and lower hemispheres of the electrostatic analyser; (4) the detector subsystem comprising a grid, the annular MCP, and the anode board, together with embedded HV coupling capacitors; (5) the application-specific integrated circuit (ASIC) 32 charge amplifiers. A representative electron trajectory through the sensor electron optics is shown by the blue dashed trace, for the case where the upper aperture deflection plate is charged positively.

Functional elements 1,2, and 3 form sub-system (i) and 4, 5, 6, and 7 form subsystem (ii). Provision of sub-systems (i) and (iii) are the responsibility of University College London's Mullard Space Science Laboratory (UCL MSSL) and sub-system (ii) is the responsibility of Laboratoire de Physique des Plasmas (LPP), Ecole Polytechnique, Palaiseau, France.

In addition, the electronics enclosure, also the responsibility of UCL MSSL, contains two identical sets of electronics boards independently servicing each of the analyser heads. These are the LV and HV electronics boards and the electronics boards hosting field-programmable gate arrays (FPGAs) for instrument control, interfaces, counters, electrical interfaces to the SWA-DPU, and the inter-experiment link (IEL).

3.1.3. SWA-EAS measurement principle

Solar wind electrons arriving at the spacecraft will enter one of the SWA-EAS sensor heads through the exterior shielding grid. The ADS uses positive voltages applied to either the upper or lower deflector electrodes, as needed, to steer electrons from a desired arrival direction into the EA section. The ADS acceptance angle can be varied through a range ±45° in 16 steps, requiring up to +2400 V on the deflector plates to accommodate the requirement for acceptance of up to 5 keV electrons at maximum deflection. The steps are selected to ensure continuous angular coverage while accounting for an increase in the acceptance angle resolution from ~2° to ~9° as the deflection angle increases. This ensures that any narrow (a few degrees) solar wind electron beams cannot fall between gaps in angular coverage and remain undetected. We note that although the deflector sweep voltages are symmetric in application, the response of the detector is asymmetric in terms of angular resolution for up and down sweeps. This is represented in the size of individual pixels shown in Fig. 3, and is discussed further in Sect. 3.1.6 below. The electrons then enter the hemispherical EA section, which permits only electrons of the selected energy to reach the detector subsystem. The design target k-factor, the ratio of the transmitted electron energy to the voltage applied between the hemispheres, is ~6.2, and the relative energy resolution is 13.5%. The maximum voltage on the inner hemisphere is +850 V. The azimuth acceptance angle of 360° for the EA is divided into 32 equal size bins, which allows determination of the electron arrival direction to within 11.25° in the detector plane. The combined ADS and EA component of each sensor thus samples the arrival direction of solar wind electrons over a 2.8π steradian solid angle range.

The 32 azimuth angle bins of each sensor head are all sampled simultaneously while the elevation angle bins must be sampled in their 16 steps sequentially by applying appropriate voltages to the upper or lower deflector plates. The sensor sweeps through 65 energy levels at each elevation, which was found to be the most efficient operation and also readily supports a scheme for tracking the magnetic field in the SWA-EAS burst mode (as detailed in Sect. 4.3.1). The usual cadence of the energy sweep is one sweep of 65 steps in 62.5 ms. Thus basic data accumulation time for any single energy-angle bin is ~0.92 ms. Combining the datasets from the two orthogonally-mounted sensor heads provides 4π steradian solid angle coverage (with 1.6π steradians in overlapping fields of view) and thus a complete measurement of the 3D VDF in $65 \times 16 \times 0.92\,\mathrm{ms} \sim 1\,\mathrm{s}$, although this is not the typically available down-linked time resolution of the VDFs.

The sensor unit is accommodated on the end of the boom in the spacecraft shadow, which both minimises the physical blockage of the spacecraft and its appendages on the SWA-EAS FoV and minimises the effect of spacecraft electrostatic interference in the measurement of the lowest-energy solar wind core electrons.

3.1.4. SWA-EAS design details

The overall functional block diagram for a single chain of the SWA-EAS unit is shown in Fig. 6. We now describe each of the key elements in that chain:

The SWA-EAS electron optics subsystem. The two annular curved deflection plates on each SWA-EAS analyser head steer incoming electrons into a hemispherical top-hat electrostatic analyser. The latter is of similar design to those flown on many previous missions (e.g. Carlson et al. 1982; Kessel et al. 1989; Johnstone et al. 1997; Carlson & McFadden 2013). Around the outside of the annular plates is wrapped a thin mesh designed to shield the incoming plasma from the voltages applied to the deflector plates. The design of the hemispherical analyser is derived from UCL MSSL heritage with instruments deployed on the Cluster, Cassini, and Double Star missions and uses parts which are precision-machined from aluminium alloy. The annular deflector plates are a new addition to this UCL-MSSL-built family of instruments and are supported on Vespel insulators to separate them electrically from the analyser top hat and the base plate. The top hat assembly is supported from the base plate by three pillars, (some of which are evident in Fig. 4). Co-aligned with the pillars are metal tubes that carry screened HV leads to the top hat assembly (also evident in Fig. 4). These support pillars are further co-aligned with anode gaps to minimise FoV loss and field distortion caused by the external and internal support pillars. The mesh is wrapped around the upper and lower end of the top and base plates. For radiation screening, the design aims to place a minimum of 2 mm of aluminium alloy around any critical instrument parts.

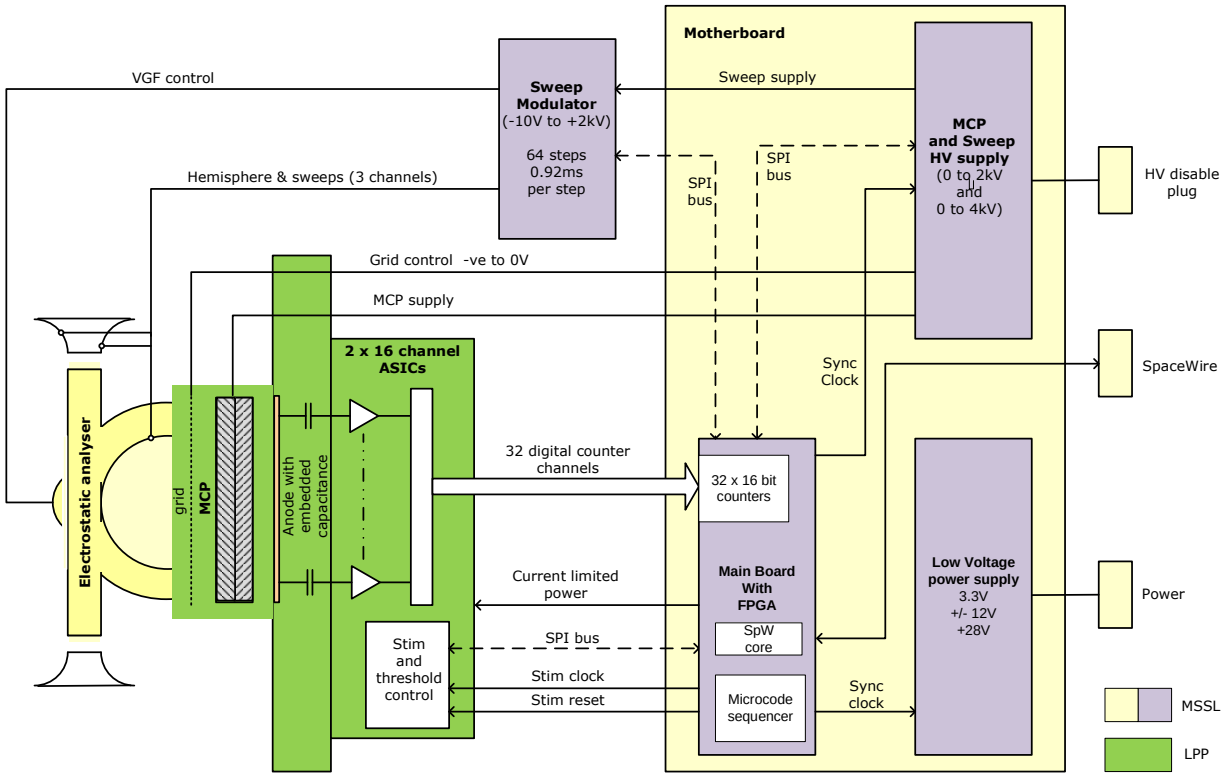

Fig. 6. Functional block diagram of single analyser head of SWA-EAS.

A second significant enhancement to the sensor heads over UCL MSSL heritage designs is the addition of a novel "top-cap" electrode, providing an electrostatic variable geometric factor (VGF) system (Collinson & Kataria 2010). The application of a commandable potential to the "top-cap" reduces the geometric factor of the system by restricting the fluxes of electrons that have passed through the ADS before they enter the EA. Addition of the VGF system increases the dynamic range of the instrument by up to two orders of magnitude, allowing the instrument to operate over the full range of solar wind conditions expected between 0.28 and >1 AU. This also provides a means to increase the lifetime of the detectors by reducing the total charge extracted from the MCPs.

Although most of the time the sensors should not be in direct sunlight, a UV photon and analyser internal photo-electron rejection scheme is required to deal with possible stray UV reflections from the spacecraft and occasional exposure to sunlight. This is achieved by use of a baffle system at the EA aperture and by use of Ebonol "C" coating for the non-reflective blacking of several internal parts. This coating also helps with trapping secondary electrons produced by energetic primary plasma electrons that contaminate the low energy end of the electron distributions. The coating produced by the Ebonol "C" process is jet black, chemically stable, heat stable, and very adherent. The finish itself will withstand temperatures up to ~190°C. This dual baffling and blackening approach has been used on previous similar flight instruments (specifically Cluster PEACE and Cassini ELS instruments) and has proven heritage.

EAS detector and readout electronics subsystem. The SWA-EAS Detector and Readout Electronics Subsystem is made up of a single printed circuit board (PCB) housed within each analyser head which also provides the MCP mount, the embedded HV coupling capacitors, and the MCP HV distribution circuitry. The detector block diagram is shown in Fig. 7. It is structurally based on an annular PCB with a circular array made up of 32 pixels printed on the top and the electronic circuitry associated with two ASICs and their associated discrete components on the bottom. A set of two annular circular MCPs of outside diameter 71.5 mm and centre hole diameter of 38.6 mm, stacked in a chevron assembly with a spacer of 50 μm between them, is positioned on the top face of the PCB. A front grid is then positioned on top of the MCP stack, with the assembly held together by a set of mechanical parts. The complete assembly, shown in Fig. 8, is then fitted in a circular housing within each analyser head. The mounting of the ASICs below the detector electronics and immediately beneath the MCPs, together with the shielding provided by housing the complete subsystem assembly in the lower part of the analyser head, is expected to provide a significant reduction of the radiation dose experienced by these sensitive components. A set of two identical such detector assemblies is needed to equip the two independent heads of the SWA-EAS.

The Anode board takes one HV input and divides the required voltages for the MCP and anodes internally. The thirty two anodes connect through small HV coupling capacitors embedded within the PCB to the two sixteen-channel ASICs containing the charge sensitive amplifiers (CSA) and leading edge discriminators. The detector PCB also receives interface commands via a dedicated Serial Peripheral Interface (SPI) bus from the SWA-EAS FPGA to configure the subsystem, including the threshold settings for the 32 CSA discriminators and a voltage (0 or −10 V) applied to the grid in front of the MCP for the rejection of low energy secondary electrons and UV induced photo-electrons. The LV connections are via a 51 way Omnetics bi-lobe nano-D type connector. The HV circuits are connected by a Reynolds HV coaxial connector.

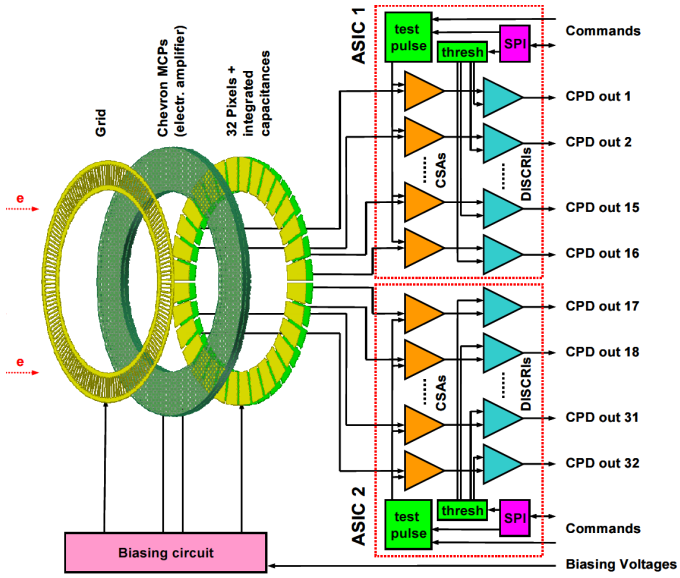

Fig. 7. EAS detector system block diagram.

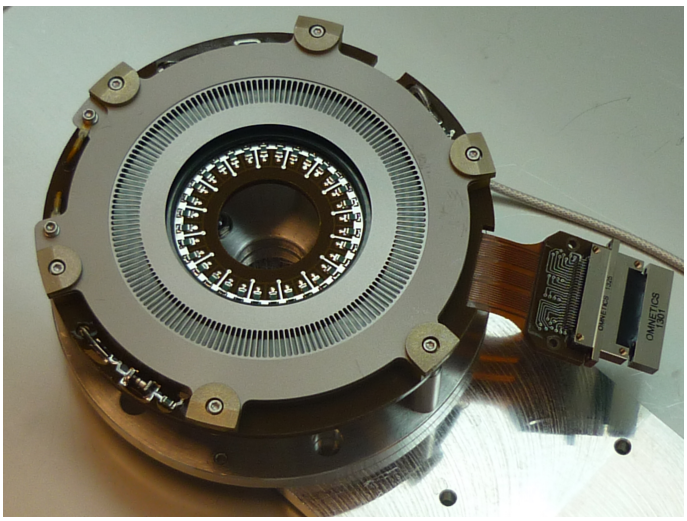

Fig. 8. EAS FM detector system.

The electrons arriving at the detector assembly through the analyser head electron optics pass through the front grid and enter the upper MCP, where they induce secondary electron emission through the micro-channels of the chevron MCPs. Electron clouds of $2-5\times10^6$ electrons (depending on the MCP voltage) are emitted from the rear of the lower MCP immediately below the impact point of the original electron, typically within a charge pulse lasting ~1 ns, and are collected on the anode. The amplitude of the associated voltage pulse generated depends on the impedance of the anode pixel and to the charge value. Due to the diameter of the charge cloud, a single electron impact may generate charge pulses on more than one anode pixels when the spot overlaps these two pixels. In addition, stray capacitances between pixels, may also generate pulses on the neighbouring pixels. To minimise this potential cross-talk, grounded tracks are placed between the anode pixels. Each one of the 32 anode pixels is connected to one of the input channels of the ASICs. Collected charges need to be in the range 16−2000 fC to match the dynamic input range of the CSAs. Charge pulse heights are assessed against the threshold applied to the 32 discriminators. These thresholds can be independently adjusted to discriminate only the main charge pulses but not the secondary charge pulses due to capacitive cross-talk. Output signals from the 32 channels which exceed the associated thresholds are then supplied to the FPGA via the motherboard as a count of the electrons arriving at each azimuth pixel of the detector during each energy-elevation angle accumulation period.

EAS HV sweep modulator subsystem. An HV sweep modulator PCB is mounted on the back of each analyser head and is connected to the electronics box via Reynolds HV coaxial connectors to enable each analyser head assembly to be readily removed as a complete testable unit. This HV sweep modulator board takes a single static HV supply at 2015 V from the Sweep HV Supply board and generates four scanning HV outputs which have high slew rates, low noise, and fast settling times. The modulator uses opto-couplers from Micropac which have been qualified for space and military use. The four outputs are assigned to the following electrodes: upper deflector plate, lower deflector plate, VGF, and inner hemisphere. The HV levels are controlled by the SWA-EAS FPGA (see below) via four SPI control busses. The subsystem uses two 12-bit digital-to-analogue converters (DACs) per channel to define the required HV levels for each sensor head subsystem. These are combined to give 20 bits of resolution with the output voltage per bit being ~1.6 mV with the smallest required step difference of ~10 mV. The maximum HV output is set to 1990 V and the minimum is ~−13 V. Read back of these voltages is provided via its housekeeping (HK) SPI to the main SWA-EAS electronics board under control of the FPGA's HK system. The LV connections are via a 31 way Omnetics bi-lobe nano-D type connector. The HV is transmitted from the HV supply by a Reynolds HV coaxial connector. The four HVs to the analyser are also transmitted via Reynolds HV coaxial connectors. The mounting of each of the analyser heads directly on to the electronics box case provides a compact unit of minimum mass with the shortest possible connections between the electronics and each analyser.

EAS LV and HV distribution and control subsystems. The remaining PCBs for each sensor head are housed in the SWA-EAS electronics box forming rear part of the structure as seen in Fig. 4. For ease of cable and connector routing and access, the PCBs for each sensor head are housed on the opposite side of the electronics box structure to that on which the related head is mounted. The forward part of the structure ahead of the front bulkhead is occupied by the cables and connectors.

To meet the minimum 2 mm structure screening thickness, the electronics case is a mixture of parts machined from both solid and sheet metal. The spacecraft boom fixing is via four threaded holes, two in each of the front and rear bulkheads with clearance holes in the top structure plate to enable the top face of the SWA-EAS to be bolted to the boom flange with thermal control bushes between them. Interface connectors are grouped in analyser sets on the rear bulkhead and a single purge connector feeds both analysers via an internal "Tee" piece. A heater interface bracket and instrument earthing stud are also positioned on the rear bulkhead.

In addition to the anode board mounted in the analyser head itself and the sweep modulator board mounted on the rear of the analyser head (both described above), the system consists of four other boards: The MCP and sweep HV supply board;

the SWA-EAS main board; and the Low Voltage Power board; these are each hosted by the fourth board, the motherboard, and are mounted within the electronics enclosure. The three motherboard mounted PCBs connect to the sweep modulator PCB, the anode PCB, and the SWA-DPU via connectors on flying leads soldered to the mother board. The exceptions are the two HV supplies, which connect to the MCP and sweep HV supply PCB via HV Reynolds connectors.

The MCP and sweep HV supply board produces one programmable HV, one static HV, and an auxiliary −30 V output. It also generates the 0 V to −8 V variable output supply for the grid in front of the MCP using a single 12-bit DAC and an op-amp to produce this output. The static HV output of ∼2 keV and auxiliary −30 V output are used to supply the sweep modulator board with a raw HV, while the other controllable output is variable between 0 V and +3700 V and supplies the MCP. This output has ripple <0.1% over the MCP operational output voltage range. The MCP voltage is controlled by SWA-DPU command over the SpaceWire (SpW) link via the SWA-EAS main board. It takes a 10 kHz clock from the main board, and uses alternate edges to synchronise the two converters, thus giving 20 kHz as its fundamental switching frequency.

The SWA-EAS main board hosts the system master crystal oscillator, supplying the 19.98848 MHz system clock, which in turn is used to synchronise all power conversion. This board also hosts the FPGA and the SpW low voltage differential signalling (LVDS) drivers and receivers. The FPGA is the master controller for SWA-EAS and provides all control of: data acquisition; HV scanning and other instrument timing, performed by a sequencer which uses an uploaded "sequence table" to control SWA-EAS; SWA-DPU communication including housekeeping, science data, and commanding (including command parsing and checking); HV and LV power supply synchronisation; the time control system; and active thermal control for the operational heater(s). The SWA-EAS main board also supports SWA-EAS sensor communication with the SWA-DPU via SpW at 10 Mbits s^{-1}. We note in passing that the FPGA design deployed for SWA-EAS also supports, without modification, the operation of the SWA-PAS unit (see Sect. 3.3.2).

The Low Voltage Power Board is designed to take switched bus power from the SWA-DPU and provide ±8.5 V, 10 V, 28 V, and 3.3 V isolated supplies to the rest of SWA-EAS. It is synchronised by the FPGA to 294 ∼ 300 kHz.

Finally, the SWA-EAS mother board provides a back plane and host for connections to other SWA-EAS electronics boards and to the SWA-DPU. It provides the low voltage and logic connections between the low voltage power board, the SWA-EAS main board, and the HV supply board. It also has the low voltage connectors for the 28 V power input, the SpW interface, the HV enable plug, and the two bi-lobe connectors to the sweep modulator and anode PCBs. It also accommodates opto-isolation for the heater control. The mother board uses the Hypertac CSD family of four row connectors for PCB interconnect. The SWA-EAS internal power returns are connected to the structure at the anode PCB. The incoming power bus return is not connected to the structure at SWA-EAS.

3.1.5. SW-EAS testing, characterisation, and calibration

The SWA-EAS instrument has been integrated and calibrated in a number of different phases. In the first phase, MCP preselection and characterisation of the MCPs were carried out at LPP, followed by characterisation and performance of the integrated detector and readout subsystem. This included a detailed characterisation of the front-end readout ASICs and a determination of temperature response of the subsystem.

Following the integration of the full SWA-EAS FM, the primary phase of the FM calibration activity was carried out at UCL MSSL, where a full calibration of both SWA-EAS sensor heads was performed using dedicated electrical ground support equipment (EGSE) to rotate the sensor within an electron beam of known energy set up in the laboratory's LEPIC (Low Energy Plasma Instrument Calibration) vacuum chamber. The purpose of this activity was to determine the sensor performance parameters, including the sensor k-factors, relative geometric factors, and the energy and angular response. These parameters must be determined for the large parameter space covered by the combination of the energy selection performed by the inner hemisphere, the look-angle selection performed by the ADS, and the geometric factor selection performed by the VGF system.

This FM sensor was bombarded by the known energy beam while performing voltage-elevation scans at various azimuth angles. For the voltage-elevation scans, the instrument is rotated to a chosen azimuth angle and set for different voltages. The number of transmitted particles at each voltage (equivalent to energy) is then recorded for an elevation angle and the process is repeated for the range of elevation angles so as to cover the full energy-elevation parameter space. The process is then repeated at all the required azimuth positions. Moreover, three sets of energy-elevation scans are carried out. First, voltage is applied to the inner hemisphere only (with elevation angle range confined typically to ±5° (for energies >100 eV) or ±10° (energies <100 eV)). Then voltages are applied to both the inner hemisphere and deflector plates, and finally to each of the inner hemisphere, deflector plates, and variable geometric factor system. In the latter two sets of tests the elevation angle range was typically ±50°, that is to say beyond the required ±45° for each sensor head. In a majority of the tests, the azimuth angles were chosen so that the beam was incident on the centre of each of the anodes. The voltage range was typically chosen to permit transmission of ±12% of the set energy.

The response of the unit to secondary electron contamination was assessed during the calibration activity and found to be satisfactory (<2% contamination level). A number of other tests, including cross-calibration of the two SWA-EAS sensor heads, determining the efficiency of UV stray light rejection, and the potential thermal drifts in the HV modulators, will be completed in flight and with reference laboratory tests performed on the flight spare.

EAS in-flight calibration. The evolution of MCP sensitivity (or "gain") as a function of applied HV can be monitored using periodic tests in which one of the two SWA-EAS sensors is operated normally while the MCP voltage on the other is slowly raised from a low level. The use of two SWA-EAS identical sensors allows a normalisation that isolates count rate changes due to MCP voltage changes from those due to changing solar wind conditions. This technique has been developed at UCL MSSL and used successfully on the Cluster PEACE instruments. The relative calibration of different parts of the MCP is very important, especially for deriving moments of the measured electron VDFs, and it will be monitored using well-established technique based on long-term symmetries in the distributions. Inter-experiment cross-calibration between the SWA experiments and between SWA and the plasma wave instrument RPW (Maksimovic et al. 2020) are envisaged in order to refine the geometric factor and directional response knowledge on all sensors, verifying and improving ground calibration knowledge.

Table 1. Summary of SWA-EAS design and build and ground calibration results for FM SWA-EAS heads.

Parameter	Range and resolution	EAS design goal	EAS build and calibration
Sensors		2 × EA	2 × EA
Mass	Species	Electrons	Electrons
Energy	Range	1 eV–5 keV	1 eV–5 keV
	Energy scan	64 steps	64 steps
	Resolution ($\Delta E/E$)	12%	13%
	Analyser constant (eV/V)	6	~6.65 (SWA-EAS1) ~6.30 (SWA-EAS2)
Angle	Range (AZ)	360°	360°
	Range (EL)	±45°	±45°
	Range scan (EL)	16 steps	16 steps
	Resolution (AZ × EL)	11.25° × 3°–8°	11.25° × 6°–12°
	Pixel FoV	11.25° × 3°–8°	11.25° × 6°–12°
Temporal	Basic accumulation period	0.96 ms	0.96 ms
	Normal mode	4 s moments	1 s moments every 4 s or 4 s moments
		100 s full 3D VDFs	1 s full 3D VDFs every 100 s (or every 400 s or every 10 s)
	Burst mode	0.125 s p.a.d.	0.125 s p.a.d.
	Triggered mode	1 s full VDF every 1 s for 5 min	1 s full VDF every 1 s for 5 min
Sensitivity	Per pixel (cm^2 sr eV/eV)	Variable, ≥8.0×10^{-5}	Variable, 8.0×10^{-5} for pixels with clear FoV

3.1.6. Summary of SWA-EAS specifications at delivery

A summary of the design goals versus the achieved characteristics of the two SWA-EAS sensor heads is given in Table 1. Overall, the performance is close to that expected on the basis of the design and simulations. The energy resolution is ~13% and the two heads show only a small difference in their analyser constant, k.

The performance in elevation angle resolution has an unusual energy dependent variation. Figure 9 illustrates the elevation angle performance of the two FM sensor heads (SWA-EAS1 in left column, SWA-EAS2 in right). The top row shows the bandwidth of each of the 16 elevation settings for the sensor head (coloured traces) and the overall passband (black line). The second row then shows the response for the peak of the transmitted elevation angle distribution as a function of the voltage applied to the aperture deflection system (ratio as a function of inner hemisphere voltage). An asymmetry in the positive-negative deflection angles is observed, consistent with the charged particle optics simulations of the sensor design. The plots in the lower row show the width of the transmitted elevation angle distribution for each elevation setting (FWHM of the passbands in the upper plots). There is a variation in the acceptance angle ranging from ~6° to ~13°. This is higher than the ~2° to ~9° observed in calibrations at higher energies, typically above 1500 eV, and predicted by the simulations. Below 1500 V, the width increases from ~2° up to ~6° as the calibration energy is lowered to below 30 eV. This energy dependent behaviour is under investigation at the time of writing this paper. The most likely explanation is a broadening of the incident beam itself at lower energies. However, if the energy dependence is found to be intrinsic to the sensor response, for example, due to stray electrostatic fields not accounted for in the simulations or increased elastic scattering within the sensor apertures at low energies, this will have to be accounted for in on-board and ground calibration parameters.

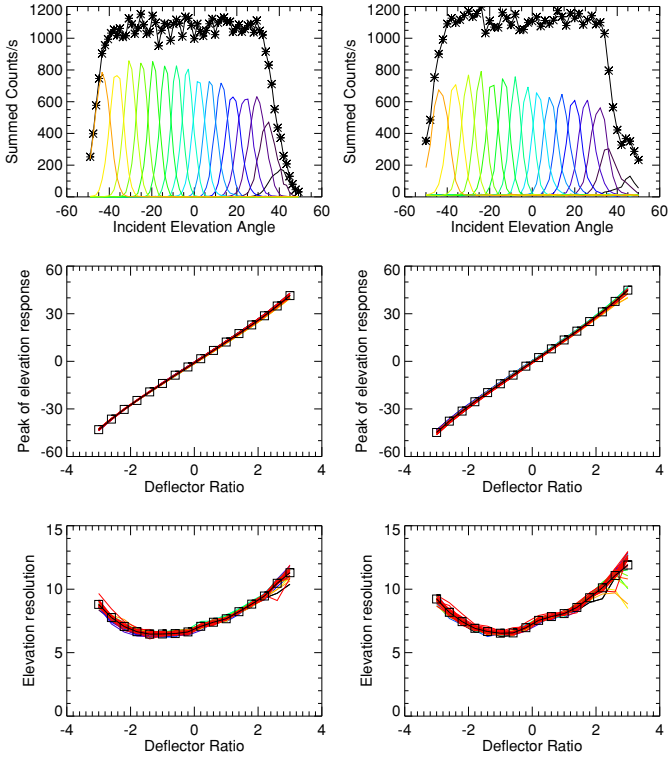

Fig. 9. Elevation response of FM SWA-EAS sensors heads (SWA-EAS1 in *left column*, SWA-EAS2 in *right column*). *Top row*: counts received in each sensor elevation bin as a function of the elevation angle of the incident electron beam. *Second row*: elevation angle showing peak response as a function of the voltage ratio applied to the deflectors, showing good linearity. *Bottom row*: FWHM of the response angle as a function of the voltage ratio, indicating that there is an asymmetry in the response for "upward" and "downward" sweeps and that the acceptance angle is larger at larger deflections.

Overall, the SWA-EAS sensor will be capable of measuring the full 3D VDF of electrons in the energy range 1 eV–5 keV with a cadence of 1 s, with measurements of a 2D pitch angle sample at 0.125 s cadence. This covers the core, halo, and strahl components of the overall solar wind electron population with high resolutions in time, energy, and angular acceptance. Due to telemetry restrictions, these data must be processed on board to form moments of the electron distribution which will be added to the telemetry stream every 4 s, or returned in their raw form only sporadically. Full 3D VDFs will be routinely returned at a nominal cadence of 100 s, but can also be returned at faster or slower rates depending on the telemetry constraints. Full-time resolution 3D VDFs will also be returned in short (~5 min) periods following occasional response to a triggered event (Walsh et al. 2020). The 2D pitch angle data will also be returned from short (5–10 min) periods of burst mode activation.

3.2. The SWA Heavy Ion Sensor (SWA-HIS)

3.2.1. SWA-HIS introduction

In support of the Solar Orbiter mission science goals, SWA-HIS will measure heavy ion composition and kinetic properties from solar wind up through suprathermal energies. To achieve these science goals, SWA-HIS must address two fundamentally different sets of measurement objectives. First, it must measure the ion and elemental composition and 3D VDFs of heavy ions (He–Fe) in the bulk solar wind between 0.5 and 18 keV/e.

Second, it must measure the ion and elemental composition and 3D VDFs of the major constituents: He, C, O, and Fe in the suprathermal energy range up to 60 keV/e. To achieve the characterisation of 3D VDFs for these populations, SWA-HIS is mounted within a cut-out in the corner of the spacecraft heat shield, with its FoV facing the solar direction. It has a FoV that spans a native 96° in the ecliptic from −30° off the Sun-Spacecraft line to +66° off the Sun-spacecraft line to account for the aberration of the solar wind due to motion of the spacecraft, and to allow for improved sampling of suprathermal and pickup ions. SWA-HIS scans through ±17° above and below the ecliptic. SWA-HIS will measure alpha particle and heavy ion 3D VDFs in solar wind, pickup ion, and suprathermal energy ranges, with native time resolution as high as 4 s in Burst Mode, 30 s in Normal Mode, and 300 s for Normal Mode (Low Cadence). This time resolution corresponds to the time it takes to scan the entire energy range from 0.5−80 keV/e in 64 steps, and sample all elevation angles in 16 steps. SWA-HIS will return a number of heavy ion rates, onboard calculated VDFs, and a statistically representative sampling of Pulse Height Analysis (PHA) event words to reconstruct high fidelity 3D VDFs of all heavy ions. From these 3D VDFs, SWA-HIS will provide measurements of elemental abundances and charge state distributions of He, C, O, Mg, Si, and Fe. SWA-HIS will provide the first-ever solar wind and suprathermal heavy ion composition measurements in the inner heliosphere.

3.2.2. SWA-HIS design overview

Figure 10 shows a photograph (left) and computer-aided design (CAD) model (right) showing a complete overview of the mechanical sections of SWA-HIS. Due to its exposure to the Sun, SWA-HIS includes its own heat shield, which wraps around the entrance system, as seen in the photograph. The aperture of the instrument is a narrow slit in the instrument heat shield, behind which the SWA-HIS pairs an electrostatic analyser (EA) with entry ion steering (IS) to form (right-upper) the upper EA-IS subsystem, which will optimise the out-of- ecliptic particle sampling. The bottom of the EA-IS is mated to a grounded housing (right middle) containing an isolated time of flight (TOF) telescope and associated electronics. The heat shield, EA-IS, and grounded housing containing the TOF telescope are mounted on top of the main electronics (ME) box (right-lower), which contains the low-voltage power supply (LVPS), post-acceleration (PA) high-voltage power supply (HVPS), and associated boards.

SWA-HIS EA-IS system. The SWA-HIS entrance system is comprised of a top-hat hemispherical EA paired with IS plates behind the entrance aperture in the instrument heat shield. The ion steering plates include top and bottom deflectors as well as a "top-cap" deflector; these deflectors steer ions in through the entrance aperture from above and below the ecliptic. Ions can be steered ±17° in the polar direction, above and below the aperture.

HIS TOF telescope. The TOF telescope measures time-of-flight and total kinetic energy of incoming ions. When paired with the EA-IS, this provides optimum separation of incoming ions by energy, mass, and charge. The TOF telescope is floated at −25 keV, supplied by the PA HVPS, which is housed in the ME box. The TOF telescope is isolated from the grounded housing by the PA vacuum gap shown in Fig. 10 (right). The TOF telescope also includes a carbon foil (CF) entrance window, MCPs paired with position sensing readout anodes, and an array of solid state detectors (SSDs), and all of the associated electronics.

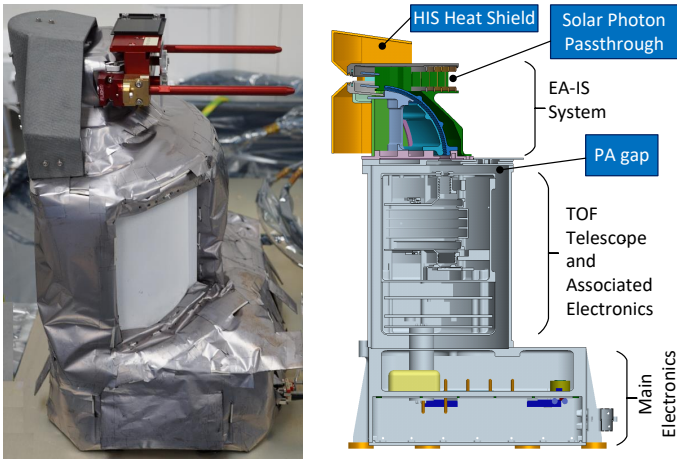

Fig. 10. *Left*: photograph of SWA-HIS in "as delivered" configuration. *Right*: schematic showing the different SWA-HIS building blocks.

The isolated detector section (DS) data interface is located in the TOF telescope.

HIS ME box. The ME box includes the PA-HVPS, the detector section LVPS, the ground side of the data interface with the TOF telescope, the EA-IS HVPS, the C&DH board, and the instrument LVPS. The C&DH board runs the flight software, which controls most aspects of the sensor.

3.2.3. SWA-HIS measurement principle

SWA-HIS requirements demand the derivation of five key properties from the measurements of all ions: mass (m), charge (q), speed (v), and direction of incidence, elevation (θ) (above and below aperture, in the polar direction), and azimuth (ϕ) (along the entrance aperture, nominally in the ecliptic). SWA-HIS provides these properties as follows: SWA-HIS EA-IS provides E/q and θ information. SWA-HIS TOF provides the ϕ information through both the SSD ID, and through the imaging of secondary electrons on the Start MCP anode, generated as the ion passes through a thin carbon foil at the entrance of the TOF telescope. These secondary electrons also serve to start the timing window for TOF (τ) measurement when they impact the Start MCP. To push solar wind ions above the SSD energy threshold, the TOF telescope floats at a potential of −25 keV. This potential accelerates the incoming solar wind ions so that their detection efficiencies are almost independent of their initial speed. Once the ion impacts the SSD, secondary electrons are emitted and steered to the Stop MCP for closure of the timing window, from which the speed of the ion within the TOF chamber can be determined. The SSD measures the total energy of the accelerated ion ($E_{\rm Tot}$). Combining E/q, τ, and $E_{\rm Tot}$ enable the calculation of ion's mass, charge, and velocity (e.g. Shearer et al. 2014). Angles of incidence are obtained as described above. This completes the five independent measurements required for unique ion identification and characterisation.

The conceptual design of the SWA-HIS EA-IS is driven by requirements that major heavy ion species should be measured up to energies of 60 keV/e ($\Delta E/E \leq 10\%$), and a maximum time resolution of 4 s for alpha particles and 30 s for heavy ions. The FoV of the instrument ranges from −33° to +66° in the azimuthal (ecliptic plane), and ±17° in the polar directions for optimum sampling of the solar wind ions, pickup ions, and suprathermal

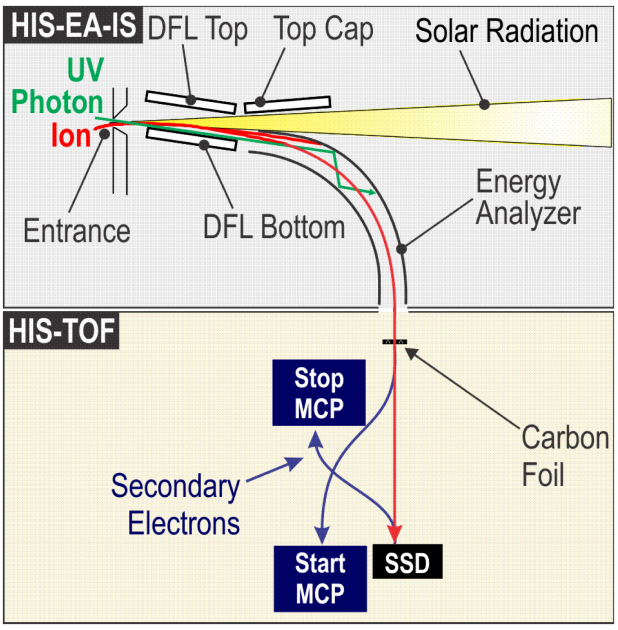

Fig. 11. Schematic of SWA-HIS with example particle trajectory. The cut-plane for the top part of the figure is that containing the Sun-spacecraft line and the direction of elevation deflection. The yellow shading represents the passage of direct solar light through the sensor and the red curve indicates a representative ion trajectory in this plane. The instrument has partial cylindrical symmetry extending from −33° to +66° out of the plane of the figure.

ions. The pixel resolution is ~6° × 6°, which corresponds to a FoV comprising 16 azimuth and six polar sectors.

Figure 11 shows the two SWA-HIS ion optics subsystems: (1) The EA-IS is designed to achieve the required FoV and energy per charge (E/q) selection. An opening in the rear side of the EA-IS allows solar radiation to pass through unhindered. (2) The TOF telescope contains start and stop MCPs for time of flight measurement (τ) and SSDs for total ion energy ($E_{\rm Tot}$) measurements. A carbon foil covers the optical path entrance to the TOF telescope as serves as a source of secondary electron to start the timing window.

Solar wind ions that enter the small aperture are steered by the IS into the EA. The EA voltage settings allow selection of ions within the appropriate E/q range to be transmitted into the TOF telescope. The IS plates, comprised of a deflector top plate (DFL Top), deflector bottom plate (DFL Bottom), and a "top-cap" serve plate to steer in ions over the range of ±17° in the polar direction. The EA-IS system is swept through voltages to scan the full elevation angle range and the full E/q range once per scan. Stray light and any ions outside this E/q range are suppressed by surface coatings and scalloping of the EA. The energy resolution of the EA is 6−10% and the elevation angle resolution is <3.5° and have been verified by both ion optics simulations and laboratory calibration. The EA subsystem has a sufficiently large geometric factor (~2×10^{-5} cm^2 sr eV eV^{-1} per 6° pixel) to to measure 3D VDFs of Fe ions at 30 s time interval even during the lower flux and density slow solar wind conditions expected outside of 0.7 AU.

After passage through the SWA-HIS-EA and -IS subsystem, the ions converge at a focal plane that is co-aligned with the carbon foil. The entire TOF telescope, including the PA voltage gap, is designed to provide measurements ϕ, τ, $E_{\rm Tot}$. The telescope has a simple interface to the SWA-HIS-EA subsystem via an aperture at ground potential. After passing through the vacuum gap, which provides a stand-off distance sufficient for safe operation at the highest voltages, an accelerated ion penetrates a segmented ultra-thin (~0.9−1.1 μg cm^{-2}) carbon foil and emits secondary electrons. These secondary electrons are deflected onto a Start MCP while maintaining their azimuthal location. The impact of secondary electrons on the Start MCP generates a start signal for TOF analysis. The ion continues through a nearly field-free volume before hitting the SSD array and emitting another set of secondary electrons that are deflected onto a Stop MCP. The electron impact generates a stop signal to complete the TOF (τ) measurement. A specially tailored electrode is situated between the start and stop MCPs to eliminate ion feedback between the two. The SSD array is comprised of 30 pixels spanning 96° in azimuth. Each pixel is comprised of a fully-depleted thin-window silicon detector with 500 μm depletion depth and <50 nm dead-layer thickness. The pixel shape is a trapezoidal approximation to an arc segment, with an average width of 4.8 mm, a radial length of 3.7 mm, and an azimuthal width of 3°. The 96° azimuthal span will cover the required FoV and also accommodate azimuthal scattering from heavy ions as they pass through the carbon foil. The angle, TOF, and energy resolutions of the TOF-SSD subsystem are sufficient to meet all of the Solar Orbiter science objectives for SWA-HIS.

3.2.4. SWA-HIS design details

Figure 12 shows the SWA-HIS block diagram, indicating the functional grouping of the subsystems shown in Fig. 10. The figure includes all the PCBs contained in each subsystem, as described below.

HIS EA-IS subsystem. The EA-IS subsystem and supporting electronics were built by Institut de Recherche en Astrophysique et Planétologie (IRAP), in Toulouse, France. With the exception of the geometric factor, it is nearly the same design as the SWA-PAS electrostatic analyser. As SWA-PAS uses channeltron detectors, the SWA-HIS EA-IS geometric factor is ~1/3 smaller to accommodate the required MCP lifetime. The EA-IS system sits behind the carbon-carbon instrument heat shield and includes a rear exit for solar photon pass-through. The EA-IS is physically mounted to the outer housing of the SWA-HIS DS. The EA-IS body is grounded with a grounding strap to this same outer housing. Ions enter the instrument through a 3.5 mm slit in the SWA-HIS EA-IS; their elevation angle is controlled by top and bottom IS plates, with maximum voltages of ±5.6 keV. The EA has a central radius of 70 mm with 2.3 mm hemisphere spacing and maximum voltage of ±5.5 keV. The EA-IS entrance has knife edges to define the opening. The curved EA plates are scalloped and surface coated for light baffling. Electrical connections from the EA-IS run via cables down the outside of the TOF telescope and around the top of the ME box before mating up to the EA-IS HVPS inside the ME box. The EA-IS HVPS can be commanded into a sweeping mode where the voltages stored in the EA-IS table are stepped through with the timing specified in the table; static voltages were used during ground testing. Commanded parameters are monitored via flight software and the analogue readback of the direct voltage when sampled. The EA-IS stepping is fully synchronised with the TOF and energy data taken by the sensor via hardware handshakes across the optical link.

HIS detector section and readout electronics subsystem. The TOF telescope and associated electronics are isolated from the grounded housing that encloses them and separated from the housing by the PA gap. This gap is sized to keep electric

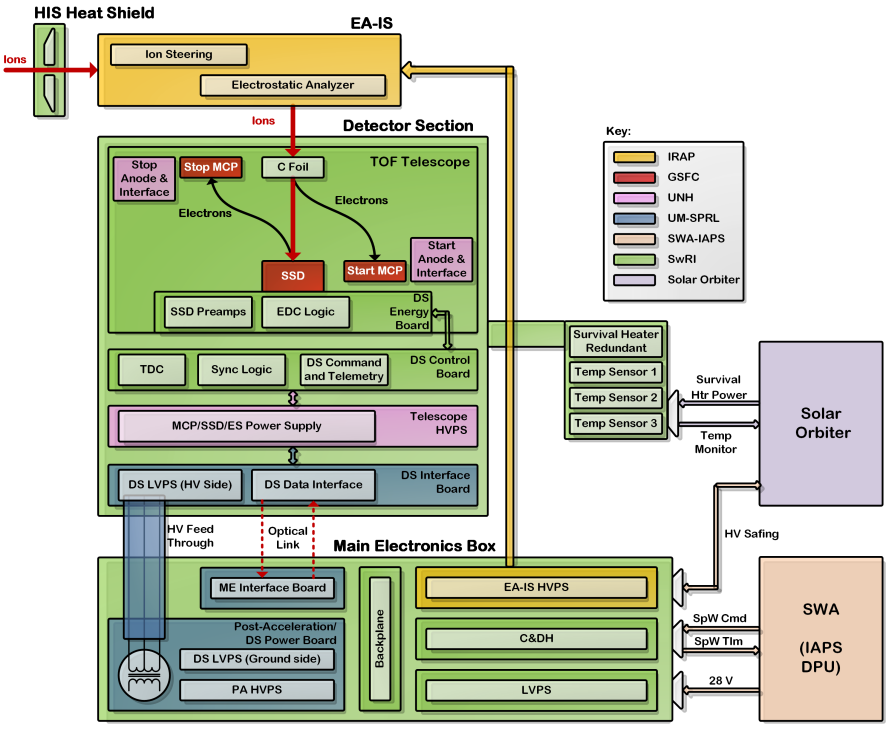

Fig. 12. HIS block diagram.

fields low according to Pachen's law in order to prevent voltage breakdown. The nominal −25 keV potential, supplied by the PA HVPS, is applied to the entire TOF telescope, accelerating ions entering from the EA-IS by 25 keV/e. The SWA-HIS TOF telescope and supporting electronics were built in the USA by a consortium comprising Southwest Research Institute (SwRI), University of Michigan (UMich), University of New Hampshire (UNH), and NASA GSFC. The interface between the EA-IS and DS subsystems is straightforward and controlled by an interface control document (ICD). This interface is an aperture at ground potential. The TOF telescope includes SSDs, MCPs, and associated electronics, control boards, and power supplies.

The ion entrance into the TOF telescope is fitted with a carbon foil and support grid. The ion path-length from the carbon foil to the SSD surface is 9 cm. The MCP Start and Stop stacks are made of two plates each in a classic chevron configuration with the front-side biased and the back side near-ground. The MCPs are mechanically clamped with tension springs and electrode contacts within the stack. Voltages are optimised for MCP throughput and vary with age, but are nominally set to 2.1 keV across the plate stacks. MCP gain is adjustable by increasing or decreasing the MCP bias voltage as needed and is anticipated to change over the mission lifetime. Azimuthal position can be obtained from the start position anode. The angular resolution is determined by the delay line with 2° strips. The TOF resolution, derived from the MCP signals, is <1.7 ns, with a TOF bin size of 0.64 ns. The TOF resolution is species and energy dependent and has been calibrated in the laboratory. Cross talk between Start and Stop MCP is virtually eliminated by a set of dedicated electrodes. The detector section's TOF and position measurements design was optimised with 3-dimensional electrostatic simulations (using SIMION[1]) and hundreds of hours of ion testing on the detector section prototype. Additionally, ion feedback at both the Start and Stop MCPs is minimised by ensuring the bias angle on the exit plate is at least 15° to the normal of the anode and applying only 50 V between the exit of the plate and the anode itself. Each SSD comprises one pixel, with 30 pixels mounted on ceramic carries spanning the azimuthal FoV. Angular resolution of 5° is limited by the size of the pixels and the required electronics for each pixel.

The isolated TOF electronics are floated at the same potential as the TOF telescope. These DS electronics include the detector section interface board (DSIB), the MCP HVPS, the DS control board (DSCB), and the DS energy board (DSEB). The DSIB supplies the low voltages for the DS (derived from the AC voltage riding on the PA-HVPS signal) and the DS side of the optical data communications link to the ME box. The MCP HVPS provides float and bias voltages for both the start and stop MCPs as well as the SSD bias voltage. All outputs are programmable. The DSCB uses an FPGA to perform the TOF measurement, time-to-digital conversion (TDC), application of commandable event logic, and combination of these signals with the energy measurement to form a partial PHA event word. DSCB event logic can be configured to trigger on events that have measurements of SSD energy only, TOF only, or both. The DSCB then sends events to the DSIB for transmission to the ME through the optical data communications link and provides fault detection, isolation and recovery (FDIR) capabilities. The DSEB houses the SSDs and collects and processes signals from the SSDs, using a specially designed, 32 channel ASIC. The DS also holds the HV side of an LVPS for powering these DS electronics. Measurement data are transmitted to the ME at ground potential via an optical link on the DSIB. The bulk of this data are PHA event words, containing the measurements of TOF (9 bits), total energy (9 bits), azimuthal angle (6 bits), SSD ID (5 bits), decimation class (3 bits) and multi-SSD flag (1 bit). These bits are streamed across the optical link and paired with the rest of their measurement information (e.g. E/q step, elevation angle) in the ME.

HIS main electronics. The ME sit below the TOF system at spacecraft potential. The ME includes: the LVPS, the Command and Data Handling Board (C&DH), the EA-IS HVPS, the optical link, and the PA-HVPS. The LVPS supplies all of the low

[1] https://simion.com/docs/simion8brochure.pdf

voltages to the other ME boards, as well as a 20 Vpp (peak-to-peak) square wave AC supply to link low voltages to the detector section. The C&DH board controls the balance of the instrument and houses the memory, processor and flight software, as well as FDIR functions. The EA-IS HVPS, built by IRAP, drives the EA-IS voltages. This HVPS consists of a pair of commandable bulk-supplies and commandable outputs for each of the electrodes in the EA-IS system. The optical link provides the ME side of the system for digital communication to the DS. The PA-HVPS provides the floating voltage to the detector section as well as a pathway for low voltages to cross the post-acceleration gap. The PA-HVPS provides DC-to-DC power conversion to lift the DS to −25 keV referenced to the ME ground potential. It also provides AC-to-DC conversion between the LVPS and the DS electronics. DC power is passed from the PA-HVPS across the PA gap into the detector section through a high voltage feed-through that provides both electrical isolation from ground potential and thermal isolation from the detector section. Heat generated by the AC-to-DC converter is coupled to the ME box chassis ground through a thermally conductive HV insulator.

The LVPS is free-running upon application of power with AC-link voltage commandable to on or off. Both HVPS supplies have enables and commanded output voltages. Electrical interface to the spacecraft is via a 28 V regulated, switched power line as well as a SpW data interface through the DPU. The DPU interface is limited to a SpW data link and the digital data that cross that link (i.e. heartbeats and FDIR information in addition to the normal HK and science data). The ME passes the event word to the C&DH, where the SWA-HIS flight software (FSW) completes it with the addition of the E/q (7 bits) and elevation step (4 bits) information. Each PHA word is a total of 46 bits. The C&DH board includes a SPARC-8 micro-controller (32-bit data bus) with 128 KB of external programmable read only memory (PROM), 2 MB of magnetic random access memory (MRAM) and 16 MB of static random access memory (SRAM). The ME also include temperature sensors and survival heaters. Radiation shielding in the ME is provided by the aluminium enclosure.

The SWA-HIS FSW controls the instrument primarily through the science programme, which is separated into several tasks. The "main" task runs at 10 Hz and performs processes such as receiving and validating commands, building and sending HK-related telemetry packets, running macros, sweeping EA-IS HV, and monitoring safety limits. The "science" task handles the fairly complex processing required to meet SWA-HIS science requirements, such as collecting PHA words and sorting them into bins subdivided by priority, counting them into priority rate and on-board VDF histograms, and randomly selecting them for inclusion in telemetry. SWA-HIS was designed to handle events at rates of up to 100 kHz, including both the hardware and software aspects of the PHA processing pipeline. Many features are table-based to allow for easier reconfiguration, including many EA-IS parameters (e.g. voltage steps, dwell & settling times), PHA handling parameters (e.g. E-TOF boxes for each priority range and E/q, sizes of buffers and number of PHA words per energy scan), and data product specifics (e.g. sizes and ions chosen for on-board VDFs). It also handles data compression, memory operations and scrubbing.

3.2.5. SWA-HIS testing, characterisation and calibration

SWA-HIS has been characterised at both subsystem and instrument levels, with subsystem testing taking place at UMich, SwRI, UNH, GFSC, and IRAP. SWA-HIS has been calibrated at the instrument level at three different facilities, during four test sessions, as summarised in Table 2.

Table 2. SWA-HIS ground calibration programme.

	Location	Dates	Configuration	Scope of calibration
1	H30 at SwRI	Sep–Oct 2015 and Jan–Mar 2016	EA-IS	Optimisation of the EA-IS voltages
2	H19 at SwRI	Sep–Nov 2016	Complete sensor minus EA-IS	Mass (1−56) and energy (0.1−450 keV) response
3	Mefisto at Bern	Jan–Feb 2017	Complete sensor	Charge (1−4), mass (1−84) and energy/charge (3−60 keV/e) response
4	H19 at SwRI	Mar–Apr 2017	Complete sensor	Geometric factor

Test session 1 involved testing the EA-IS subsystem at SwRI. Testing lasted 36 days where the EA-IS was combined with a mock-up TOF section with a phosphorus screen in the SSD plane. Particle interactions with the phosphorus screen were imaged with a camera. This setup did not allow for TOF measurement, but was dedicated to evaluating the electro-optics and ion trajectories, with full post-acceleration. The ion beam consisted of Ar^+ with energies ranging from 1 keV to 40 keV. Illumination of the EA-IS aperture was completed with a broad, uniform, parallel beam larger than EA-IS aperture. During this test, the EA-IS and mock-up TOF were powered by laboratory equipment.

Calibration of the EA-IS addressed a number of aspects of performance. These included determination of: Energy-angle response of EAIS; optimal tuning of the EAIS voltages; elevation and azimuth response; energy-per-charge resolution; elevation angle resolution; ion optics and ion focus onto SSD; and relative efficiency.

Test session 2 was completed at SwRI with only the TOF telescope and associated electronics. It consisted of 5 days of beam testing without post-acceleration and 4 days of testing with full post-acceleration of the ion beam. The TOF telescope was subjected to a beam of H^+, H_2^+, He^+, N^+, H_2O^+, Ne^+, Mg^+, N_2^+, Ar^+, Ar^{2+}, Ar^{3+}, and Fe^+. Beam energies ranged from 0.3 keV to 450 keV (1.35 MeV for Ar^{3+}), with beam intensities in the kHz range. The ion beam was vignetted by a 3 mm dia hole (7 mm^2) to simulated a pencil beam incident on the TOF aperture. Flat ion beam illumination of the TOF aperture was also conducted. During 80 h of operations there were no spurious events detected.

Test session 3 was completed in the Mefisto vacuum chamber at the University of Bern with the full integrated sensor. Testing lasted 21 days and was conducted with all voltages operating at nominal flight-like settings. The instrument was subjected to a beam of H, H_2, He, C, N, O, F, S, Ar, Ca. Beam energies ranged from 3 keV to 60 keV, with beam intensities in the kHz range. A vignetted beam through a 2 mm diameter hole illuminated the instrument aperture. The testing included over 200 h of operations with no spurious events record.

Test session 4 was conducted at SwRI and included 5 days of testing of the integrated instrument with full PA voltages applied. The instrument was subjected to a beam of H, He, and N. Beam energies ranged from 0.3 keV to 60 keV, with beam intensities in the kHz range. The instrument aperture was illuminated with a flat beam. In over 80 h of operations no spurious events were recorded.

Overall, during test sessions 2−4, a number of aspects of sensor performance were assessed. These included the following: aliveness of the sensor; communication at various speeds;

Table 3. Species and charge states used during calibration.

HIS elements and charge states						
	1	2	3	4	5	6
H	Yes					
He	Yes					
C	Yes	Yes	Yes	Yes		
N	Yes	Yes	Yes			
O	Yes	Yes	Yes			
F	Yes	Yes				
Ne	Yes	Yes	Yes	Yes		
S	Yes	Yes	Yes	Yes		
Ar	Yes	Yes	Yes	Yes	Yes	Yes
Fe	Yes	Yes				
Kr	Yes	Yes	Yes	Yes		

Notes. "Yes" indicates the ion species was generated and measured, blank cells indicate the ion species was not able to be generated in the lab, and greyed out cells indicate the ion does not exist in nature.

coincidence logic; energy, elevation, and azimuth acceptance and resolution; TOF and energy resolution for various species; TOF and energy range; constant fraction discrimination thresholds on detectors; operation at high fluxes; and proton and alpha rejection capability. Table 3 shows the elements and the charge states collected during ground calibration.

Figure 13 shows the dependency of collected TOF bin and collected energy bin as functions of beam energy. Data collected using the Bern facility and the SwRI accelerator agree very well to each other and can be well approximated by a forward model that takes into account losses through the foil, and the dependency of detected energy to particle mass and energy.

HIS in-flight calibration. HIS will be calibrated in-flight to check the instrument performance parameters established during ground calibrations. Internal calibration of the SWA-HIS sensor will include validating instrument efficiencies and comparing the instrument response to various ions. Start, Stop, and SSD rates will independently measure instrument efficiencies, which will be monitored as a function of time, as detector responses may decline with age. In particular, the SSD may experience an increase in dead layer or reduced signal amplification over time, and MCP performance may degrade due to large cumulative radiation events. The MCP gain will be monitored and bias voltages increased to compensate for losses in gain. The measurements will be compared with our forward model for ion identification and adjustments made as necessary. Internal calibration capabilities include time and energy test pulse generators. Further calibration includes a test of the cross suite data link as well as cross-calibrations with SWA-PAS. Such internal test and suite-level cross calibrations will be performed routinely at UMich. Gain measurements for SSD and MCPs will be made every six months and after major SEP events, potential temperature increases near perihelion, or other spacecraft occurrences that could affect efficiencies. MCP and SSD voltage adjustments will be made as appropriate.

3.2.6. Summary of SWA-HIS specifications at delivery

The SWA-HIS calibration campaign had two major goals. Firstly, to establish all needed parameters to be able to invert the measurements to be collected in flight into physical units.

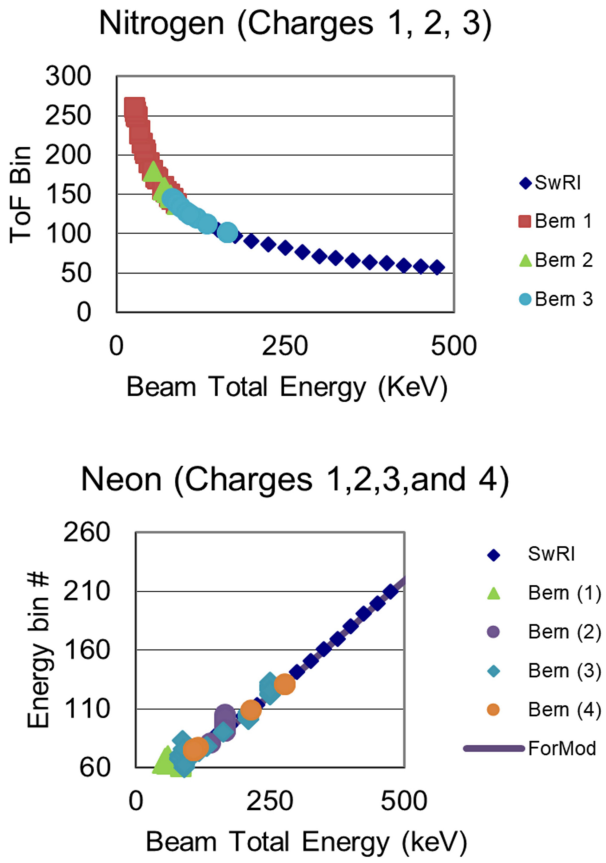

Fig. 13. Time-of-flight (*top*) and energy (*bottom*) response to beams of N and Ne as function of beam energy.

Secondly, to prove that the instrument has performance that will fulfil all Level-1 requirements.

Table 4 summarises the most important characteristics of the SWA-HIS sensor; rows colour-coded in blue show the project-defined Level-1 requirements. All properties of the SWA-HIS sensor are as expected from the design, and are compatible (and indeed most of the time better) with those needed to fulfil the Level-1 requirements. Some of the parameters reported in Table 4 are for an average configuration of the sensor: specifically, while the normal E/q resolution is ~8% and the geometric factor per pixel is $\sim 1 \times 10^{-5}$ ($\mathrm{cm^2\,sr\,eV\,eV^{-1}}$), by tuning the EA and IS voltages it is possible to increase the E/q resolution while lowering the GF, and vice versa. In-flight performance will be used to establish the most appropriate compromise between these two values.

It must be noted that for large azimuthal angles (ϕ) and for elevation angles (θ) out of the nominal orbit plane of the spacecraft ($\theta > 7°$, $\theta < -7°$), the centres of the elevation look-directions change slightly from the nominal. This property was expected for both SWA-HIS and SWA-PAS, and has been factored into the calibration files, such as to enable proper reconstruction of the VDFs.

The mass separation capabilities of SWA-HIS are illustrated in Fig. 14, which shows an energy versus TOF spectrogram obtained during laboratory testing. The track of Ar (doubly ionised in this series) is well separated from the track of Ne for all energies down to 100 keV. This energy corresponds to a charge state of 4, smaller than that expected for Ne in the solar wind. For higher charge state, the energy after PA will be larger (TOF smaller), and the mass resolution better.

Table 4. Summary of SWA-HIS performances at delivery.

	SWA-HIS L1 requirement or needed inversion parameter	SWA-HIS measured capability
Particle species	He^{2+}, C^{+4} to C^{+6}; O^{+5} to O^{+8}, Fe^{+6} to Fe^{+20}, Mg^{+6} to Mg^{+12}, Ne^{+6} to Ne^{+9}, Si^{+6} to Si^{+12}, He^{+}, C^{+}, and O^{+}	H, ^{4}He, ^{3}He, C, N, O, Mg, Ne, Si, Fe (see Table 3 for details on masses and charges measured)
Energy per charge range	0.5–60 keV/e	0.5–~78 keV/e
Energy per charge resolution ΔE/E at FWHM	Between 6 and 10%	~8–9%
Mass resolution M/ΔM at FWHM	4	>5
Mass/charge resolution (m/q)/Δ(m/q)	N/A	> 30
FoV		
In ecliptic	–33° to +66°	–33° to +66°
Out of ecliptic	±17°	±20°
Pixel resolution (Az × El)	6° × ~6° pixels	6° × ~4° pixels
G-factor/pixel (cm^2 sr eV/eV)	N/A	$\sim 1 \times 10^{-5}$
Time resolution	≤30 s	4 s (Burst mode); 30 s (Normal mode); 300 s (Normal Low Cadence mode)

Notes. Rows colour-coded in blue show the Project-defined Level-1 requirements.

One of the science goals of SWA-HIS is the characterisation of the full VDF for pickup ions. As their typical charge state is +1, they gain only a single 25 keV step from the post-acceleration, as opposed to multiples of this value for higher charge states. For energies <10 keV, they do not produce a detectable energy signal in the solid state detector and therefore must be identified by their TOF only. Figure 15 shows a histogram of counts collected for a beam energy of 0.3 keV (25.3 keV after post-acceleration) representative of the characteristics of pick-up ions in the inner heliosphere; the beam was composed of 20% each of H_2, He, N_2, Ne, and Ar, with H_2O and CO_2 as contaminants in the chamber. Even at this very low energy, TOF measurement enables clear identification of the single-charge species.

3.3. The SWA Proton-Alpha System (SWA-PAS)

3.3.1. SWA-PAS introduction

SWA-PAS is designed to measure the 3D VDFs of solar wind protons and alpha particles with high time cadence, energy and angular resolution. In the solar wind, the proton and alpha-particle thermal velocity is generally much smaller than the bulk velocity, which itself is usually strongly radially directed. Thus most of the individual ions within the distribution arrive at the spacecraft with at most a few 10's of degrees deviation from the radial direction. Thus SWA-PAS is mounted behind the spacecraft heat shield which has a dedicated cut-out in one corner. This cut-out allows a SWA-PAS FoV that covers the angular range of −22.5° to 22.5° in nine elevation (or polar) angle bins and has 11 azimuth angle bins covering a total width in this direction of 66°. In order to account for the expected aberration of the solar wind arrival direction due to the motion of the spacecraft, the FoV is offset from the solar direction by 9° such that the angular coverage is from −24° to +42°. In addition, the SWA-PAS sensor operates with a maximum resolution of 96 energy steps, from 200 eV/e to 20 keV/e.

The sensor will measure proton and alpha particle fluxes at a 4 s cadence, which will be returned to ground within the SWA telemetry stream. The SWA-DPU will also calculate moments of the associated distributions, which will be shared onboard with other instruments and returned to ground as a low-latency (<1 day following acquisition) data product for quick-look and mission planning purposes.

A complete 3D measurement of a VDF is a matrix of (96, 9, 11) elements (energy, elevation, azimuth), each element corresponds to the counts measured during a defined elementary time

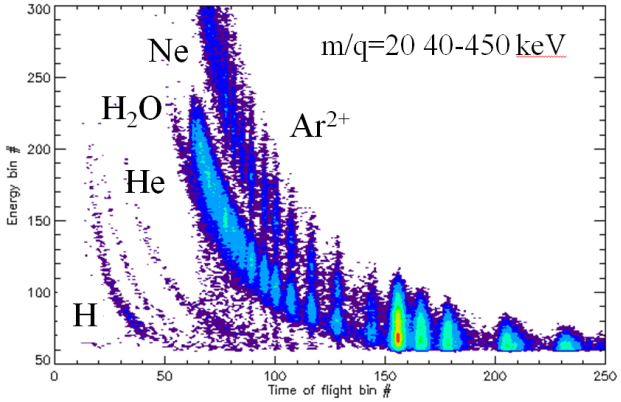

Fig. 14. E vs TOF spectrogram of $m/q = 20$ amu/e for various energy beams.

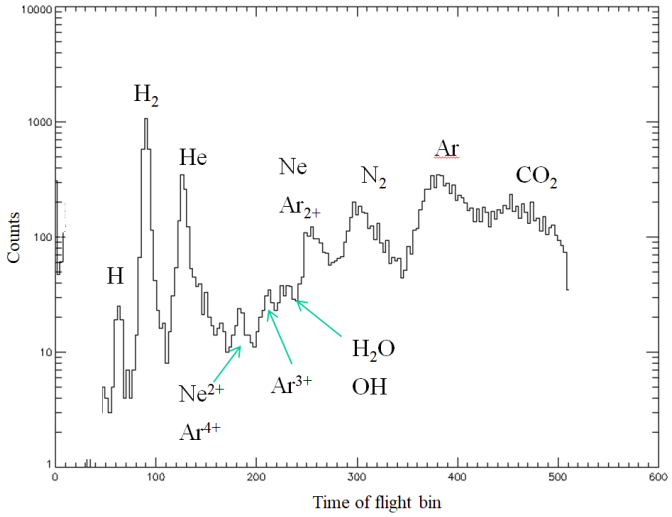

Fig. 15. Time-of-flight spectrum of a mixed beam of pickup ions of 0.3 keV energy.

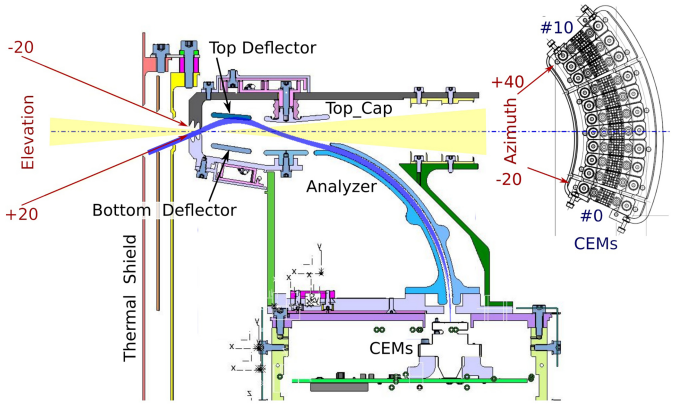

Fig. 16. *Left*: cut-away representation of the SWA-PAS analyser head. The cut-plane is that containing the Sun-spacecraft line and the direction of elevation deflection. The yellow shading represents the direct solar light and the blue curves show the extreme ion trajectories in this plane. The instrument has partial cylindrical symmetry extending from +40° to −20° out of the plane of the figure. *Right*: the insert shows the top view of the CEMs array detector arrangement and its angular range.

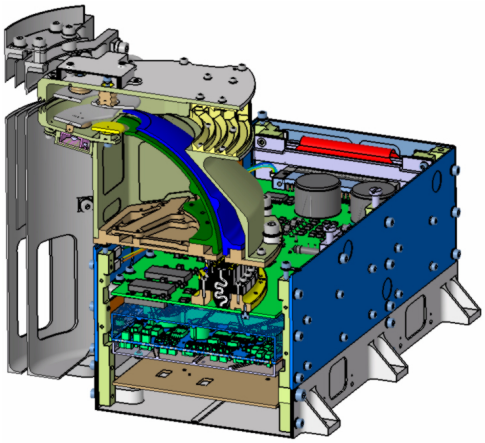

Fig. 17. Three-dimensional cut of the full SWA-PAS instrument illustrating the three main elements of SWA-PAS design: (1) the analyser (sensor head); (2) the electronics box containing the CEM detectors, HV sources, and other electronics boards; (3) the front thermal shield.

period by a specific bin. It is possible to reduce the number of energy and angular bins in one sample in order to significantly increase the sampling rate. SWA-PAS can automatically change the position of the reduced matrix to keep the maximum of the ion velocity distribution at the centre of the sampling window. Thus SWA-PAS is capable of taking a wide variety of "snapshot" and "burst" mode data products in which the time resolution of the sensor is increased. These high frequency modes consist of continuous acquisition of full or reduced VDFs, at second or sub-second cadences. The snapshot data products will be generated over periods of 8 s every 5 min in order to align with the operation of the RPW snapshot facility (Maksimovic et al. 2020; Walsh et al. 2020).

3.3.2. SWA-PAS design overview

Figure 16 shows the SWA-PAS sensor head which is comprised of the electrostatic analyser and an array of conventional channel electron multipliers (CEM) used to detect the solar wind ions. Since the instrument line-of-sight points to the Sun, the main driver of the sensor design was to provide reasonable defence against direct sunlight and heat radiation. In order to protect the sensor, it has a narrow aperture slit in front of the optical surfaces located outside of the solar light path through the sensor (yellow triangle in Fig. 16). This geometry avoids any interaction of the light beam with the internal elements of the sensor. The rear of the SWA-PAS analyser head is open to allow sunlight to pass straight through the head. In addition, the sensor has its own heat-shield system to locally protect the analyser.

The entrance deflection system, comprising two deflector plates and the "top-cap" plate, steers the incident particles towards the entrance of the electrostatic analyser. The deflection of the particles is achieved by applying specific potential on the plates. Figure 16 shows the ion trajectories calculated for the case of the maximum deflector voltages. The spherical shape electrostatic analyser filters out ions with energies outside a narrow energy band and focuses the remaining particles on to the CEM array. The azimuthal position of the focal point corresponds to the azimuthal direction of the incident ions. Thus the instant count rate of each CEM is a function of the solar wind ions flux in the corresponding bin of the SWA-PAS 3D sampling matrix. The azimuth index of this bin is the CEM number, the energy index of the bin is defined by the electrostatic analyser instant voltage and the elevation index of the bin is defined by the deflector voltage to analyser voltage ratio. The averaged geometrical factor of one bin is $5{\times}10^{-6}$ cm^2 sr eV eV^{-1}. This geometrical factor restricts the maximum count rate for an individual CEM to 10^7 s^{-1} when Solar Orbiter is at its closest approach to the Sun. Moreover, SWA-PAS still can produce a statistically valid 3D ion VDF every 4 s when the spacecraft is at 1 AU distance from the Sun. Details of the SWA-PAS measurement scheme are described in Sect. 3.3.3.

Figure 17 shows the three mechanical sections of SWA-PAS: the titanium multi-layer heat shield, the sensor head, and the electronics box. The sensor head is mounted on the top of the electronics box and is insulated from it thermally and electrically. The CEM detectors are located inside the box on the dedicated CEM board. The fast-varying HV voltages for the optical surfaces of the analyser head are generated by the HVPS. Other boards provide the HVPS controls, data acquisition, the SWA-DPU interface and LV power. We provide the details of these in Sect. 3.3.4.

Figure 18 shows the SWA-PAS assembly and its position on Solar Orbiter. The upper right insert shows the SWA-PAS installed on the spacecraft. SWA-PAS looks towards the Sun through a rectangular cut-out in a corner of the spacecraft heat-shield which has a stepped profile which acts to reduce the stray light. The charged particles pass across this cut-out, enter through the slot in the SWA-PAS heat shield, and then enter the sensor aperture. Most of the SWA-PAS external surfaces are protected by a high temperature "black Kapton" MLI. Other surfaces, shadowed against the solar heat flux, as well as against the heat radiation from other Solar Orbiter units, are coated by PCBE white paint and serve as radiators.

3.3.3. SWA-PAS measurement principle

A complete 3D measurement of an ion VDF is a matrix of (96, 9, 11) elements (energy, elevation, azimuth). Each bin of this matrix corresponds to the counts measured during a defined elementary time period of ∼1 ms by a specific channeltron, for a given energy and elevation angle bin. SWA-PAS accumulates counts in all azimuthal bins simultaneously, but to cover all

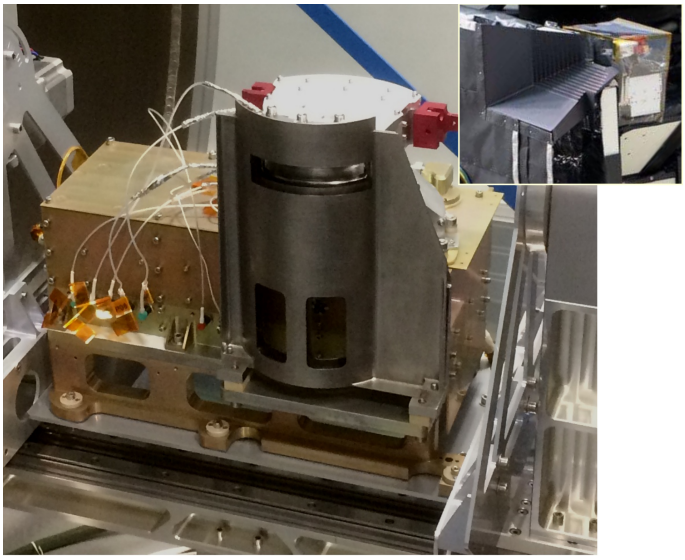

Fig. 18. Flight model of the SWA-PAS unit in the vacuum chamber during its calibration. The white analyser head is mounted on the top of the electronics box. Both are located behind the SWA-PAS-specific heat shield. Inset to the top right shows the sensor mounted behind its scalloped cut-out in the main spacecraft heatshield.

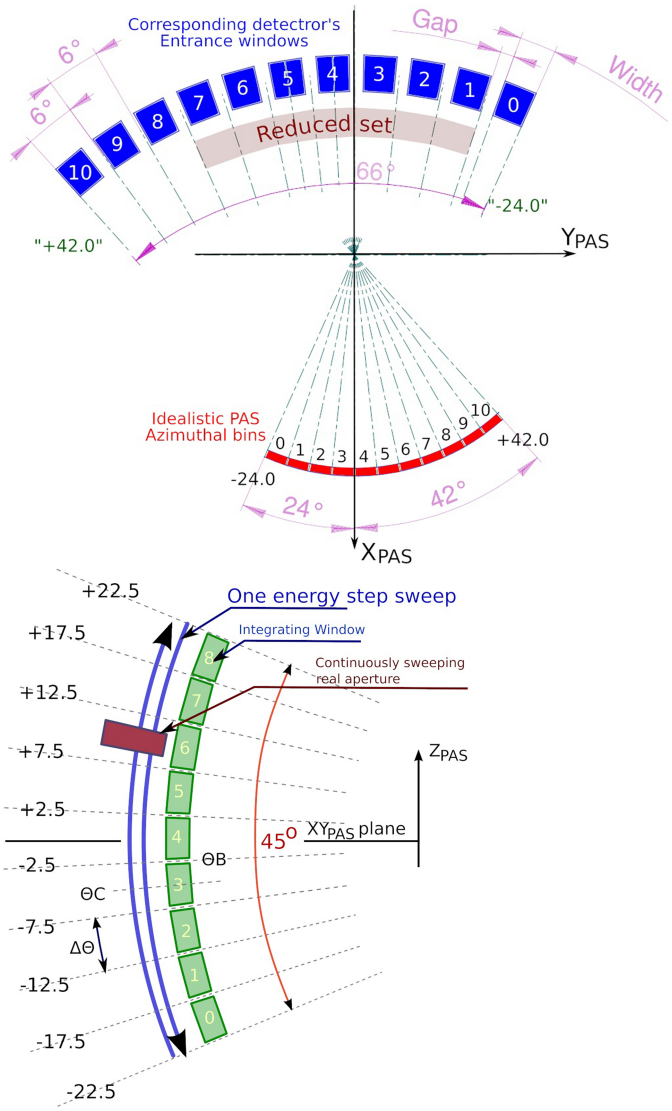

Fig. 19. SWA-PAS detector angular bins defined by the sensor geometry for the azimuth bins (*top panel*) and by deflector sweep for the elevation bins (*bottom panel*).

elevation and energy bins, SWA-PAS performs elevation sweeping and energy stepping (see Figs. 19 and 20). For a given energy, SWA-PAS makes a continuous sweep over the elevation range. The width of the instant elevation response is ~3°. To fill one bin, SWA-PAS opens the corresponding counter when the elevation scan enters the corresponding elevation bin, and stops the counter when the scan leaves the bin. As soon as one full elevation sweep is completed, SWA-PAS transfers to another energy step (Fig. 20). The transition time, ~2 ms, is that needed to stabilise the deflector HVPS. SWA-PAS transmits the data from the eleven CEMs to the SWA-DPU as soon as counts from one elevation bin are accumulated.

The duration of the full 3D sampling period consisting of (96, 9, 11) elements is exactly 1 s. The SWA-PAS design allows for the reduction of the number of energy steps and elevation angles, and also the use of seven rather than eleven channeltrons. Reduced VDFs are then obtained: for example, samples of (48, 9, 7) or (24, 3, 7), etc. Importantly, in these cases the reduced set of the energies is a subset of the energies of the full 3D sampling. The same is true for the elevation subsets. This allows placement of the 2D energy-elevation sub-window of the reduced sample in any position inside the full sampling window. If the duration of the reduced sample accumulation is less than the full sampling duration, SWA-PAS can perform several samplings per second. This fundamental advantage of the SWA-PAS operation allows the sensor to capture short-duration, high-cadence snapshots. The full set of the constants defining the SWA-PAS instant energy-elevation window is shown in Table 5.

In nominal operation, one VDF (one 1 s 3D VDF sample) will be measured each 4 s, with 3 s idle time between samples. This provides the basis to determine the density, velocity, and pressure of the solar wind at the required 4 s cadence.

3.3.4. SWA-PAS design details

From the functional point of view, SWA-PAS can be divided into five subsystems (see Fig. 21) as follows: (1) the electrostatic analyser, (2) the CEM board with the detectors, (3) the HVPS board providing HVs for the sensor head optical surfaces, (4) the FPGA board hosting the necessary digital data processing, and (5) the DC-DC converter providing the corresponding LV power. All electronics boards are located the SWA-PAS electronics box. It is not expected that the electronics box will need to be heated when the spacecraft is far from the Sun. However, for safety reasons, an operational heater is located on the side of the electronics box. The heater is powered via the same primary power line as SWA-PAS itself. The FPGA provides very simple open-loop heater control.

The SWA-PAS electrostatic analyser has no direct heritage in past space plasma instruments. Since corresponding instruments flown on HELIOS and on Bepi-Colombo are, or were, on spinning spacecraft, their plasma instrument designs did not need to include elevation steering. The Parker Solar Probe ion instrument is completely protected by the spacecraft heat shield and does not need special design to accomodate direct exposure to sunlight. However, the SWA-PAS sensor head must look directly at the Sun, which has driven the need to design the SWA-PAS analyser from the scratch. No existing coating can survive in such conditions, thus the entrance collimator and the

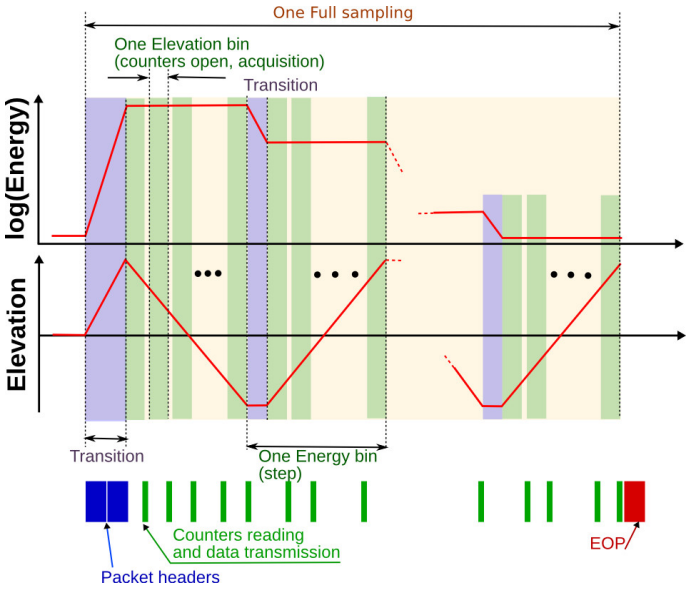

Fig. 20. SWA-PAS Energy – Elevation sampling waveform. The transition time, 2 ms, is needed to stabilise the deflector HVPS. Without this delay, the slope on the HV is perturbed at higher elevations.

Table 5. Constants controlling the SWA-PAS reduced energy-elevation window.

Parameter	Description	Possible values
Ne	Number of energy bins	2, 4, 6, ... 92
Se	Start position of the energy window	Any if the window does not exceed 0 or 95
Nel	Number of elevation bins	1, 3, ... 9
Sel	Start position of the elevation window	Any if the window does not exceed 0 or 8

deflector plates exposed to sunlight are made of polished aluminium. The electrostatic analyser spheres, less impacted by thermal flux, are scalloped and coated by Ebonol "C" UV absorbing film. The insulation of the deflector plates must be maintained up to 10 keV, since the steering of 20 keV charged particles requires at least 5.5 keV sweeping voltage. We describe the analyser properties in more detail in Sect. 3.3.5.

The CEM board is the uppermost board in the SWA-PAS electronics box. It serves as a base-plate for eleven ceramic CEMs mounted via two semi-metallised Ultem holders (Fig. 22). A corresponding set of eleven anodes lies under the CEM assembly, surrounded with a grounded guard fencing, made as a part of the outer golden metallisation layer. The anodes are internally routed and capacitively coupled to the hybrid charge-sensitive pre-amplifier-discriminators. The pre-amplifier digital output signals exit the board via logical buffers and level shifters and are passed to the FPGA board where the detected particles are counted. Each pre-amplifier-discriminator can register 6×10^6 Poisson-distributed pulses per second and their thresholds are set by fixed resistors to $\sim1.5\times10^5$ e^-. In order to save electrical power, the pre-amplifiers are switched off during the idle phases of the measurement (independently for the central and lateral sections).

The channeltron exits are kept at a potential ~-100 V, while the CEM entrance grids are biased to the CEM bias (-3900 V maximum). Two CEM variants with different resistances are used in the SWA-PAS detector to decrease the total power consumption. CEMs with nominal resistance of 80 MΩ, allowing maximum count rate 10^7 s^{-1}, are used for the azimuthal sectors 2−6. Sectors 0, 1, 7−10 utilise CEMs with nominal resistance of 200 MΩ (maximum count rate 10^6 s^{-1}) (see Fig. 19 and Table 6). Two independent HV converters (HVC) provide CEM bias for the central CEMs (sectors 1−7) and the lateral CEMs (sectors 0, 8−10). The count versus HV bias profile of both types of central CEMs are very similar, so it is unnecessary to provide separate voltages on them. Both HV converters work at 25 kHz, synchronised by a phase-locked loop (PLL) circuit to the 5 kHz clock signal provided by the FPGA board. When working with the reduced set of azimuthal sectors, the lateral pre-amplifiers and the lateral CEM HVC are always off. To minimise electromagnetic emissions and channeltron noise, the CEM board provides a single point connection between the SWA-PAS internal electrical and mechanical (chassis) grounds.

Table 6. SWA-PAS CEM properties.

CEM #	0	1	2−6	7	8−10
Resistivity, MOhm	200	200	80	200	200
Central or lateral	L	C	C	C	L

Two temperature sensors are glued near the two outermost channeltrons to monitor their operational temperatures. The CEM operational temperatures are a critical factor for detector lifetime and the SWA-DPU continuously monitors the corresponding HK values. If the temperature becomes too high, the CEMs are switched off immediately.

The SWA-PAS HVPS board provides four very fast varying HV voltages for the electrostatic analyser optical surfaces. Figure 23 shows the wave-forms of HVPS outputs. The deflector voltage linearly sweeps from -2000 V up to 5500 V over 10 ms. To provide the necessary waveform, the HVPS switches the output voltage sign and changes the internal gain of the source to transfer from the highest voltages to the lower voltage range needed for the low energy measurements.

The SWA-PAS HVPS provides a static voltage source, ±6500 V, which powers four opto-coupler-based fast HV drivers. The design includes dedicated opto-couplers, maintaining 12 keV bias, for the HVPS. The HPVS instant output is controlled by FPGA via a very fast LVDS data line.

As shown in Fig. 21, the FPGA code functionality is divided into several subsystems: (1) SpW interface; (2) SWA-DPU command decoder; (3) operational heater control; (4) HVPS control; (5) CEM HV control; (6) 11 fast counters; (7) HK acquisition unit; and (8) sequencer. The HV control system is a fast multi-channel LVDS control of the DACs integrated with the dedicated boards. The HK control is a multiplexing multi-channel analogue-to-digital converter control. Several channels needed for critical control, such as the operational heater, can be measured and transmitted to SWA-DPU at a factor of 20 times faster than other HK parameters. The counters can count up to 10^7 events per second.

The main FPGA subsystem is the sequencer, which gives significant flexibility to the system. The sequencer is an embedded programmable controller which allows simple mathematical operations, performs simple execution control loops, and "if-else" switching. The sequencer calculates HV values for the next substep using appropriate constants held in a small look-up table (LUT), and sends the commands to the HVPS board. It opens and closes the counters at the required times and forms

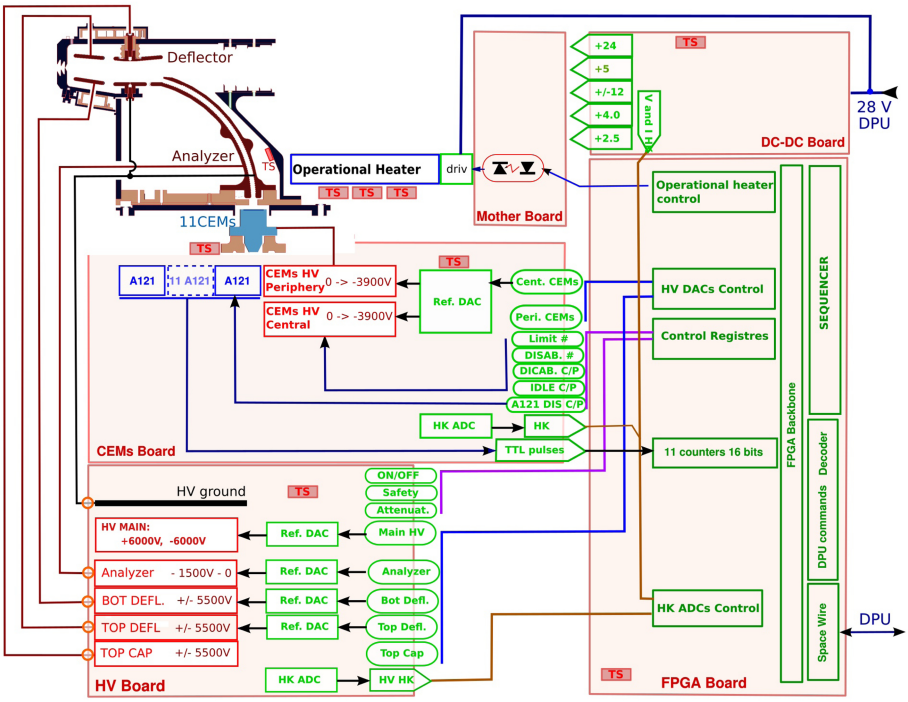

Fig. 21. Block diagram of the SWA-PAS system.

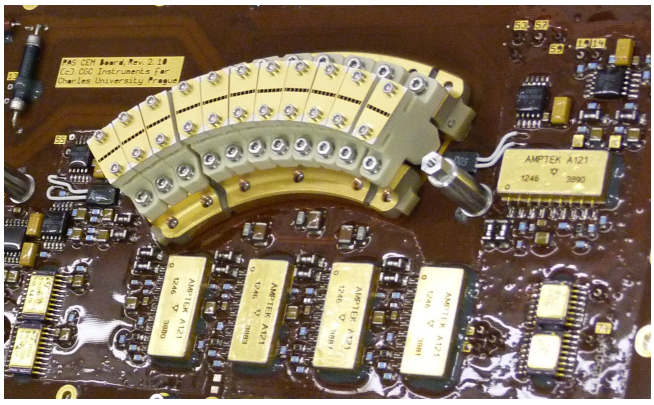

Fig. 22. Detail of the SWA-PAS CEM board depicting the assembly of the eleven ceramic channel electron multipliers. Two HV isolation gaps between the seven central CEMs and one + three lateral CEMs allow their independent operation. Hybrid charge sensitive pre-amplifiers-discriminators are placed on both the top and the bottom sides of the PCB near the lower voltage side of the channeltrons. Two temperature sensors are glued left and right of the channeltron set to monitor the temperatures of the CEM board.

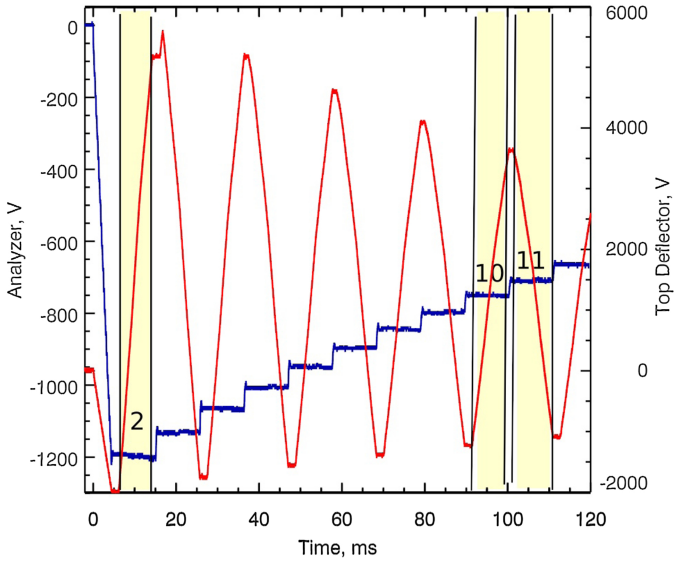

Fig. 23. SWA-PAS HVPS waveforms taken at the beginning of a sampling period. Blue trace: energy analyser voltage; red trace: top deflector voltage. The yellow bars show the time intervals for count accumulations.

the data packet. The sequencer controls the HK acquisition and performs all other actions needed to control the sensor.

3.3.5. SWA-PAS characterisation and calibration

A summary of the steps in the characterisation and calibration of SWA-PAS elements and the whole sensor is shown in Table 7.

As shown in Fig. 24 the "top-cap" voltage can be varied over a relatively large range for a given elevation bin. The analyser properties vary significantly with the "top-cap" polarisation. A trade-off is thus required between the bin geometrical factor, the energy, and the angular resolutions, in order to establish the optimised combination of parameters for operation. The FPGA sequencer can be programmed with the optimal values, as shown in Fig. 25.

Once SWA-PAS optical surface voltages are optimised and SWA-PAS FPGA tables are uploaded in flight, we can perform a full SWA-PAS calibration procedure, measuring the energy-angular-response of each angular bin. The integration of these responses provides the full matrix of SWA-PAS geometrical factors. An example of such responses are shown in Fig. 26.

3.3.6. Summary of SWA-PAS specifications at delivery

A summary of the design goals versus the obtained SWA-PAS properties is given in Table 8. The performance is close to that expected on the basis of numerical simulations of the design, with minor exceptions. The energy resolution varies between 3%

Table 7. Steps of SWA-PAS characterisation and calibration.

#	Action	Comment
1	CEM lifetime characterisation	
2	Detection system integrity	Check the signal propagation from the CEM to the telemetry with the real ion beam
3	CEM characterisation	CEM uniformity, working biases, etc.
4	Sensor optimisation	Optimal HVs for each elevation step
5	"Static" calibration	Determine SWA-PAS properties with quasi-static HVs
6	"Flight-like" calibration	Determine SWA-PAS properties with flight sweeping HVs

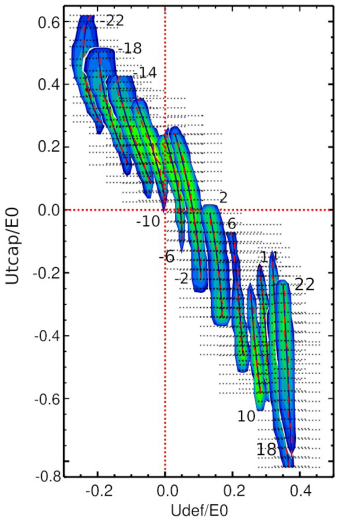

Fig. 24. SWA-PAS count rate (colour coded) as a function of "top-cap" voltage (Utcap, vertical axis) and deflector voltage (Udet, horizontal axis), normalised to the central energy of the hemisphere analyser (E0), for several elevation angles (labelled values adjacent to the responses). Black dots indicate the points of the measurement.

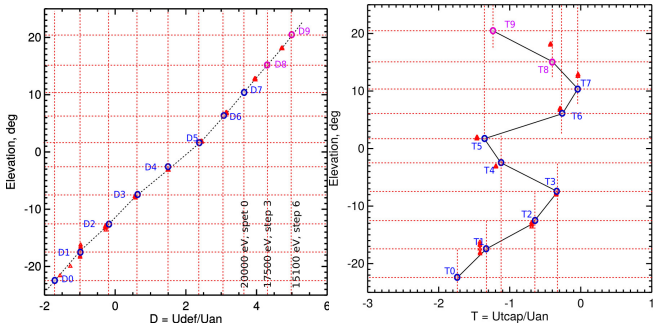

Fig. 25. SWA-PAS optimisation results that provide the basis for FPGA sequencer code inputs. *Left panel*: variation of the elevation angle as a function of the ratio between the voltage on the deflector (Udef) and that on the analyser (Uan), *right panel*: variation of the elevation angle as a function of the ratio between the voltage on the top cap (Utcap) and Uan.

and 9.3%, a range that brackets the target resolution of 5.5%. This deviation is a result of the trade-off between the instrument geometrical factor and the energy resolution. This is a generic property of the instrument which has a thin slit as an entrance aperture and a deflector behind this slit. The elevation range is

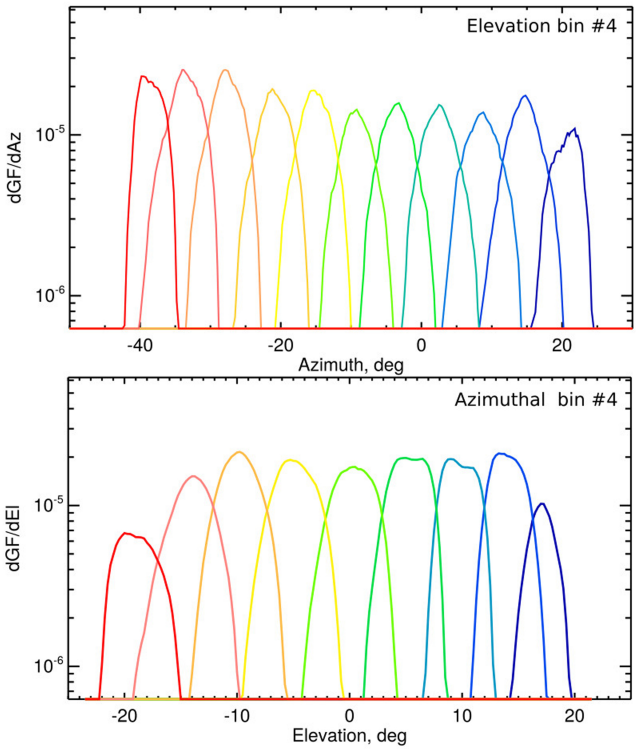

Fig. 26. *Top*: SWA-PAS azimuth responses for the elevation bin #4. This shows the differential geometric factor of each azimuth bin as a function of azimuth angle. *Bottom*: SWA-PAS elevation responses for Azimuthal bin #4. This shows the differential geometric factor of each elevation bin as a function of elevation angle.

Table 8. SWA-PAS design target goals with build and calibrated properties for PFM instrument.

Parameter	Range and resolution	Design goal	Build and calibration
Energy	Range	200 eV–20 keV	70 eV–20 keV
	Resolution ($\Delta E/E$)	5.5%	3.0–9.3%
	Number of steps	96	92
	Analyser constant (eV/V)	13	13–14
Angle	Azim. range	−24° to 42°	−24° to +42°
	Elev. range	±22.5°	−20° to +23°
	Azim. resolution	<6°	5°
	Elev. resolution	<6°	5°
Temporal	Basic accumulation period	~1 ms	0.95 ms
	Normal mode	4 s moments and 3D VDFs	4s moments and 3D VDFs
	Burst mode	15 VDFs/s	15 VDFs/s
Sensitivity	Per angular bin (cm^2 sr eV/eV)	≥4×10^{-6}	From 4×10^{-6} to 6×10^{-6}

slightly asymmetric. The 3D sampling energy range used for an individual measurement is reduced to 92 steps, although there remain 96 steps covering the total possible range. Other properties are very close to the corresponding targets.

3.4. The SWA Data Processing Unit (SWA-DPU)

3.4.1. SWA-DPU introduction

The SWA Data Processing Unit (SWA-DPU, Fig. 27) is the "heart" of SWA. It represents the only SWA interface with

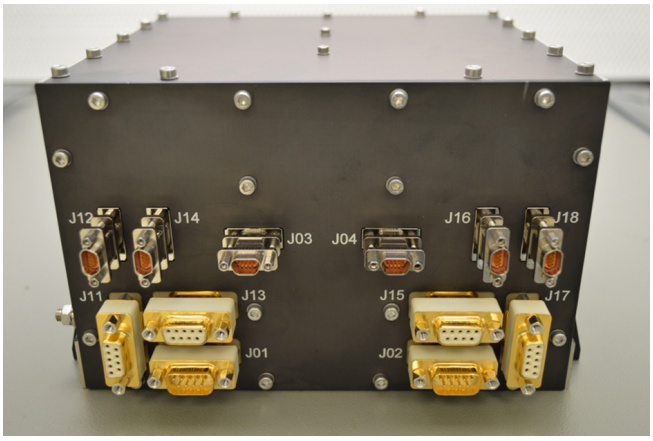

Fig. 27. SWA-DPU flight model hardware.

the spacecraft as far as commanding and communication are concerned: the SWA-DPU implements the data and command interfaces with the spacecraft via redundant SpW data links and the redundant HV-high power command (HV-HPC) interfaces. The SWA-DPU is also interfaced with SWA-EAS, SWA-PAS, and SWA-HIS sensors via SpW dedicated links. For SWA-EAS and SWA-PAS this interface supports functionality control, temporary storage, communication, and computational capability. In addition, the SWA-DPU will support SWA-HIS with communication to the spacecraft. The SWA-EAS and SWA-PAS sensors receive redundant power inputs from the SWA-DPU, although the SWA-HIS sensor draws power directly from the spacecraft bus.

3.4.2. SWA-DPU hardware design

The SWA-DPU architecture is derived from trade-off analyses to define a system able to perform the needed computational tasks while keeping mass, volume, and power consumption within the constraints imposed by spacecraft resources. Additionally, the SWA-DPU has been designed to be "single fault" tolerant and the "cold-spare" concept has been adopted as the redundancy philosophy. The SWA-DPU hardware architecture is based on:

- 1 × backplane and SpW splitter (BSS) front-end interface circuits;
- 2 × data processing module (DPM), each composed of:
  - 1 × communication and scientific data processing (CSP) Board;
  - 1 × central processing unit (CPU) Board;
- 2 × power conditioning and distribution module (PCDM).

Apart from the BSS, representing the SWA-DPU redundant communication node, the SWA-DPU is comprised of two sub-units (SWA-DPU-nominal and SWA-DPU-redundant), each of which includes one DPM and one PCDM and is capable of implementing separately all the functions of the SWA-DPU (see Fig. 28 for details). The BSS is a rigid-flex board that, in addition to the backplane board, includes the SpW front-end circuits serving the SWA sensors and the spacecraft communication interfaces (nominal and redundant); these circuits provide connections for the two DPMs, deployed in cold redundancy, and each SpW data link must have a connection to both the DPMs. For this purpose, each of the six independent SpW physical layer "splitter" circuits act as a repeater and distributor on two independently buffered outputs. Each splitter is composed of LVDS drivers and receivers, a local regulated power supply, and sectioning circuits. This design avoids fault propagation, ensuring the isolation of possible failure. It also provides independent switch-on and off capability for each splitter, thus saving power when the corresponding interface is unused. The SWA-DPU data communication and processing capabilities, provided by the DPM, are realised by the joint use of a CPU board and a FPGA-based CSP board. The latter acts as communication controller and can be also used as a processing engine for intensive computation. This architecture allows the implementation of a wide range of complex processing algorithms, by adopting appropriate hardware and software partitioning solutions.

The CPU board is based on the Leon2FT ASIC AT697F processor by ATMEL, running at 100 MHz and working under the VxWorks Real Time Multitasking Operating System. The CPU is equipped with EDAC-protected volatile and non-volatile memories, including a 64 Kbyte Boot EPROM, a 2 Mbyte + 2 Mbyte MRAM for onboard software and permanent data, and an 8 Mbyte SRAM for code execution and run-time data.

The CSP board is based on two RTAX2000 FPGAs (primary and secondary). It also has a 2.5 Gbit synchronous dynamic random access memory (SDRAM) mass-memory needed for buffering of the scientific data generated by the SWA-EAS and SWA-PAS sensors. The primary FPGA is directly interfaced with the CPU and the SDRAM, performing all the SWA-DPU communication tasks and the data handling functionalities not covered by the CPU. The secondary FPGA is used as a possible hardware accelerator, dedicated (as needed) to the implementation of parts of algorithms, in order to reduce CPU overhead and to ensure a significant margin in the overall SWA-DPU processing capabilities.

Each DPM module is supplied with a separate and protected power supply line from its associated sub-unit PCDM. It also directly interfaces with the PCDM via a SPI interface, for reception of HK data and for power distribution management for the SWA sensors by means of low-level control and status signals.

The PCDMs primary role is to implement the power-related functionalities, including: (i) power inputs (main and redundant) interface front-end, including EMI filter, inrush current limiter, protection circuits, etc; (ii) interface for the external HV-HPC commands from the spacecraft and BSM status towards the spacecraft (main and redundant); (iii) power conditioning, distribution, and protection for the internal SWA-DPU electronics; (iv) power distribution and protection for the sensors, by means of power switches controlled by opto-isolated circuits; and (v) acquisition of HK data related to currents and temperatures.

3.4.3. SWA-DPU software design

The overall SWA-DPU software consists of two separate independent executable software images: the boot software (BSW) and the FSW. The top-level software architecture for the SWA-DPU is shown in Fig. 29. The BSW is non-patchable software resident in a PROM. At start-up, the BSW performs the basic hardware initialisation, namely processor and memory controller initialisation. It then starts a memory check, which consists of a write and read test of the SRAM (8 MB) and an integrity check of the FSW stored in MRAM, based on the FSW code cyclic redundancy check (CRC) verification. Should the SRAM test fail, the redundant section of the SWA-DPU will be used. Should the FSW code CRC test fail, the BSW enters its diagnostic mode and waits for ground intervention. Upon successful execution of SRAM and MRAM tests, the BSW loads the FSW from MRAM to SRAM and starts it. Upon entering the diagnostic mode,

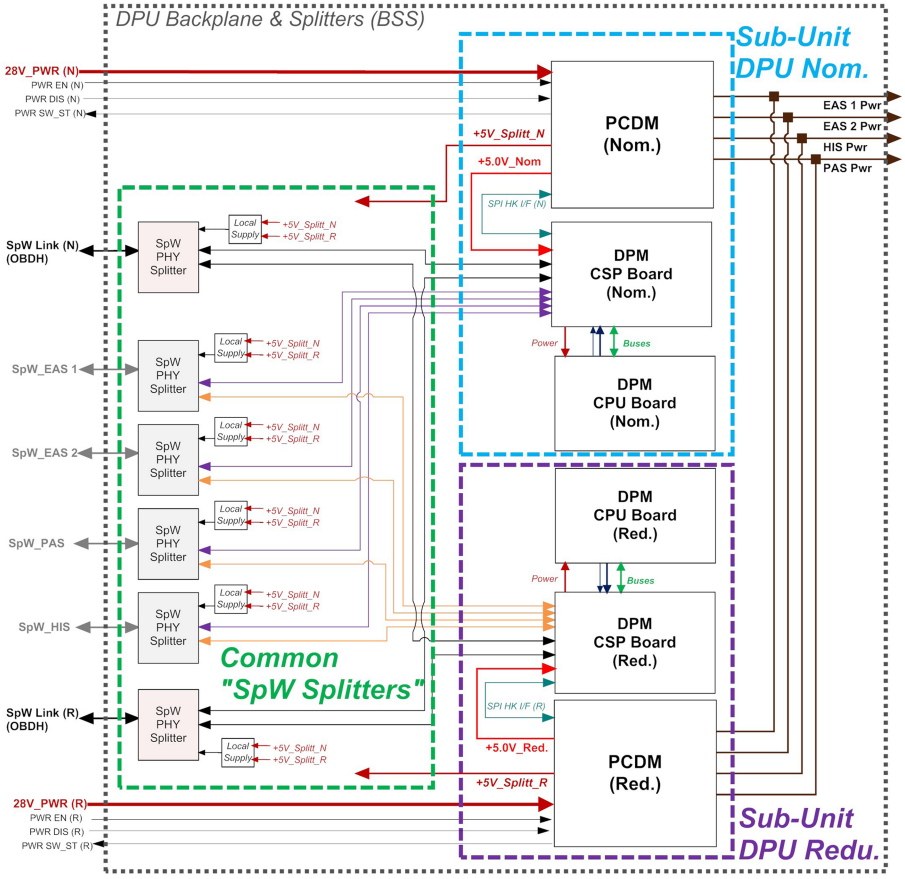

Fig. 28. Schematic of the SWA-DPU hardware architecture.

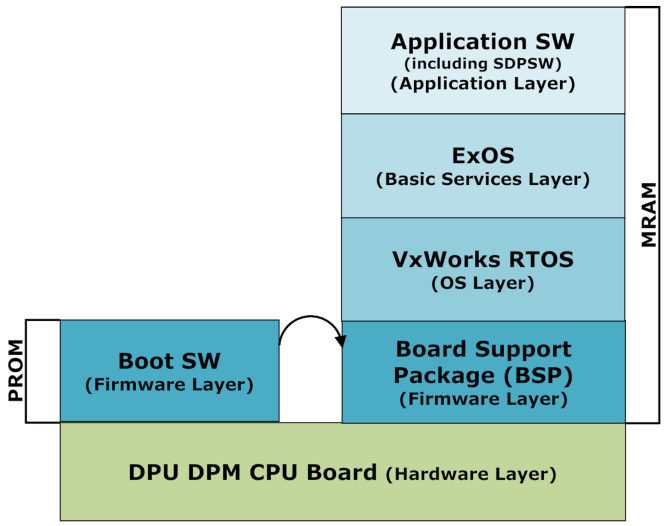

Fig. 29. SWA-DPU top-level software architecture.

the BSW initialises the communication through the main and redundant SpW interfaces with the spacecraft on board computer (OBC) in order to manage a reduced set of TM and TC services. These include Service 9 TC, to synchronise the SWA-DPU internal reference time with the spacecraft event time (SCET), Service 3 TM, to generate and transmit the SWA-DPU HK telemetry, and Service 6 TC, to perform check, dump, and load of memory blocks (for FSW patching).

The FSW is composed of three software layers: the application software layer (ASW), the application service software layer (ASSW), and the machine services software layer (MSSW). The ASW includes SWA-DPU TC and TM and process control management software (PCMSW), and the scientific data processing software (SDPSW). The PCMSW is a logical composition of sub-components which manage TC validation and execution, SWA-DPU and sensor state management, the SWA sensors (SWA-EAS1, SWA-EAS2, SWA-PAS, and SWA-HIS) themselves, and the science data acquisition. It also controls algorithm execution on acquired scientific data (i.e. moment computation, compression, etc.), SWA-DPU HK data handling, FDIR, and time management. The SDPSW provides post-processing functionalities on the SWA-EAS and SWA-PAS acquired science data (moment calculation, raw data compression, formatting of compressed stream for downlink). The ASSW includes the packet utilisation standard library software (PUS) and mission services for the ASW. It provides the set of functions for implementing the PUS services required for the SWA-DPU ASW. The MSSW includes the real time operating system (RTOS) kernel, the extended operating system service (EXOS) software, and the low level drivers in the board support package (BSP). The RTOS provides the SWA-DPU DPM runtime resource management, the basic mechanisms for task execution, and inter-process communication. The EXOS provides a library used by the ASW and ASSW layer components to gain access to the SWA-DPU hardware resources (memory, registers, time, SpW, sensors, etc.). The EXOS also efficiently executes some basic functions for the configuration and management of the system and its various subsystems. It provides appropriate functionalities to support the exchange of information among the subsystems and between the SWA-DPU and spacecraft. The BSP provides access services to all SWA-DPU internal hardware and physical interfaces of the system to the above software layers.

3.4.4. Scientific data processing

The SDPSW is the component handling the processing of data collected by the SWA-EAS (1 and 2) and SWA-PAS sensors, while SWA-HIS processes scientific data on its own. Due to the limited bandwidth available to SWA for downlink, the full set of SWA raw data collected cannot be transmitted back to ground at all times. Indeed, even to return full resolution data products at relatively low time cadences requires compression rates (CR) in the range from 2 to 7.6, depending on the different kinds of data and their associated data product volumes. In order to return information on the nature of the solar wind at higher cadences, data processing within the SWA-DPU is used to evaluate derived scientific properties of the solar wind, in particular the moments of the particle VDF (Paschmann et al. 1998). These quantities are transmitted instead of the full raw data, with the transmission of full VDFs only at lower cadence or after appropriate compression. The processing of SWA-EAS1, SWA-EAS2, and SWA-PAS scientific data generated during their normal and burst modes is handled by the PCMSW that calls the services offered by the SDPSW, within its cyclic activities routine. Accordingly, the execution of scientific algorithm requests, such as "Compress Data Product" or "Calculate Moments", is distributed across several different run-time intervals. This is managed by means of dedicated activity tables defining the actions the SDPSW has to perform for each "activation" by the PCMSW. These tables define the software behaviour for both compression and moment calculation functions for each sensor and for each operating mode, according to the specific data collection rate and order. In this way, the SDPSW prepares data as they are ingested by the SWA-DPU from sensors, and, when the complete data sample to be processed has been reconstructed, the SDPSW's services start data compression (or moments calculation) and continue, with cyclic activation, until that operation is completed.

On board moments calculation. The SDPSW provides the functionality for the calculation of the number density (moment of order zero), number flux density (first order moment), pressure tensor (second order moment: computed in the satellite reference frame for SWA-EAS and SWA-PAS), and energy flux density vector (third order moment: computed only for SWA-EAS). Moments are computed starting from the counts accumulated in each elementary volume in phase space and with reference to the sensor' resolution in energy, azimuth, and elevation angles (Paschmann et al. 1998). From an operational point of view, all the equations defining the moments have been captured within a series of LUTs allowing the performance of the moments calculation by means of only sums and products, with the counts of each elementary volume in phase space "modulated" by a combination of these factors. This algorithm has an initialisation phase that is performed only at SWA-DPU start-up and must be repeated each time the configuration values are updated from ground. It is a deterministic set of computations, and can be completely verified on-ground. Algorithm configuration values are read from memory (MRAM) and used to evaluate a set of "constant" parameters used as LUTs at run-time. Some of these tables contain configuration parameters derived on the ground from the sensor physical and geometrical properties. Others parameters which are expected to show slow time variation are held in LUTs which can be readily updated from the ground. For some parameters, particularly those which are directly linked with the way sensors are commanded to sweep energies or elevations, the same inputs are shared for both sensor and SDPSW configurations. For example, both the SWA-EAS-Sequencer and the SWA-DPU-SDPSW rely on the same ground commandable parameters defining the hemisphere voltage ratio and maximum voltage. The output is the same hemisphere LUT composed of 64 values expressed in volts and eV. Other commandable LUT parameters include those fixing the range of variability and the precision at which a given set of moments will be telemetered to ground; this is done by defining the couplet of information (LSB, Offset) to be applied to the raw and scientific data in order to define the transmitted value within the data packet.

The calculation of accurate moments from the SWA-EAS sensor is dependent on identifying and removing data from those low energy bins which may be contaminated by the presence of spacecraft photo-electrons. Since such electrons are generally found at energies below the spacecraft potential, the baseline algorithm involves the use of a measurement of that potential passed to the SWA-DPU from the RPW experiment (Maksimovic et al. 2020), if it proves reliable, or otherwise using a fixed but ground-commandable level. This information is transmitted via the Service 20 IEL. The moment calculation then does not include SWA-EAS1 and SWA-EAS2 energy bins with ranges which are partially or fully below the value of the spacecraft potential. Moreover, the ranges of the energy bins above the spacecraft potential are reduced by the value of the spacecraft potential. In addition, moments are calculated as partial summations across three energy ranges (see Sect. 4.3 for details), so that even if the lower range is contaminated, some useful science data will remain in the upper ranges.

Data compression. Representative sample data have been produced by extrapolating real measurements by the Cluster mission to the conditions in which SWA is expected to operate. These have been evaluated for their information content, using both the data entropy measure and the actual CR. Results from this exercise demonstrate that SWA-EAS data CR can vary between ~1.9 and ~12.1, while for SWA-PAS data this ranges from ~3.4 to ~17.5. Data compression is performed by means of a customised implementation of the lossless Consultative Committee for Space Data Systems (CCSDS) 121.0 standard. This choice has been made as a trade-off between compression and computational efficiency. In fact, the CCSDS 121 technique allows full exploitation of the intrinsic structure exhibited by all data products, together with information theory methods, while remaining within the computational resource limitations. In particular, a specific customisation was designed for SWA-EAS data in order to reach the compression ratio needed, by detailed consideration of the specific data structure. SWA-EAS samples produce 3-dimensional matrices (cubes) whose dimensions cover the elevation and azimuth of incoming particle directions and their energy levels. These cubes are stored in a rolling buffer, within the SWA-DPU's memory, in a specifically defined one-dimensional array, mostly dependent on the acquisition sequence (simply meaning the first sample acquired is the first in the array). However, a preferential scanning sequence, which is different to that of the actual acquisition, has been identified from simulations using existing solar wind data. This sequence is identified by measuring similarities in each direction within the 3D data in order to identify which demonstrates the slowest variation rate. Thus, a further processing step is preliminarily applied to sampled SWA-EAS electron distributions in order to increase the algorithm's performance in terms of better prediction efficiencies, smaller prediction errors, and ultimately higher achievable compression ratio. This "complex reordering" mechanism has thus been designed in order to exploit the preferential direction in data similarity. It switches the data order

after acquisition (this mechanism is identified as the "simple" reordering step), and then ensures that the highest degree of spatial continuity is established between contiguous samples (this mechanism is identified as the "complex" reordering step).

For SWA-EAS data, it has been found that a simple reordering of the data from the original order, that is elevation angle, energy level, azimuthal angle to energy level, azimuthal angle, elevation angle, brings clear improvements in the compression efficiency. In addition, the complex reordering step further improves compression performances by avoiding periodic jumps between acquisition directions. Re-ordered data are then passed to the unit-delay predictor and the standard pre-processing module. In the final compression step, the coder applies Rice's technique, in which several algorithms are concurrently applied to a block of consecutive pre-processed samples. The algorithmic option that yields the shortest encoded length for the current block of data are selected for transmission.

Book-keeping algorithm (BKA). The SWA-DPU ASW is responsible for controlling data collection, mode use, and imposing telemetry generation restrictions on each of the three SWA sensors separately, in order to keep each of them within the respective assigned allocations. In principle, during burst modes the sensors generate raw data at a rate which is significantly higher than their orbit-averaged allocation, while in normal mode they generate data products at a slightly slower rate than is consistent with the orbit allocation for each sensor. Thus, the book-keeping algorithm (BKA) is a software tool able to monitor and control the amount of burst mode used against the pro-rata expectation for any given point along the orbit. The principles underpinning the BKA are:

1. The BKA will be used by the ASW to assess the generation rate of science data by each of the three SWA sensors over an established time interval that starts at time T_0 and ends at time $T_0 + \Delta T$. ΔT is variable to allow for lessons learnt in flight, but the initial baseline should be the orbital period of the spacecraft or duration of a stable telemetry corridor (Sanchez et al., in prep.);

2. The ASW will hold record of two limits per sensor, set by the SWA team (changeable in flight to account for lessons learnt) representing: (a) the fractional level, O_S, against which the sensors may be allowed to become overdrawn against the pro-rata allocation, and; (b) the fractional level, U_S, against which an unacceptable "under-drawing" against the pro-rata allocation is deemed to have occurred;

3. At regular intervals the ASW will update the accumulated total volume, $V_{BM,S}(t)$, of post-processed data which has been originated by sensor S since time T_0.

4. At regular intervals, the ASW will calculate $A_{BM,S}(t)$, the expected pro-rata data accumulation for each sensor, S, since time T_0, based on the orbit-averaged allocation, $A_{BM0,S}$, for that sensor:

$$A_{BM,S}(t) = A_{BM0,S} \times \frac{(t - T_0)}{\Delta T} \tag{1}$$

5. The ASW will ensure that each sensor, S, does not produce so much BM data that the difference between the actual accumulated total volume, $V_{BM,S}(t)$, of data from sensor S which has been sent to the spacecraft solid state mass memory (SSMM) since time T_0, and the pro-rata orbit allocation $A_{BM,S}(t)$ does not exceed the fraction O_S of the remaining allocation. If the fraction is exceeded, then the SWA-DPU will disable trigger event capture and disable further optional scheduled burst modes until the excess is reduced to a factor of, at most, $M \times O_S$. Specifically, the SWA-DPU will disable optional scheduled BM and trigger event capture if:

$$V_{BM,S}(t) > A_{BM0,S} \times \left[\frac{(1 - O_S)(t - T_0)}{\Delta T} + O_S \right] \tag{2}$$

and will subsequently re-enable schedule BM and trigger event capture once:

$$V_{BM,S}(t) < A_{BM0,S} \times \left[\frac{(1 - MO_S)(t - T_0)}{\Delta T} + MO_S \right] \tag{3}$$

6. In a similar way the SWA-DPU will ensure that $V_{BM,S}(t)$ does not fall below the fraction U_S of the remaining allocation. If the fraction is not achieved, then the SWA-DPU will enable additional scheduled burst modes until the underspend is reduced to a factor of less than $M \times U_S$ enabling additional scheduled BM;

7. In any case, the assessment period can be restarted once the period ΔT has elapsed. At this time, the accumulated data should have only a relatively small difference from the maximum allowed total for the orbit or period. Thus the assessment can be restarted by carrying over the small difference to the next assessment period;

8. The BKA is also able to handle ground commands for the ASW operation, which set the trigger-enable flag and control the amount of scheduled burst mode for limited specific periods, and automatically recover the required average telemetry rate in the following period;

9. All the parameters controlling the operation of the BKA are configurable in flight to allow the ASW to control the data production when the available telemetry rate is reduced below the nominal level. In practice this is likely to require (temporary) changes to the parameters O_S, U_S, and $A_{BM0,S}$ by ground command for the duration of such periods, with possible compensatory changes to allow catch-up outside these periods;

10. The ASW is able to restart the BKA and resume correct operation in the event of a reboot or restart of the SWA-DPU.

The requirement to steer the SWA data accumulation through a telemetry corridor (defined for any given period at mission level) is equivalent to choosing a particular set of the BKA configuration parameters defined above. This will allow the SWA BKA to control SWA telemetry generation to remain within a defined telemetry corridor. This is illustrated in Fig. 30.

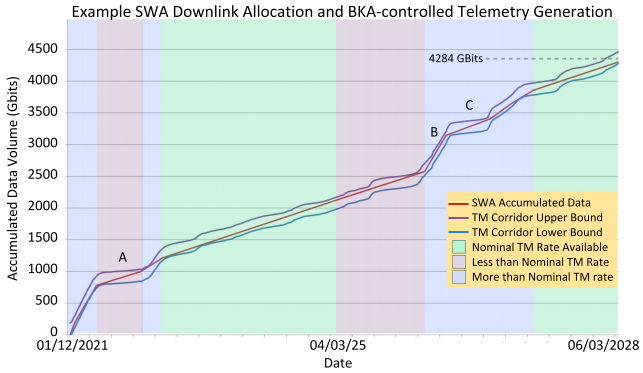

Fig. 30. Operation of the SWA BKA. Mission periods occur when less than (pink shading), more than (blue), and actual (green) nominal data rates will be available. The SWA BKA will steer data production (red line) through a project defined telemetry corridor with upper and lower limits (purple and blue lines respectively). Periods of low download rates (e.g. marked A and C) can be optimally negotiated by the BKA using higher rates on ether side (e.g. at point B).

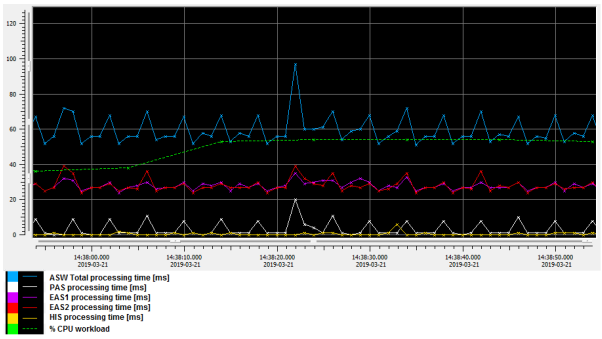

Fig. 31. Illustration of SWA-DPU performance. DPU activity enhancements associated with the 4 s cadences of SWA-EAS and SWA-PAS in normal mode are clearly visible.

3.4.5. SWA-DPU testing and characterisation

Figure 31 shows the ASW performance in the worst case condition occurring in periods in which all sensor scientific activities are activated, the compression algorithm is enabled, and a freeze of the trigger mode rolling buffer has been activated following the simulated receipt of a flag from the RPW instrument (Maksimovic et al. 2020) via PUS Service 20. Even under these conditions, the ASW performance remains under the required limit. In particular, we note that during each ASW processing slot (ASW activity cycles at 8 Hz) the ASW total processing time is lower than the maximum allowed time of 125 ms with the maximum time measured being 97 ms. In addition, the SWA-EAS and SWA-PAS processing times are largely uniform during science processing, and peaks are due to moment computation performed each 4 s and full 3D distribution extracted each 100 s. In contrast, SWA-HIS contribution is negligible as the ASW acts just as pass through for incoming SWA-HIS telemetry packets. Overall, typically the ASW CPU load is under 40% with a peak of 56% which is reached during RPW-trigger buffer freeze operations.

The data depicted in Fig. 31 are derived from housekeeping data dumped at its maximum frequency of 1 Hz (reporting the ASW processing time) and represents the maximum processing time measured in an observation window of 1 s for the management of each of the four SWA sensors (SWA-EAS1, SWA-EAS2, SWA-PAS, and SWA-HIS), and for the sum of all ASW activities (including the sensor management). In conclusion, the processor does not need to work under stressed conditions. It has more than 40 % margin in the worst case, and the time consumed by the ASW processing tasks is well under its maximum limit of 125 ms. So the risk of breaching operational limits, and the consequent possibility of losing a processing slot and the associated science data is very low (an overrun event report is generated in any such case).

4. SWA science operations

The suite of three SWA sensors plus its SWA-DPU will be operated in a variety of modes in order to address the overall Solar Orbiter mission science goals (Müller et al. 2020; Zouganelis et al. 2020). The SWA operations activities are distributed across three centres, primarily to allow key hardware institutes for the three sensors to address the health and calibration issues of their relevant sensor. The primary SWA operations group is based at UCL MSSL, and will take lead responsibility for SWA-level communications, coordinating activities across the suite, and for processing of the SWA-EAS data products. In this case, "communications" includes liaison and data exchange with the Mission Operations Centre (MOC) at the European Space Operations Centre (ESOC) in Darmstadt, Germany, the Solar Orbiter Science Operations Centre (SOC, Sanchez et al., in prep.) near Madrid, the Solar Orbiter Archive, as well as with partner SWA operations groups in Toulouse (for SWA-PAS related activities) and UMich (for SWA-HIS related activities). This section summarises the key operational issues, mode, and data product information likely to be of use to the scientific user of SWA data.

4.1. SWA telemetry

The baseline operations planning driving the original design of the SWA sensors and their operations was based on returning an orbit average data telemetry rate of ~14.5 kbps. Considering the required data products, the cadences at which they would be required, and the useful duty cycle for higher time resolution (burst mode) data products, a baseline target data production rate for the three sensors was established as ~5.5 kbps for SWA-HIS, ~4.5 kbps for SWA-PAS, ~4.3 kbps for SWA-EAS, and ~300 kbps for the SWA-DPU. Given the uncertainties associated with both the CRs achievable in flight and with the capture of data products associated with irregular triggers, the SWA team planned to maintain broad compliance with these rates by monitoring and internally controlling data taking by the SWA-DPU through the operation of the BKA (see Fig. 30 and associated text). Under this scheme, periods of poor compression ratio or numerous trigger responses would be compensated for by the cancellation of some planned burst mode intervals and switching off of the response to further trigger flags. In extreme cases, autonomous commanding of the sensors into low-cadence data taking would also occur. Conversely, if the sensors supply less data volume to the SSMM (due to a period of efficient data compression or lack of triggers) then the instruments can be commanded to take more burst mode data or to take higher volume data products at higher cadences.

More recent analyses of the mission orbits by the Solar Orbiter project have led to the realisation that there will be times when the instruments can produce significantly more data than the original baseline volumes, and conversely times when data taking cannot proceed at baseline rates without overfilling the SSMM data stores and overwriting previously taken data. For this reason the ESA SOC will, as part of the planning for the mission, define "telemetry corridors" for each instrument. These will define the upper and lower bounds for the data volume acquired by a given instrument at a given point in time. This thus sets the rate, as a function of time, and over periods that may be shorter than the orbital period, at which the instruments may accumulate data. For SWA, the prior existence of the BKA means that this development is readily accommodated in the instrument planning by simply changing the control parameters of the BKA, such that they match the requirements of the telemetry corridors. Although we describe later in this section the various modes and data products produced by SWA, the descriptions are largely based on the nominal behaviour, and we note that a key outcome of the wide range of telemetry rate availability will mean that there will be variances in SWA data cadences and resolutions to accommodate this.

4.2. SWA commanding

SWA commanding is the responsibility of the UCL MSSL SWA operations team, who lead the activity in close consultation with

SWA partners and the SOC. On the basis of mission-level planning by the Solar Orbiter Science Working Team (SWT) and Science Operational Working Group (SOWG), the SWA operations teams will have a baseline operational plan, defining instrument telemetry and power constraints against which to fix the detailed commanding of the three sensors for a given period. In general, the SWA operations team will attempt to plan for the sensors to operate to return the highest volume of best quality science data consistent with those constraints, in particular within the telemetry corridors defined by the SOC. However, coordinated data taking with other instruments (e.g. joint burst mode observations, Walsh et al. 2020) will also be factored in to maximise the potential science return. Compliance of the data taking by the SWA sensors will be monitored and controlled on board by the SWA BKA (see Fig. 30). Instrument operations request (IOR) files will be constructed and submitted to the SOC for compliance testing, before upload to the spacecraft a few weeks before execution.

4.3. SWA modes of operation

4.3.1. SWA-EAS modes of operations

The SWA-EAS instrument can operate in various modes that will return different subsets of the original 3D VDF data. Together with the HK data from each SWA-EAS, there are also various engineering modes that allow instrument health monitoring and fault diagnosis to be performed on a semi-regular basis (about once per week, for a limited duration) in order to ensure that the sensor is maintained in optimum configuration. Of more relevance here are the science modes. These are:

SWA-EAS normal mode. The two SWA-EAS sensors each send their respective sampling of the 3D VDF to the SWA-DPU every second. The SWA-DPU stores these data in a 5 min rolling buffer. Every 4 s the SWA-DPU selects the measurements from each sensor, performs a partial moment calculation (over three subsets of energy range and two angular ranges for each sensor), and adds the resulting 168 parameters to the SSMM for inclusion in the telemetry stream. Optionally, in the event of low counts, the SWA-DPU will add four consecutive measurements from SWA-EAS and then perform the moment calculation. Every 100 s of the full set of $64 \times 32 \times 16$ 3D measurements from each SWA-EAS is compressed and sent to the SSMM. In addition, every 100 s (offset by 50 s from the selection above) a single energy bin slice of the full 3D measurement of each SWA-EAS sensor is compressed and sent to the SSMM for telemetry as a low-latency data product (see Sect. 4.4.5). The data array dimensions for this product are thus $2 \times 1 \times 32 \times 16$;

SWA-EAS burst mode. On command, the SWA-DPU will place the SWA-EAS sensors into burst mode. The SWA-DPU will steer the SWA measurements with reference to the magnetic field unit vector provided by the MAG instrument (Horbury et al. 2020) over the Service 20 IEL feed at 0.125 s cadence. In response, the SWA-EAS sensor whose central plane of FoV passes closest to the magnetic field direction makes measurements at only two elevations (but at full energy and azimuth). These two elevations are chosen such that one set of observations includes the direction along the B-field direction, and the other along the anti-parallel direction. Given that only two elevations are sampled in this mode, the resulting $1 \times 64 \times 32 \times 2$ array of data can be captured every 0.125 s and transmitted to the SWA-DPU for addition to the SSMM and the telemetry stream. These data products will be reassembled on the ground to provide a measurement of the 2D PAD of electrons (with some limited gyrophase information) at 0.125 s cadence.

SWA-EAS triggered mode. Autonomously, and following the receipt of a trigger flag over the Service 20 IEL feed, the SWA-DPU will freeze the rolling buffer containing 5 min of 1 s-cadence samples of the full 3D velocity distribution from each SWA-EAS sensor. The SWA-DPU will transmit the resulting 300 samples of $2 \times 64 \times 32 \times 16$ data arrays to the SSMM for inclusion in the SWA telemetry stream. It is expected that the trigger flag will be set by the RPW instrument (Maksimovic et al. 2020) in response to an autonomous evaluation of whether combined in situ data suggests the passage of an event of scientific interest (e.g. an interplanetary shock) passed the spacecraft in the previous 5 min period.

4.3.2. SWA-PAS modes of operations

SWA-PAS is capable of producing one $96 \times 11 \times 9$ array of data every second. However, due to restrictions of telemetry and power, SWA-PAS will operate in various modes and states that will return different subsets of the original 3D data. These modes are:

SWA-PAS normal mode. SWA-PAS can be operated across a range of parameter space. However, typically in normal mode SWA-PAS will operate on a repeating 300 s cyclogram. The data taking activities during each 300 s cyclogram are illustrated in Fig. 32. The upper part of the figure shows SWA-PAS operation around a 300 s cyclogram boundary, while the lower part shows the operation at each of the two intervening 100 s boundaries. In each case the boundary is marked by the thick vertical dashed lines. The scheme is based on making a measurement of the proton-alpha particle VDF over 1 s every 4 s. This is achieved by taking a series of "normal samples", represented by the grey boxes marked "S" in Fig. 32 over 48 energies, seven azimuths, and five elevations. However, these samples are replaced near the 100 and 300 s boundaries by "full 3D" samples, represented by the orange boxes marked "FS", in which the measurement is extended to all nine elevations. This is to ensure (checked by the SWA-DPU) that the sensor scans to correctly capture the ion distribution in the "normal samples". One such distribution is taken near the 100 s boundary, while two are taken a few seconds before and after each 300 s boundary. Between the latter two full sample measurements, SWA-PAS will be commanded into snapshot mode (see below). Figure 32 also shows, for completeness, the commanding requirements for the scheme (green boxes) and an illustration of the power saving profile (pink lines) in which the sensor voltages are ramped down between measurements. Under this scheme the SWA-PAS sensor makes a sampling of the full 3D VDF of the protons and alpha particles every 4 s, which are passed by the SWA-DPU to the SSMM for telemetry to the ground.

SWA-PAS snapshot mode. For a period of 7 s every 300 s, the SWA-PAS sensor is commanded by the SWA-DPU into snapshot mode. During these periods the sensor will sample over 48 energies, seven azimuths but only three elevations. However, the measurement cadence will be raised to a rate of 4 per second over the 7 s snapshot period. The timing of this mode will be such that it covers the period that the RPW sensor (Maksimovic et al. 2020) will perform its nested snapshot mode. This nested timing of the observations will enable detailed analyses of wave-particle interactions through the combination of high-cadence field and particle measurements.

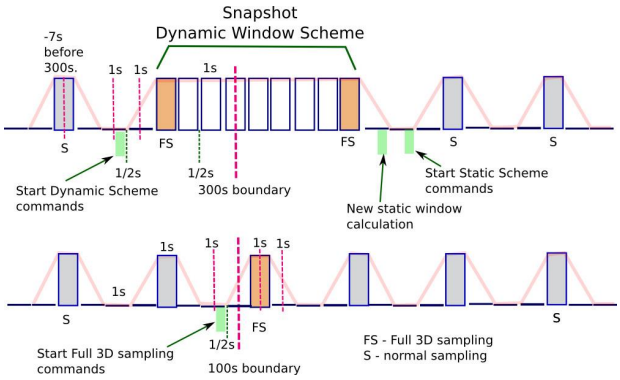

Fig. 32. Schematic illustration of the SWA-PAS cyclogram for data capture during SWA-PAS normal mode (for details see text).

SWA-PAS burst mode. On command, the SWA-DPU will place the SWA-PAS into burst mode. In this mode SWA-PAS returns samples of the full 3D proton and alpha particle distribution in a variety of formats, and for a limited period depending on telemetry constraints. Typically we expect to be able to support measurements of 48 energies, seven azimuths, and three elevations at 0.25 s cadence for periods of order 5 min. However, more complete samples over all nine elevations can also be made at 1 s cadence over similar periods, depending on scientific goals.

4.3.3. SWA-HIS modes of operations

The SWA-HIS sensor measures heavy ions arriving at the sensor aperture over a range of azimuths and elevations and distributed over a spectrum of energies, together with a measure of the TOF of these particles across a known distance in order to determine species. Each individual heavy ion entering SWA-HIS represents an event. The rates of events over different ranges (energy, elevation, TOF) are recorded, which can form the basis of a determination of a phase space distribution for individual elements. SWA-HIS will provide the full PHA, and the rates of PHA, at different cadences and resolutions since events can be selected to fill the available telemetry rates. The selection algorithm works as follows: All ion event words from an E/q scan are divided into five priority ranges, based on their average abundance in the solar wind. Priority ranges are defined by large Energy-TOF boxes, defined separately for each E/q. Events are chosen at random from each of these ranges, with more events selected from ranges containing less abundant ions. In cases where there are insufficient events present in a given range, that number is added to those to be taken from the next range (and so on). On this basis, we anticipate that in normal mode SWA-HIS will provide packets to the SSMM for telemetry which correspond to a cadence of 30 s for Helium ions and 300 s for heavier ions. Limited periods of burst mode data are possible within the telemetry constraints during which (if there are sufficient counts) Helium data will be returned every 4 s and heavier ions at 30 s. However this mode can only be run on average 1% of the time due to telemetry constraints. Conversely a low-cadence mode will also be employed at larger distances from the Sun or during periods of telemetry restriction, in which the data return would be significantly slower than in normal mode.

SWA-HIS also has a number of engineering modes which, together with the housekeeping data, allows instrument health monitoring and fault diagnosis to ensure that the sensor is maintained in optimum configuration.

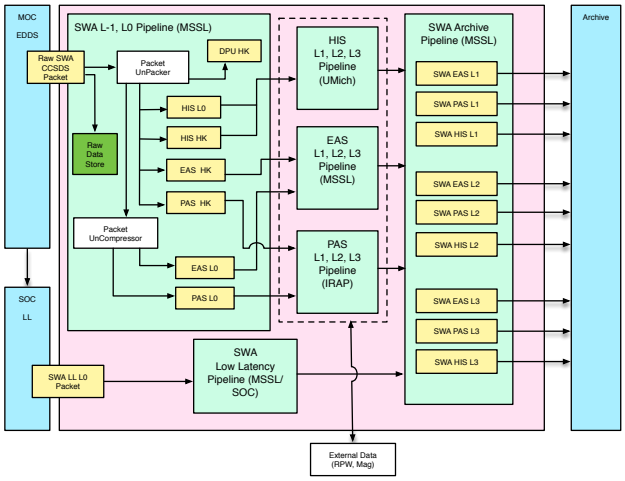

Fig. 33. Schematic of the structure of the SWA data processing pipelines from receipt of telemetry by the MOC to deposit within the ESA science archive.

4.4. SWA data products

In this subsection we detail the SWA data products that we expect to be made available through the Solar Orbiter Archive for the purposes of supporting the science goals of the mission and the community. It is expected, in accordance with the mission Science Management Plan, that best-effort science-quality level-2 data will be made generally available through the archive at 90 days after the receipt of the relevant telemetry by the ESOC. However, some SWA data products may need additional effort to produce or understanding of calibration parameters may evolve, so it is likely that further releases of the data may occur to update the available data to "current best quality" at various points after the initial release.

The SWA data processing flows from the MOC data delivery service through a series of processing pipelines and back out to the SOC archive and other archives as illustrated in Fig. 33. There are six distinct pipeline elements (shaded light green in the figure) dealing with the processing and calibration of the various data products collected by the three SWA sensors and distributed among the SWA operations teams at UCL MSSL, IRAP, and UMich. The remainder of this section provides a top level description of the data types and products produced from these pipelines.

4.4.1. SWA house-keeping and engineering data

The sensor teams for all three of the science sensors within SWA, and the SWA-DPU team have defined a set of house-keeping and engineering parameters for priority download from the spacecraft. It is anticipated that these are available immediately after the ground station pass following their acquisition. An archive of these data products will be maintained by the instrument teams and the project, although it is not foreseen that these will routinely be released to the wider community. However, these data can be made available to researchers should a specific need be identified.

4.4.2. SWA Level 0 and Level 1 data

Data collected by the SWA sensors and SWA-DPU are returned in the telemetry stream as individual CCSDS packets. Once on the ground, these packets are decommutated into relevant files

containing the separate SWA-EAS, SWA-PAS, and SWA-HIS data, and uncompressed to form the L0 raw data packets. These files are still in CCSDS format and are saved and archived in binary format. The process used to create these data files is a simple C code that searches on the data type, subtype, and SID. Data which are compressed are passed through a decompressor. The decommutated and uncompressed CCSDS packet files are grouped into appropriate files for each sensor and each 24 h period. They are stored at UCL MSSL and made available to the wider SWA team.

The SWA L1 data are the uncalibrated, uncompressed L0 data converted into CDF format. The individual sensor teams are responsible for generating SWA L1 data from the L0 packets. These CDF files will have the CCSDS header data and the CCSDS science data combined. All data products are stored as CDF files according to "SOL-SGS-TN-0009 Metadata Definition for Solar Orbiter Science Data". As well as being stored in the SWA Master Repository at UCL MSSL with the L0 data, these files will be be converted to NetCDF format to fit the AMDA tool specification and stored in the Centre de Données de la Physique des Plasmas (CDPP) data archive.

SWA-EAS L1 data. UCL MSSL is responsible for generating the SWA-EAS L1 data from the L0 source. The SWA-EAS L1 data products are, for each SWA-EAS sensor, as follows:

– Normal Mode Spectra in counts, one set for each SWA-EAS sensor. The angular bin directions are in the SWA-EAS sensor reference frames;

– Burst Mode spectra in counts, from one sensor viewing the magnetic field direction. The angular bin directions are in the relevant SWA-EAS sensor frame;

– Triggered Mode Spectra in counts, one set for each SWA-EAS sensor. The angular bin directions are in the SWA-EAS sensor reference frames. These data are at the highest cadence of one 3D sweep per second for a period of 5 min;

– Partial moments calculated on board (6 sets per SWA-EAS sensor) in physical units. The frame references are the SWA-EAS sensor reference frames;

– Engineering mode and calibration data.

SWA-PAS L1 data. IRAP is responsible for generating the SWA-PAS L1 data from the L0 source. The SWA-PAS L1 data products are as follows:

– Normal Mode Spectra in counts. The angular bin directions are in the SWA-PAS frame;

– Normal Mode Snapshot Spectra. The angular bin directions are in the SWA-PAS frame;

– Burst Mode spectra. The angular bin directions are in the SWA-PAS frame;

– Onboard moments in physical units and in the SWA-PAS frame of reference;

– Engineering and Calibration data;

An example of the expected output from the SWA-PAS sensor is shown in Fig. 34. We used the SWA-PAS Proto-Flight Model (PFM) calibration data to simulate the SWA-PAS response, together with very high sampling rate solar wind data from the Faraday cup instrument BMSW onboard of RadioAstron mission (Šafránková et al. 2013) as an input for the simulation. The resulting E-T colour-coded spectrogram in the lower panel of the figure illustrates to the expected output in the SWA-PAS normal mode when the instrument takes a full 3D ion VDF every 4 s.

To illustrate the SWA-PAS ability to resolve the proton and He^{2+} peaks, we have made also a realistic simulation of SWA-PAS energy spectra for two different solar wind conditions

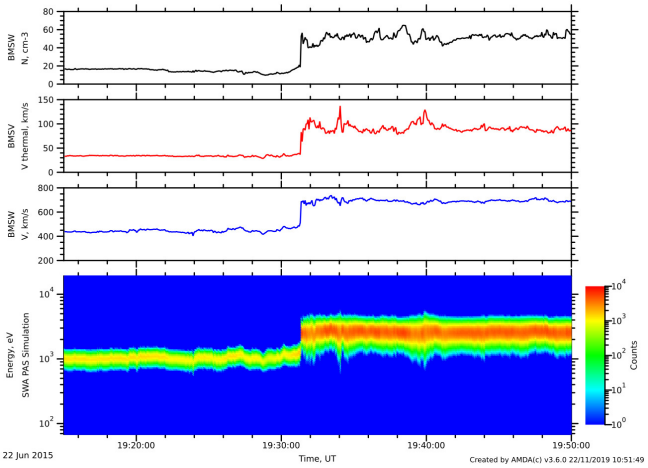

Fig. 34. Simulation of a SWA-PAS Energy-Time Spectrogram. *Three top panels*: input parameters to the simulation as measured by the BMSW instrument onboard the RadioAstron mission. *Bottom panel*: expected sensor response integrated over all angular bins. The time of the measurements is shifted relative to UT by about 1.5 h.

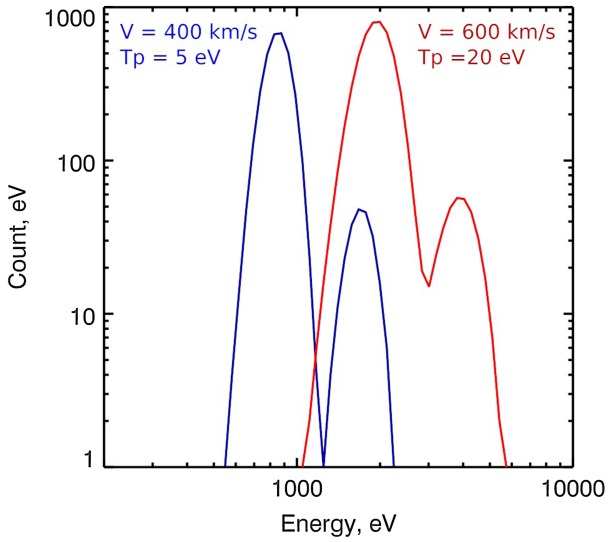

Fig. 35. Simulated examples of SWA-PAS energy spectra for different solar wind conditions. The temperature of He^{2+} peak is assumed as Tp × 4.

(Fig. 35). In both cases the He^{2+} temperature is factor 4 higher than proton temperature. We can see that the He^{2+} peak should be easily resolved by the sensor.

SWA-HIS L1 data. UMich is responsible for generating the L1 SWA-HIS data from the L0 source. These data will be in CDF format. SWA-HIS L1 data products are as follows:

– Ion Event (PHA) words: Individual ion event data, containing full information on incident angles (elevation and azimuth), E/q, TOF, and SSD energy in digital units. The number of PHA words telemetered for each energy scan is fixed (the same for each scan) but configurable, based on available resources. A sampling algorithm is employed to select the sample sent to the ground (see Sect. 4.3.3).

– Priority Rates: Counts of PHA events within a priority range, as a function of E/q and elevation. See below for description of typical use;

– Sensor Rates: Counts of unclassified ion event words on the SWA-HIS detectors (start MCP, stop MCP, SSD) as a

function of E/q, integrated over incident angles, TOF, and Energy. Includes full counts of events subject to decimation. Sensor rates also include two coincidence rates, the number of events with a valid TOF and energy (triple coincidence), and a count of those with only a valid TOF (double coincidence). These rates are primarily used to evaluate the performance of the instrument, rather than for science. In particular, they can be used for calculation of ion detection efficiency in-flight (von Steiger et al. 2000);

– Decimation Rates: Counts of ion event words in each of three decimation ranges as a function of E/q. In order to reduce the on-board processing load caused by light ions and low-TOF noise sources, only a fraction (1 in N) of those events are transmitted to the SWA-HIS C&DH board from the HV bubble. Separate decimation ranges in E/q and TOF are included for alpha particles, protons, and low-TOF events caused by accidental coincidences. The fraction transmitted is commandable, from typically one in four for alphas to zero for low-TOF noise events;

– Matrix Rates: Counts of ion event words within a specified Energy-TOF range, classified and counted onboard, for each E/q step. These are summed over incident angle. SWA-HIS has 32 such species boxes intended to roughly select counts of ion event words measured for particular ion species. Classification transforms E/q, TOF, and residual energy into the two dimensions of Energy and TOF. Classification is primarily used for other data products (below and in low-latency). This data product is not in telemetry for most instrument data rates. If resources allow, He^{2+}, C^{4-6+}, O^{6-7+}, and Fe^{10+} ions may be included. Additional ions and charge states may be produced according to science needs and as counting statistics allow;

– Rate-Based VDFs: Counts of ion event words for a set of ions subdivided by E/q, elevation, and azimuth. The selection of ions will include He^{2+}, C^{5+}, O^{6+}, and Fe^{10+}. Additional ions and charge states may be produced according to science needs and as counting statistics allow. Since these counts are not subject to the effect of the priority sampling algorithm, they represent the best possible statistics. However, because species are separated simply by boxes and no peak overlap removal is performed (see below), the counts are not as accurately assigned to a given species as they would be if formed on the ground, especially for lower abundance heavy ions;

– Engineering and calibration data.

4.4.3. SWA Level 2 data

We define SWA L2 data products as those that have been fully processed and calibrated such that parameters have physical units and are in a common, scientific frame of reference. These are intended as the primary science quality data sets from the SWA project, and the intention is to release these products to the open Solar Orbiter Mission Archive at 90 days after the receipt of the corresponding telemetry from the spacecraft, consistent with the requirements of the mission Science Management Plan. The validation of some L2 data products requires information from other instruments on the spacecraft (e.g. the spacecraft potential measure from RPW and the B-field unit vector from MAG) or extended periods of data taking to validate calibration parameters (e.g. for very low flux heavy ion populations) which may compromise science quality at 90 days and necessitate later updates to the data products.

All SWA L2 data products will be placed, with appropriate metadata, within CDF files according to the format specified in "SOL-SGS-TN-0009 Metadata Definition for Solar Orbiter Science Data". The L2 files from all three SWA sensors will be collected and stored in the SWA master repository at UCL MSSL, along with the auxiliary data generated from the mission. These data files will be submitted to the official ESA Solar Orbiter Archive, from where they will be shared with the NASA Space Science Data Coordinated (NSSDC) archive and the CDPP data archive in France. These files may also be converted by the UCL MSSL team to appropriate format (e.g. NetCDF format to fit the AMDA tool specification) as requested by the archives.

In the remainder of this subsection we provide an overview of the SWA L2 data products that we expect to be readily available from the archive and suitable for science purposes. Full details can be found in SWA technical documentation, particularly the SWA Data Product Definition Document (SO-SWA-MSSL-IF-006).

SWA-EAS L2 data. The Operations team at UCL MSSL is responsible for generating SWA-EAS L2 data. The generation of the full set of SWA-EAS L2 data products from the L0 data products depends a number of sources of auxiliary information including:

– SWA-EAS ground calibration files held at UCL MSSL;

– SWA-EAS flight calibration files, regularly updated during the mission from ESA L0 engineering and calibration data and held at UCL MSSL;

– Spacecraft orbit and attitude information files (e.g. SPICE kernels) available from the SOC;

– Spacecraft potential data associated with each set of SWA-EAS moment calculations (i.e. at 4 s cadence), provided by the RPW instrument;

– Magnetic field direction associated with each SWA-EAS burst mode sample (i.e. at 0.125 s cadence), provided by the MAG instrument.

The set of SWA-EAS L2 data products includes the following primary scientific outputs:

– Onboard moments: A complete set of 14 parameters comprising the best estimation of the moments of the electron velocity distribution (i.e. density, bulk velocity vector, components of the pressure tensor, heat flux vector, and including total counts in the distribution) available from the onboard-generated L1 moments data. This product is available for periods in which the SWA-EAS sensors are in normal mode, and will be provided in physical units and in a relevant heliospheric reference frame. This product will be produced by appropriately combining the L1 partial moments data from each sensor including reference to the spacecraft potential from RPW in order to minimise the effect of spacecraft charging and presence of photo- and secondary electrons of spacecraft origin. The data product will be available at 4 s time resolution;

– Full 3D electron distributions: Electron distributions expressed as a VDF, differential energy flux, and differential number flux provided with appropriate physical units and in a relevant heliospheric reference frame. These distributions are produced by appropriately combining spectra from the two sensors, taking into consideration those parts of the FoV which have an overlap between the two SWA-EAS sensors. In their fullest form these data products will cover the energy range 1 eV−5 keV in 64 energy steps, and with the two orthogonally-mounted sensors each covering ±45° and ±180° in elevation (in 16 steps) and azimuth (in 32 steps), the combined system is capable of covering more than the full 4 π steradian FoV. Measurements at low energy steps contaminated by photo- and secondary electrons will be replaced by fill values, as well as angular bins which may have been affected by a blockage to arrival electrons

by the spacecraft and its appendages. These products are available for periods in which the SWA-EAS sensors are in normal mode. The nominal time resolution for these data products is 100 s, although they can be made available with 10 s resolution when the spacecraft is relatively close to the Earth and higher than average telemetry rates can be made available. Conversely, these products may only be available at 400 s resolution during periods when the project needs to limit overall telemetry below the baseline allocation to instruments;

– Ground moments: A complete set of 14 parameters comprising the ground-calculated moments of the electron VDF (i.e. density, bulk velocity vector, components of the pressure tensor, heat flux vector, and including total counts used to derive the distribution). This product is generated from the normal mode combined 3D electron distributions following calibration and correction for the spacecraft potential derived from RPW data. These data products will have two variants, the moments resulting from both a direct moment summation across the corrected and validated full 3D VDF and, where appropriate, a fit to a model core, halo, and strahl distribution. This product is again available for periods in which the SWA-EAS sensors are in normal mode, and will be provided in physical units and in a relevant heliospheric reference frame. It will be generated on the same resolution as the available 3D VDF's (i.e. nominally at 100 s time resolution, but with variants at 10 s and 400 s depending on telemetry rates);

– Trigger Mode distributions: Full 3D electron distributions derived from L0 data captured and telemetered to ground in response to a freeze of the internal SWA rolling memory buffer following the receipt and acceptance by the SWA-DPU of an appropriate trigger flag via the S20 inter-instrument communications link from RPW. This "trigger mode" data product will be assembled in the same way as the normal mode full 3D distributions functions discussed above (i.e. combined data from both sensors) but will be available at 1 s cadence for a period of 5 min per triggered event. As for the normal mode distributions, these data will be available in appropriate physical units expressed as a VDF, a differential energy flux, and a differential number flux, each in a relevant reference heliospheric frame.

– Trigger Mode Moments: These moment parameters are calculated on the ground in the same way as the "Ground Moments" described above, but are derived from the combined trigger mode VDF's following calibration and correction for the spacecraft potential derived from RPW data. They will thus be available at 1 s time resolution over the trigger mode periods of 5 min per event accepted by the SWA-DPU;

– Burst mode electron pitch angle (2D) distributions: SWA-EAS data collected in burst mode, comprising two full azimuth scans from two elevations from one sensor, will be rebinned into pitch angle space on the ground with reference to the validated magnetic field unit vector. The resulting 2D electron pitch-angle distributions thus will be delivered in physical units (in distribution function, differential energy flux, and differential number flux formats), and in a frame defined by the magnetic field direction. The data product can contain up to 64 energy bins and 64 pitch angle bins, although these will likely be reduced in size by removing energy bins contaminated by photo-electron fluxes and combining the individual pitch angle measurements into a regular set of pitch angle bins. The time cadence of this product is 0.125 s, and it will generally be available for limited periods (average of less than 12 min per day) due to telemetry constraints. Longer periods may be available during enhanced telemetry periods or by reducing the duty cycle and combining available burst mode periods over a longer period of time;

– Single energy angle-angle electron distributions: This data product is equivalent to the ground validated and enhanced SWA-EAS low-latency data product (see Sect. 4.4.5). It is available for periods in which the sensor operates in normal mode, and contains a full angular distribution (i.e. combined data from both sensors) for a single energy bin, usually chosen in the range expected for the solar wind strahl population. The data product will be made available in physical units (in distribution function, differential energy flux, and differential number flux formats), and in a relevant heliospheric frame. The raw L0 data forming the corresponding low-latency product is only available at a time resolution 100 s. However, given the operation of the sensor to capture that product between measurements of the normal mode VDF's the ground produced L2 version of this product will usually be available at 50 s time resolution or better;

SWA-PAS L2 data. The SWA operations team at IRAP, Toulouse, is responsible for generating SWA-PAS L2 data. The generation of the full set of SWA-PAS L2 data products from the L0 data products depends a number of sources of auxiliary information including:

– L0 data products;
– SWA-PAS ground calibration files;
– SWA-PAS flight calibration files (Obtained from L0 data);
– Spacecraft orbit and attitude information files (e.g. SPICE kernels);

The set of SWA-PAS L2 data products includes the following primary scientific outputs from the SWA-PAS sensor:

– Full and reduced 3D ion distributions: Ion distributions expressed in scientific units (as differential fluxes and as VDFs), and in a relevant physical frame (e.g. the solar-ecliptic frame). These data are available from periods of normal mode operation, usually with 4 s time resolution;

–Snapshot mode fast 3D ion distributions: Ion distributions obtained during periods of snapshot operation expressed in scientific units (as differential fluxes and as VDFs), and in a relevant physical frame. Snapshot mode measurements are made at a cadence of one distribution per second over a period of 7 s, recurring every 300 s during normal mode operation;

– Burst Mode fast 3D ion distributions: Ion distributions obtained during periods of burst mode operation expressed in scientific units (as differential fluxes and as VDFs), and in a relevant physical frame. SWA-PAS burst mode measurements can be made at a variety of cadences (extending down into the sub-second range) depending on the trade-off between time and angular or energy resolution. The duration of the burst mode period is variable, depending on available telemetry, but will generally occur in 5 min periods. Details of the operation for a given burst mode interval will be included in the meta-data for the data product.

– Ground-calculated H^+ moments: The 3D ion distributions will be appropriately processed on the ground to produce moments (density, bulk velocity, pressure tensor) for the proton component of the solar wind captured by SWA-PAS. Data will be in scientific units in an appropriate physical reference frame, and will generally be available with 4 s cadence;

– Ground-calculated He^{2+} moments: As above for protons, but separating out the moments for the alpha particle component of the solar wind capture by SWA-PAS;

– Onboard-calculated Moments: This data product is essentially the ground-validated SWA-PAS low-latency data product (see Sect. 4.4.5). It is provided for reference, but essentially

Table 9. SWA-HIS Level 2 derived data products in physical units.

Data product	Time resolutions [1]
Ion event (PHA) words	30 s, 300 s, 4 s [2]
E/q (keV/e)	
Elevation and azimuth (deg)	
Time-of-flight (ns)	
Total energy (keV)	
Priority range	
Decimation range	
Sensor rates (flux)	30 s, 300 s, 4 s [2]
Start	
Stop	
SSD	
Double coincidence	
Triple coincidence	
Normalisation rates	30 s, 300 s, 4 s [2]
Decimation	
Priority	
Matrix rates [3]	30 s, 300 s, 4 s [2]
He^{2+}	
C^{4-6+}	
O^{6-7+}	
Fe^{10+}	
Rate-based velocity distributions [3]	
He^{2+}	30 s, 300 s, 4 s [2]
C^{5+}	30 s, 300 s, 4 s [2]
O^{6+}	30 s, 300 s, 4 s [2]
Fe^{10+}	30 s, 300 s, 4 s [2]

Notes. [1]These are the possible time resolutions. For some periods in the solar wind, the highest time-resolution will not provide data with sufficient statistical accuracy. The best, most scientifically useful averaging intervals will be determined ground analyses of the counting accuracy achievable. [2]Data at this resolution corresponds to SWA-HIS Burst mode, which can only be run on average 1% of the time due to telemetry constraints. [3]Data product not included for most telemetry rates.

is superceded in terms of quality by the ground-calculated moments described above.

SWA-HIS L2 data. The SWA operations team at UMich is responsible for generating SWA-HIS L2 data. The generation of the full set of SWA-HIS L2 data products from the L0 data products depends a number of sources of auxiliary information including:

– L0 data products;
– SWA-HIS ground calibration files;
– SWA-HIS flight calibration files (Obtained from L0 data);
– Spacecraft orbit and attitude information files (e.g. SPICE kernels);

The set of SWA-HIS L2 data products is summarised in Table 9 and includes the following primary scientific outputs from the SWA-HIS sensor:

– Ion event (PHA) words: Full information about measured ion events, including E/q, TOF, energy, and incident angles (elevation and azimuth) in physical units. These are the primary science data product from SWA-HIS, and make up the bulk of SWA-HIS telemetry volume in normal and low cadence modes;

– Priority rates: Total counts of ion event words in each priority range, divided by E/q and elevation angle bin. (Duplicate of L1 version). These rates are used to correct the weighting of telemetered ion event words for the effect of the sampling algorithm. For example, if the priority rate for a given E/q step and elevation bin is ten, but only five of these ion event words were included in telemetry, then each counts for two in further processing;

– Sensor rates: L1 sensor rates converted to differential number flux units, $(cm^2\ s\ sr\ keV)^{-1}$;

– Decimation rates: Duplicate of L1 version since conversion to flux units is not useful;

– Matrix rates: L1 Matrix Rates converted to number flux units, $(cm^2\ s)^{-1}$;

– Rate-based VDFs: L1 Rate-Base VDFs converted to differential number flux units, $(cm^2\ s\ sr\ keV)^{-1}$.

4.4.4. SWA Level 3 data

It is anticipated that during the course of the mission the primary science data products, as represented by the SWA L2 data products submitted to the archives and discussed above, will be supplemented by the creation of higher order, or Level 3, SWA data products. These products may arise either through further reduction of the L2 products or perhaps through further combinations of data products either within the SWA suite or with other instruments on Solar Orbiter. For SWA-EAS and SWA-PAS, possible examples of this might include SWA-EAS PADs generated from the Trigger Event 3D distributions with reference to the magnetic field direction (providing a cadence of 1 s for a 5 min period), or electron or ion moments calculated over narrower energy ranges, etc.

In the case of SWA-HIS, the most accurate and scientifically useful data products are formed via a peak overlap removal algorithm to assign counts to individual ion species in ground processing (von Steiger et al. 2000; Shearer et al. 2014). This algorithm uses a forward model to predict the peak centre location of each of the >75 analysed ions in TOF – energy space at each E/q step. This forward model, which includes estimated peak width as well as centre, is developed from ground calibration and in-flight accumulated data. A set of two-dimensional Gaussian curves is formed from these centres and widths and provides an initial estimate of count vectors assigned each species. A maximum-likelihood estimation (MLE) method then shuffles counts among these vectors to remove overlap in the statistically optimal way. Events at each pair of incident angle bins are processed independently to preserve distributions in these dimensions. Count vectors from all angle bins are then recombined and converted to phase-space density ($s^3\ km^{-6}$) to form 3D VDFs. Moments of density, velocity, and temperature are then computed from these VDFs and used to produce the following data products from SWA-HIS (see Table 10):

– Elemental abundances: This data product contains the sum of all ion densities for a particular element provided as a ratio to those of oxygen;

– Ionic charge states: Density ratios for specified ion pairs or average charge states, computed as density-weighted average;

– Charge state distributions: Normalised distribution of all charge states analysed for a specified element;

– Kinetic properties: Moments of VDFs for specified ions. This data product includes the density (cm^{-3}), bulk velocity ($km\ s^{-1}$), and temperature (K) for the specified ions;

– Velocity distributions: Phase space density ($s^3\ km^{-6}$) of the specified ions in instrument frame, binned according to speed and incident angles (elevation and azimuth).

Table 10. SWA-HIS Level 3 derived data products in physical units.

Data product	Time resolutions [1]
Elemental abundances	
Fe/O	30 s, 300 s, 4 s [2]
C/O	30 s, 300 s, 4 s [2]
He/O	30 s, 300 s, 4 s [2]
Mg/O	30 s, 300 s
Si/O	30 s, 300 s
Ne/O	30 s, 300 s
S/O	>300 s [2]
N/O	>300 s
Ionic charge states	
O^{7+}/O^{6+}	30 s, 300 s, 4 s [2]
C^{6+}/C^{4+}	30 s, 300 s, 4 s [2]
C^{5+}/C^{4+}	30 s, 300 s, 4 s [2]
$\langle Q_O \rangle$	30 s, 300 s, 4 s [2]
$\langle Q_C \rangle$	30 s, 300 s, 4 s [2]
$\langle Q_{Fe} \rangle$	30 s, 300 s, 4 s [2]
Ionic charge state distributions	
$Q_i(O)$, $i = 5, \ldots, 8$	30 s, 300 s
$Q_i(C)$, $i = 4, \ldots, 6$	30 s, 300 s
$Q_i(Fe)$, $i = 6, \ldots, 20$	30 s, 300 s
$Q_i(Si)$, $i = 6, \ldots, 12$	30 s, 300 s
$Q_i(Ne)$, $i = 8, \ldots, 10$	30 s, 300 s
$Q_i(Mg)$, $i = 5, \ldots, 12$	30 s, 300 s
$Q_i(N)$, $i = 5, 6$	30 s, 300 s [3]
$Q_i(S)$, $i = 6, \ldots, 14$	30 s, 300 s [3]
Bulk properties (n, v_{bulk}, T)	
He^{2+}	30 s, 300 s, 4 s [2]
C^{5+}	30 s, 300 s, 4 s [2]
O^{6+}	30 s, 300 s, 4 s [2]
Fe^{10+}	30 s, 300 s, 4 s [2]
Velocity distributions [4]	
He^{2+}	30 s, 300 s, 4 s [2]
C^{5+}	30 s, 300 s, 4 s [2]
O^{6+}	30 s, 300 s, 4 s [2]
Fe^{10+}	30 s, 300 s, 4 s [2]

Notes. [1]These are the possible time resolutions. For some periods in the solar wind, the highest time-resolution will not provide data with sufficient statistical accuracy. The best, most scientifically useful averaging intervals will be determined by ground analyses of the counting accuracy achievable. [2]Data at this resolution corresponds to SWA-HIS Burst mode, which can only be run on average 1% of the time due to telemetry constraints. [3]These elements are more difficult to resolve. Appropriate time resolutions will be determined in flight. [4]Additional charge states may be produced during periods of high counting statistics.

It is expected that some elements of the processing or analyses of the SWA sensor data will in time become routine. In such cases, the SWA operations teams will include these in the SWA processing pipelines and the results will be stored in the master SWA archive at UCL MSSL and submitted to the archives with the corresponding level 2 data.

4.4.5. SWA low-latency data

The Solar Orbiter project reserved a small amount of telemetry within the download budget for priority download of a subset of the data from each of the instruments on board the spacecraft. These data are downloaded from the instrument packet stores with priority second only to the house-keeping data. It is thus anticipated that these data would also normally be available immediately after the ground station pass following their acquisition, and thus with a latency which will generally be low in comparison to that of the full, regular instrument data set for the same observing period. For this reason, the volume of such low-latency data generated by each instrument is very limited ($\sim$1 Mbyte day^{-1}), corresponding to a maximum of $\sim$100 bits s^{-1} within each instruments telemetry stream.

The primary purpose of the low-latency data is to aid in the "last-minute" pointing of the remote sensing instruments on the platform, although there are also obvious benefits to instrument operation to have visibility of the science data production with short turn-around times. However, this also has potential uses as a "space weather beacon" data set, and indeed to provide some context for early identification and assessment of periods of potentially high scientific interest (e.g. for those instruments that may wish to use a selective data download capability). Given these "fast-turnaround" functions, the low-latency data from SWA will be produced immediately after receipt of the telemetry by an automated pipeline within a virtual machine which has been delivered to the ESA SOC. It will be made available immediately to the community through the Solar Orbiter archive.

The specific SWA low-latency data products that, at the time of writing, are intended to be made available are described below:

SWA-EAS. Following acquisition of a full 3D VDF from the two SWA-EAS sensor heads, the SWA-DPU will, with 100 s cadence, select a single (ground-commandable) energy level and extract all electron counts from all angular bins for both heads. The resulting data (2 heads $\times$ 32 azimuths $\times$ 16 elevations $\times$ 1 energy $\times$ 2 byte words compressed by factor 4 every 100 s $\sim$ 43 bits s^{-1}) will be added to the SWA low-latency telemetry stream. In flight it is intended that the SWA-DPU will select an energy in the range which generally isolates the strahl population in the solar wind, and thus has been termed "single (strahl) energy distribution". Thus after processing by the SOC virtual machine, this low-latency data product should indicate the presence (or not) of narrow beams directed parallel or anti-parallel to the magnetic field direction, which provides key information indicating the nature of the connection of the magnetic field line passing through the spacecraft location to the Sun. We note also that this data product will be derived from a full 3D distribution measurement that otherwise would not fall in the downloaded normal mode data (see below). Thus this SWA-EAS single (strahl) energy distribution product will be offset by 50 s from the 100 s cadence full 3D data product. This is in order to avoid duplication of telemetered data and to allow subsequent on-ground data processing to generate an equivalent data product at twice the cadence ($\sim$50 s). The data product can only be generated while the SWA-EAS sensor is in normal mode.

SWA-PAS. From the SWA-PAS normal mode measurements, the SWA-DPU will calculate on board a set of proton and alpha particle moments every four seconds. These SWA-PAS moments will consist of a single density value, a 3-element velocity vector, and a 9-element pressure tensor, which will be added to the SWA low-latency telemetry stream, where they typically require $\sim$46 bits s^{-1}. This data product will regularly provide the community with near-immediate (<1 day delay) context of the solar wind conditions (fast or slow stream, etc.) at the spacecraft.

SWA-HIS. SWA-HIS will contribute four items to the low-latency telemetry stream, one charge state ratio, one elemental abundance ratio, and two rate spectra. The charge state and elemental abundance ratios will be on-board computed versions of those described in the L3 data products (above). The rate spectra will be selected from one of the sensor or matrix rates. These data, normally containing a total of 131 8-bit words, will be sent every 300 s, contributing 4 kbps to the telemetry stream, including packet overhead (although an option for 30 s cadence is available). These can be used for payload-wide science planning and end-to-end instrument health monitoring. Charge state and elemental abundance ratios enable monitoring of solar wind type (slow, fast, shock) and baseline tracking of structures in the solar wind, while the rate spectra are a valuable measure of the plasma environment and the correct end-to-end operation of the SWA-HIS sensor.

5. Summary and conclusions

The SWA instrument is a suite of scientific sensors on-board Solar Orbiter that is designed and developed to measure the thermal and suprathermal charged particle populations in the inner heliosphere. SWA is comprised of three distinct sensor systems, plus a coordinating SWA-DPU, or electronics box, which together will make key measurements of electron, protons and alpha particle, and heavy ion populations arriving at the spacecraft location. Details of the sensor designs and characteristics have been summarised in this paper: SWA-EAS is located in the spacecraft shadow at the end of the boom, and is capable of detecting electrons arriving from all directions (except those blocked by the spacecraft or its appendages) across the energy range of 1 eV to ~5 keV. The SWA-PAS samples protons and alpha particles with energies in the range 0.2−20 keV/e arriving from within a few tens of degrees of the solar direction. Given the ratio of the solar wind bulk flow speed to the proton thermal speed, this FoV through a cut-out in the spacecraft heat shield is sufficient to capture the full distribution of arriving particles under most expected circumstances. The SWA-HIS samples and categorises heavy ions (masses from He to Fe) with energies in the range <0.5−100 keV/e, also arriving from within a few tens of degrees of the solar direction. The sensor is also located behind the spacecraft heat shield with a FoV extending through a cut out in one corner. Finally, the SWA-DPU provides all sensor commanding and control functions, power supply, and data processing for SWA-EAS and SWA-PAS and data communications from all sensors to the spacecraft SSMM, as well as monitoring sensor operations and health.

The broad range of operating modes and data products expected from the suite of sensors have also been described in this paper. Normal mode data products, including electron on-board-calculated moments and proton and alpha particle velocity distributions, are expected to be available on a time cadence of 4 s. Electron velocity distributions and heavy ion composition and charge state information will generally be available at a lower cadence (normally ~100 s and ~300 s respectively, due to telemetry restrictions or expected count rates), but each of these data products is expected to make a key contribution to the scientific objectives of the mission. In particular, SWA has a critical role in establishing the links between measurements made by the in situ instruments on the spacecraft and those remote sensing instruments observing potential source regions of the solar wind, either through establishing solar wind speed by which to map solar wind streamlines back to the Sun, through comparison of ion composition and FIP information to verify connections, to the presence of electron strahl to establish magnetic connections to the Sun. Moreover, the SWA sensors will operate in several possible burst modes and triggered modes (at sub-second cadences for SWA-EAS and SWA-PAS and down to 4 s for SWA-HIS) which will provide unique inputs to mission goals that focus on solar wind kinetics, turbulence, and the nature of relatively small-scale structures.

In all cases, the SWA sensors, as delivered to the spacecraft, meet or exceed the performance requirements originally set out to achieve the mission science goals. The successful operation of the SWA sensors throughout the course of the Solar Orbiter mission will result in the provision to the solar and heliospheric science community of unique data products revealing the nature of the solar wind depending on both heliocentric distance and solar latitude. The SWA data will underpin efforts to link the in situ measurements of the solar wind made at the spacecraft with remote observations of the candidate source regions. This will lead to very significant advances in our understanding of the mechanisms accelerating and heating the solar wind, driving eruptions and other transient phenomena on the Sun, and controlling the injection, acceleration and transport of the energetic particles in the heliosphere.

Acknowledgements. The Solar Orbiter Solar Wind Analyser (SWA) scientific sensors, SWA-EAS, SWA-PAS, SWA-HIS, and the SWA-DPU have been designed and created, and are operated under funding provided in numerous contracts from the UK Space Agency (UKSA), the UK Science and Technology Facilities Council (STFC), the Agenzia Spaziale Italiana (ASI), the Centre National d'Etudes Spatiales (CNES, France), the Centre National de la Recherche Scientifique (CNRS, France), the Czech contribution to the ESA PRODEX programme, and NASA. The very significant efforts by a wide team of engineers, scientists, industrial partners, and subcontractors to the development of the instrument suite are gratefully acknowledged.

References

Auchère, F., Andretta, V., Antonucci, E., et al. 2020, A&A, 642, A6 (Solar Orbiter SI)
Bale, S. D., Kasper, J. C., Howes, G. G., et al. 2009, Phys. Rev. Lett., 103, 211101
Carlson, C. W., & McFadden, J. P. 2013, Design and Application of Imaging Plasma Instruments (American Geophysical Union (AGU)), 125
Carlson, C., Curtis, D., Paschmann, G., & Michel, W. 1982, Adv. Space Res., 2, 67
Collinson, G. A., & Kataria, D. O. 2010, Meas. Sci. Technol., 21, 105903
Dusenbery, P. B., & Hollweg, J. V. 1981, J. Geophys. Res., 86, 153
Feldman, U., & Widing, K. 2003, Space Sci. Rev., 107, 665
Feldman, W. C., Asbridge, J. R., Bame, S. J., Montgomery, M. D., & Gary, S. P. 1975, J. Geophys. Res., 80, 4181
García-Marirrodriga, C., Pacros, A., Strandmoe, S., et al. 2020, A&A, in press, https://doi.org/10.1051/0004-6361/202038519 (Solar Orbiter SI)
Gary, S. P. 1991, Space Sci. Rev., 56, 373
Gary, S. P. 1993, Theory of Space Plasma Microinstabilities (Cambridge, UK: Cambridge University Press), 193
Gary, S. P., & Karimabadi, H. 2006, J. Geophys. Res.: Space Phys., 111, A11224
Gary, S. P., Feldman, W. C., Forslund, D. W., & Montgomery, M. D. 1975, J. Geophys. Res., 80, 4197
Gary, S. P., Montgomery, M. D., Feldman, W. C., & Forslund, D. W. 1976, J. Geophys. Res., 81, 1241
Gary, S. P., Foosland, D. W., Smith, C. W., Lee, M. A., & Goldstein, M. L. 1984, Phys. Fluids, 27, 1852
Gary, S. P., Yin, L., Winske, D., & Reisenfeld, D. B. 2000, Geophys. Res. Lett., 27, 1355
Gloeckler, G., Zurbuchen, T., & Geiss, J. 2003, J. Geophys. Res.: Space Phys., 108, A4
Hellinger, P., Trávníček, P., Kasper, J. C., & Lazarus, A. J. 2006, Geophys. Res. Lett., 33, L09101
Horbury, T. S., O'Brien, H., Carrasco Blazquez, I., et al. 2020, A&A, 642, A9 (Solar Orbiter SI)
Hundhausen, A. J., Gilbert, H. E., & Bame, S. J. 1968, J. Geophys. Res. (1896–1977), 73, 5485
Isenberg, P. A., & Hollweg, J. V. 1983, J. Geophys. Res., 88, 3923
Johnstone, A., Alsop, C., Burge, S., et al. 1997, Space Sci. Rev., 79, 351

Kessel, R., Johnstone, A., Coates, A., & Gowen, R. 1989, Rev. Sci. Instrum., 60, 3750
Klein, K. G., & Chandran, B. D. G. 2016, ApJ, 820, 47
Ko, Y., Fisk, L., Geiss, J., Gloeckler, G., & Guhathakurta, M. 1997, Sol. Phys., 171, 345
Laming, J. M. 2015, Liv. Rev. Sol. Phys., 12, A2
Landi, E., Gruesbeck, J. R., Lepri, S. T., & Zurbuchen, T. H. 2012, ApJ, 750, A159
Lynch, B. J., Reinard, A. A., Mulligan, T., et al. 2011, ApJ, 740, A112
Maksimovic, M., Bale, S. D., Chust, T., et al. 2020, A&A, 642, A12 (Solar Orbiter SI)
Marsch, E. 2006, Liv. Rev. Sol. Phys., 3, 1
Marsch, E., Goertz, C. K., & Richter, K. 1982, J. Geophys. Res., 87, 5030
Marsch, E., Vocks, C., & Tu, C. Y. 2003, Nonlinear Process. Geophys., 10, 101
Matteini, L., Hellinger, P., Goldstein, B. E., et al. 2013, J. Geophys. Res.: Space Phys., 118, 2771
Mewaldt, R. A., Cohen, C. M. S., Haggerty, D. K., et al. 2003, Int. Cosm. Ray Conf., 6, 3313
Müller, D., Marsden, R. G., St. Cyr, O. C., & Gilbert, H. R. 2013, Sol. Phys., 285, 25
Müller, D., St. Cyr, O. C., Zouganelis, I., et al. 2020, A&A, 642, A1 (Solar Orbiter SI)
Nicolaou, G., Verscharen, D., Wicks, R. T., & Owen, C. J. 2019, ApJ, 886, 101
Owens, M. J., Crooker, N. U., & Schwadron, N. A. 2008, J. Geophys. Res.: Space Phys., 113, A11104
Owens, M. J., Lockwood, M., Riley, P., & Linker, J. 2017, J. Geophys. Res.: Space Phys., 122, 10,980
Paschmann, G., Fazakerley, A. N., & Schwartz, S. J. 1998, ISSI Sci. Rep. Ser., 1, 125
Pilipp, W. G., Miggenrieder, H., Mühlhaüser, K. H., et al. 1987, J. Geophys. Res., 92, 1103
Reinard, A. A., Lynch, B. J., & Mulligan, T. 2012, ApJ, 761, A175
Rodríguez-Pacheco, J., Wimmer-Schweingruber, R. F., Mason, G. M., et al. 2020, A&A, 642, A7 (Solar Orbiter SI)
Rouillard, A. P., Pinto, R. F., Vourlidas, A., et al. 2020, A&A, 642, A2 (Solar Orbiter SI)
Šafránková, J., Němeček, Z., Přech, L., et al. 2013, Space Sci. Rev., 175, 165
Šafránková, J., Němeček, Z., Němec, F., et al. 2019, ApJ, 870, 40
Schwadron, N., & McComas, D. 2003, ApJ, 599, 1395
Shearer, P., von Steiger, R., Raines, J. M., et al. 2014, ApJ, 789, 60
SPICE Consortium (Anderson, M., et al.) 2020, A&A, 642, A14 (Solar Orbiter SI)
Stansby, D., Perrone, D., Matteini, L., Horbury, T. S., & Salem, C. S. 2019, A&A, 623, L2
Steinberg, J. T., Gosling, J. T., Skoug, R. M., & Wiens, R. C. 2005, J. Geophys. Res.: Space Phys., 110, A06103
Tu, C., Zhou, C., Marsch, E., et al. 2005, Science, 308, 519
Velli, M., Harra, L. K., Vourlidas, A., et al. 2020, A&A, 642, A4 (Solar Orbiter SI)
Verscharen, D., Bourouaine, S., & Chandran, B. D. G. 2013, ApJ, 773, 163
Verscharen, D., Chandran, B. D. G., Bourouaine, S., & Hollweg, J. V. 2015, ApJ, 806, 157
Verscharen, D., Klein, K. G., & Maruca, B. A. 2019, Liv. Rev. Sol. Phys., 16, 5
von Steiger, R., Schwadron, N. A., Fisk, L. A., et al. 2000, J. Geophys. Res., 105, 27217
von Steiger, R., Zurbuchen, T., Geiss, J., et al. 2001, Space Sci. Rev., 97, 123
Walsh, A. P., Horbury, T. S., Owen, C. J., et al. 2020, A&A, 642, A5 (Solar Orbiter SI)
Wu, H., Verscharen, D., Wicks, R. T., et al. 2019, ApJ, 870, 106
Yoon, P. H., & Sarfraz, M. 2017, ApJ, 835, 246
Zhao, L., Zurbuchen, T. H., & Fisk, L. A. 2009, Geophys. Res. Lett., 36, L14104
Zouganelis, I., De Groof, A., Walsh, A. P., et al. 2020, A&A, 642, A3 (Solar Orbiter SI)
Zurbuchen, T. H. 2007, ARA&A, 45, 297
Zurbuchen, T., Hefti, S., Fisk, L., Gloeckler, G., & Von Steiger, R. 1999, Space Sci. Rev., 87, 353
Zurbuchen, T., Fisk, L., Gloeckler, G., & von Steiger, R. 2002, Geophys. Res. Lett., 29, A1352

[1] Mullard Space Science Laboratory, University College London, Holmbury St. Mary, Dorking, Surrey RH5 6NT, UK
e-mail: c.owen@ucl.ac.uk
[2] INAF-Istituto di Astrofisica e Planetologia Spaziali, Via Fosso del Cavaliere 100, 00133 Roma, Italy
[3] Southwest Research Institute, 6220 Culebra Road, San Antonio, TX 78238, USA
[4] Institut de Recherche en Astrophysique et Planétologie, 9, Avenue du Colonel ROCHE, BP 4346, 31028 Toulouse Cedex 4, France
[5] Laboratoire de Physique des Plasmas, Ecole Polytechnique, Palaiseau, France
[6] Centre National d'Etudes Spatiales, DCT/PO/EU – B.P.I. 2220, 18, Avenue Edouard Belin, 31401 Toulouse Cedex 9, France
[7] Techno System Developments S.R.L., Via Provinciale Pianura 2, Int. 23, San Martino Zona Industriale 80078, Pozzuoli, Italy
[8] NASA Goddard Space Flight Center, 8800 Greenbelt Road, Greenbelt, Maryland 20771, USA
[9] Planetek Italia S.R.L., Via Massaua, 12, 70132 Bari, BA, Italy
[10] Space Science Center, University of New Hampshire, Morse Hall, Durham, NH 03824, USA
[11] University of Michigan, 2455 Hayward St, Ann Arbor, MI 48109, USA
[12] LEONARDO, Viale del lavoro, 101, 74123 Taranto, Italy
[13] SITAEL S.p.A., Via San Sabino 21, 70042 Mola di Bari, BA, Italy
[14] ESA-ESTEC/SCI-PS, Keplerlaan 1, 2201 AZ Noordwijk, The Netherlands
[15] Department of Surface and Plasma Science, Faculty of Mathematics and Physics, Charles University, V Holesovickach 2, 18000 Prague 8, Czech Republic
[16] NASA Goddard Space Flight Center, 8800 Greenbelt Road, Greenbelt, MD 20771, USA
[17] CGC Instruments, Chemnitz, Germany
[18] Space and Atmospheric Physics, The Blackett Laboratory, Imperial College London, London SW7 2AZ, UK
[19] LESIA, Observatoire de Paris, Universite PSL, CNRS, Sorbonne Universite, Universite de Paris, 5 Place Jules Janssen, 92195 Meudon, France
[20] Space Research Group, University of Alcalá, 28801 Alcalá de Henares, Spain
[21] Agenzia Spaziale Italiana, Via del Politecnico, snc, 00133 Roma, Italy
[22] ESA-ESAC, Camino bajo del Castillo s/n, 28692 Villafranca del Castillo, Madrid, Spain
[23] Institute of Experimental and Applied Physics, Kiel University, Leibnizstrasse 11, 24118 Kiel, Germany
[24] Physikalisches Institut, Universitat Bern, Sidlerstrasse 5, 3012 Bern, Switzerland
[25] Incom, Inc., 242 Sturbridge Road, Charlton, MA 01507, USA